Techno-economic feasibility analysis of low-temperature geothermal heating and cooling

Zur Erlangung des akademischen Grades eines

Doktors der Naturwissenschaften (Dr. rer. nat.)

von der KIT-Fakultät für
Bauingenieur-, Geo- und Umweltwissenschaften
des Karlsruher Instituts für Technologie (KIT)

genehmigte

DISSERTATION

von

M.Sc. Simon Schüppler

Tag der mündlichen Prüfung
07.06.2021

Referent: Prof. Dr. habil. Philipp Blum
Korreferent: Prof. Dr. habil. Peter Bayer

Karlsruhe 2021

Abstract

Feasibility analyses in the early stages of project development are crucial for a smooth planning process and significantly contribute to a successful implementation of shallow geothermal energy (SGE) systems for heating and cooling supply. Even though the supply reliability and operational efficiency of SGE are widely proven, a broad market distribution is still impeded by high initial capital costs, site-specific and complex planning procedures as well as existing conventional technologies that are often characterized by simpler planning and utilization. Hence, comprehensive feasibility analyses considering economic and technical aspects are crucial not only to facilitate a rapid project development but also to point out associated economic benefits and technical capabilities to customers and decision-makers. Despite the successful realization of a few best practice examples of SGE supplying large-scale industrial, commercial or public facilities, there is a lack of knowledge transfer regarding coordinated site characterization and successful project development. Furthermore, only little is known about the actual heating and cooling requirements of buildings and their related supply costs, which not only impede the demonstration of economic benefits of SGE systems but also jeopardizes overall project success. To address these shortcomings and to demonstrate the required scope of holistic and sound techno-economic feasibility (TEF) analyses of large-scale SGE systems, this thesis analyzes individual stages of the TEF at selected sites using four different approaches.

In study 1, a straightforward approach to determine the cooling requirements of buildings is introduced by quantifying installed cooling capacities of compression chillers using aerial images. This is demonstrated at the Campus North of the Karlsruhe Institute of Technology (KIT) considering 36 air-cooled chillers with a total installed cooling capacity of 16 MW. With increasing capacities, improved accuracies of up to 85 % are achieved, indicating higher suitability of the method for large-scale installations.

Considering the findings of study 1, study 2 further analyzes the current cooling supply at the Campus North and examines the cooling demand and associated supply costs of 23 campus buildings. This study is performed considering the intended transition from the current decentralized cooling supply using chillers to promising district cooling (DC) networks fed by renewable cooling sources. Since the obtained parameters are subject to uncertainties, a Monte Carlo simulation is performed revealing cooling costs between 5.4 and 11.4 euro cents kWh^{-1}. Cumulative annual costs of €4.5 million of all considered buildings, mainly resulting from the

electricity costs to operate the chillers, request for a rapid shift to a decentralized and more efficient cooling supply by integrating renewable cooling solutions. The holistic analysis of the current cooling supply facilitates the discussion on further optimization measures and enables benchmarking with other universities or facilities, where DC systems are already implemented.

Study 3 analyzes the economic viability of SGE systems considering the investment costs and operating expenses of a potential Aquifer Thermal Energy Storage (ATES) for the heating and cooling supply of a specific building of the municipal hospital in Karlsruhe, Germany. The determined capital costs amount to €1.3 million, with underground installations accounting for the largest share of costs (60 %). The subsequent cost-benefit analysis between the considered ATES and the current supply technology consisting of compression chillers and district heating (DH) reveals a payback time of about 3 years for the ATES system. The most efficient supply option is direct cooling using ATES resulting in an electricity cost reduction of 80 %. Furthermore, the ATES achieves CO_2 savings of about 600 tons per year, hence clearly demonstrating its potential economic and environmental benefits. This analysis addresses the existing lack of awareness of ATES in general and its related economic potential in particular to especially promote ATES usage in Germany, where the technology has not yet penetrated the thermal energy market.

As the reliability of measured data during exploration is related to optimized system designs affecting SGE economics, a holistic analysis of errors and uncertainties related to wireless temperature measurement (WTM) is provided in study 4. The encountered errors are determined in the laboratory and subsequently applied to vertical temperature profiles of the undisturbed ground recorded at a borehole heat exchanger (BHE) site. The resulting precision of 0.011 K and accuracy of -0.11 K ensure a high reliability of the WTMs. The largest uncertainty is obtained within the first five meters of descent and results from the thermal time constant of 4 s. The fast and convenient measurement procedure results in substantial advantages over Distributed Temperature Sensing (DTS) measurements using fiber optics, whose recorded temperature profiles at the site serve as a qualitative comparison. This study aims to raise awareness on the importance of detailed exploration as part of the TEF analysis of SGE in general and to specifically contribute to the advancement of wireless measurement technology.

Kurzfassung

Machbarkeitsanalysen in der frühen Phase der Projektentwicklung sind entscheidend für einen reibungslosen Planungsprozess und tragen maßgeblich zu einer erfolgreichen Umsetzung von oberflächennahen geothermischen (ONG) Systemen zur Wärme- und Kälteversorgung bei. Obwohl die Versorgungssicherheit und Betriebseffizienz der ONG hinreichend demonstriert ist, wird eine weite Marktverbreitung noch immer durch hohe Anfangsinvestitionen, standortspezifische und komplexe Planungsverfahren sowie konventionelle Technologien, die sich meist durch einfachere Planung und Nutzung auszeichnen, erschwert. Daher sind umfassende Machbarkeitsanalysen, die sowohl wirtschaftliche als auch technische Aspekte berücksichtigen, nicht nur entscheidend, um eine schnelle Projektentwicklung zu ermöglichen, sondern auch, um Kunden und Entscheidungsträgern die wirtschaftlichen Vorteile und technischen Möglichkeiten aufzuzeigen. Trotz der erfolgreichen Umsetzung einiger Best-Practice-Beispiele der ONG für die Versorgung großer industrieller, gewerblicher oder öffentlicher Einrichtungen fehlt es an Wissenstransfer hinsichtlich koordinierter Standortcharakterisierung und erfolgreicher Projektentwicklung. Darüber hinaus ist nur wenig über den tatsächlichen Wärme- und Kältebedarf von Gebäuden und die damit verbundenen Versorgungskosten bekannt, was nicht nur den Nachweis der wirtschaftlichen Vorteile von ONG-Systemen erschwert, sondern auch den gesamten Projekterfolg gefährdet. Um diesen Unzulänglichkeiten zu begegnen und den erforderlichen Umfang einer ganzheitlichen und fundierten technisch-wirtschaftlichen Machbarkeitsanalyse (TWM) großer ONG-Systeme aufzuzeigen, werden in dieser Arbeit einzelne Stufen der TWM an ausgewählten Standorten mit vier verschiedenen Ansätzen analysiert.

In Studie 1 wird ein einfacher Ansatz zur Ermittlung des Kühlbedarfs von Gebäuden vorgestellt, indem die installierten Kühlleistungen von Kompressionskältemaschinen anhand von Luftbildern quantifiziert werden. Dies wird am Campus Nord des Karlsruher Instituts für Technologie (KIT) unter Berücksichtigung von 36 luftgekühlten Kältemaschinen mit einer installierten Gesamtkühlleistung von 16 MW demonstriert. Mit zunehmender Leistung werden verbesserte Genauigkeiten von bis zu 85 % erzielt, was auf eine bessere Eignung der Methodik für Großanlagen hinweist.

Unter Berücksichtigung der Ergebnisse von Studie 1 wird in Studie 2 die aktuelle Kälteversorgung am Campus Nord weiter analysiert und der Kältebedarf von 23 Campusgebäuden

sowie die damit verbundenen Versorgungskosten untersucht. Diese Studie wird im Hinblick auf den beabsichtigten Übergang von der aktuellen dezentralen Kälteversorgung mittels Kältemaschinen zu einem zukunftsfähigen Kältenetz, das durch erneuerbare Kältequellen gespeist werden soll, durchgeführt. Da die erhaltenen Parameter mit Unsicherheiten behaftet sind, wird eine Monte Carlo Simulation durchgeführt, die Kühlkosten zwischen 5,4 und 11,4 Eurocent pro kWh offenbart. Die kumulierten jährlichen Kosten aller betrachteten Gebäude, die hauptsächlich aus den Stromkosten für den Betrieb der Kältemaschinen resultieren, liegen bei 4,5 Mio. € und fordern einen schnellen Umstieg zu einer dezentralen und effizienteren Kälteversorgung durch die Integration von erneuerbaren Kälteversorgungslösungen. Die ganzheitliche Analyse der aktuellen Kälteversorgung erleichtert die Diskussion über weitere Optimierungsmaßnahmen und ermöglicht ein Benchmarking mit anderen Universitäten und Einrichtungen, in denen Kältenetze bereits erfolgreich betrieben werden.

Studie 3 analysiert die Wirtschaftlichkeit der ONG unter Berücksichtigung der Investitions- und Betriebskosten am Beispiel eines potenziellen Aquiferspeichers (ATES) zur Wärme- und Kälteversorgung eines spezifischen Gebäudes des Städtischen Klinikums in Karlsruhe, Deutschland. Die ermittelten Investitionskosten beziffern sich auf 1,3 Mio. €, wobei die unterirdischen Installationen mit 60 % den größten Kostenanteil ausmachen. Eine Kosten-Nutzen-Analyse zwischen dem betrachteten ATES und der aktuellen Versorgungstechnologie bestehend aus Kompressionskältemaschinen und Fernwärme zeigt eine Amortisationszeit des ATES-Systems von ca. 3 Jahren. Die effizienteste aller Versorgungsoptionen ist die direkte Kühlung des Gebäudes mittels ATES, was zu einer Stromkostenreduktion von 80 % führt. Darüber hinaus ermöglicht das ATES-System eine CO_2-Einsparung von ca. 600 Tonnen pro Jahr, wodurch die potentiellen wirtschaftlichen und ökologischen Vorteile der Technologie verdeutlicht werden. Diese Analyse adressiert das fehlende Bewusstsein für ATES im Allgemeinen und das damit verbundene wirtschaftliche Potenzial im Besonderen, um die ATES Nutzung speziell in Deutschland zu fördern, wo die Technologie den Wärmemarkt bislang noch nicht durchdrungen hat.

Da die Verlässlichkeit von gemessenen Untergrundparametern während der Erkundungsphase sich auf die Auslegung und Wirtschaftlichkeit eines ONG-Systems auswirkt, wird in Studie 4 eine ganzheitliche Analyse von Fehlern und Unsicherheiten im Zusammenhang mit kabellos durchgeführten Temperaturmessung vorgenommen. Die auftretenden Fehler werden im Labor ermittelt und anschließend auf vertikale Profile der ungestörten Untergrundtemperatur übertragen, die an einer Erdwärmesonde aufgenommen wurden. Die ermittelte Präzision von 0.011 K

und Genauigkeit von -0.11 K gewährleisten eine hohe Zuverlässigkeit der Messungen. Die größte Unsicherheit ergibt sich innerhalb der ersten fünf Meter und resultiert aus der thermischen Zeitkonstante von 4 s. Das schnelle und komfortable Messverfahren führt zu Vorteilen gegenüber herkömmlichen Glasfasermessungen, deren aufgezeichnete Temperaturprofile am Standort als qualitativer Vergleich dienen. Diese Studie soll das Bewusstsein für die Bedeutung einer detaillierten Exploration als Teil einer ganzheitlichen Machbarkeitsanalyse von SGE im Allgemeinen schärfen und speziell zur Weiterentwicklung der kabellosen Messtechnik beitragen.

Table of contents

Abstract ..... **i**

Kurzfassung ..... **iii**

Table of contents ..... **vi**

1. Introduction **1**

1.1 General motivation 1

1.2 Techno-economic feasibility of SGE 3

1.3 Considered heating and cooling supply technologies 5

1.4 Study sites 10

1.5 Objectives 13

1.6 Structure of the thesis 14

2. Quantifying installed cooling capacities using aerial images **16**

Abstract 16

2.1 Introduction 17

2.2 Material and methods 18

2.2.1 General approach 18

2.2.2 Study site 19

2.3 Results and discussion 22

2.3.1 Data evaluation 22

2.3.2 Potential and optimization requirements 24

2.4 Conclusion 26

Acknowledgments 27

3. Cooling supply costs of a university campus **28**

Abstract 28

3.1 Introduction 29

3.2 Material and methods 31

3.2.1 Workflow 31

3.2.2 Study site 32

3.2.3 Economic analysis 35

3.2.4 Monte Carlo simulation 38

3.3 Results and discussion 40

3.3.1 Reference buildings 40

3.3.2 Monte Carlo simulation 41
3.3.3 Cooling costs of the university campus 43
3.3.4 Optimization and benchmarking 46
3.4 Conclusion 49
Acknowledgments 51

4. Techno-economic analysis of an Aquifer Thermal Energy Storage in Germany 52
Abstract 52
4.1 Introduction 53
4.2 Material and methods 56
4.3 Results and discussion 67
4.4 Conclusion 78
Acknowledgments 79

5. Uncertainty analysis of wireless temperature measurement in borehole heat exchangers 80
Abstract 80
5.1 Introduction 82
5.2 Material and methods 84
5.2.1 Wireless temperature measurement (WTM) 84
5.2.2 Temperature calibration 87
5.2.3 Measurement error 88
5.2.4 Dynamic properties of WTMs 90
5.2.5 Site 94
5.3 Results and discussion 95
5.3.1 Calibration procedure 95
5.3.2 Thermal time constant 96
5.3.3 Sinking behaviour 98
5.4 Conclusion 108
Acknowledgments 109

6. Synthesis 110
6.1 Conclusion 110
6.2 Perspective 116

Acknowledgments 120
Declaration of Authorship 122
References 124

Publications and contributions 159

Chapter 1

Introduction

1.1 General motivation

In the frame of the European Green Deal, the European Union (EU) strives to reduce greenhouse gas emissions to at least 50 % of 1990 levels by the year 2030 and to achieve climate neutrality by 2050 [1]. To become the first climate-neutral continent, a fundamental paradigm shift from a fossil-based to a renewable energy supply in the heating and cooling sector is indispensable. Hitherto, the majority of public and political debates on energy transition are, however, related to the electricity sector focusing on the decarbonization of the power generation. Consequently, the total share of 20 % of renewable energy in the EU is mainly attributed to the disproportionate amount of renewables in the power sector (32 %) [2, 3]. At the same time, the EU consumes half of its energy for heating and cooling purposes mostly required for industrial processes or to supply buildings [4].

To pave the way towards a low carbon thermal energy sector, the replacement of combustion heating and electricity-intensive cooling technologies with different portfolios of shallow geothermal energy (SGE), also described as beneficial electrification [5], is considered an elementary component [6, 7]. SGE represents different types of usage ranging from closed or open-loop systems to seasonal storage or direct usage applications. These different designs have in common the exploitation of thermal energy stored at a maximum depth of 400 m to heat or cool an above-ground facility [8, 9]. As the most commonly allowed temperature values for heating and cooling supply range between 5 and 25 °C [10], SGE is also referred to as low-temperature (LT) or low-enthalpy geothermal technology. Hence, the additional application of electrically powered heat pumps (HPs) is required to raise the extracted subsurface temperatures to a level suitable for space heating. For cooling supply, reversible HPs transport heat from the building to the subsurface [11, 12]. Depending on the subsurface properties and the facility requirements, SGE also allows direct cooling, operating as a natural heat sink without auxiliary power [13].

Even though SGE is a proven technology demonstrating operational robustness, it can still be considered a niche technology with a fairly small market share even within renewable heating and cooling applications (2 %) [14]. In most cases, energy planners and customers are familiar with and used to the handling of conventional technologies in both planning and operation. In contrast, planning of SGE systems is site-specific and requires multidisciplinary competencies regarding geology, geotechnics, drilling, heat pump technology and building service. Furthermore, high initial capital costs, which are usually higher than those of conventional systems, are considered as a financial barrier to broader market dispersion [15]. To face this competition, feasibility analyses in the early stage of project development that examine both economic and technical factors are required. This not only provides a sound basis for subsequent planning and implementation but also demonstrates potential benefits and opportunities to users, stakeholders and decision-makers.

In recent years, some approaches were developed to investigate the feasibility of SGE systems on a site-specific basis. For instance, Tissen et al. [16] show that various SGE applications are technically suitable to meet the heat demand of an urban quarter pointing out that ground-source heat pumps (GSHPs) are most appropriate at the site. Further case studies examining the technical feasibility of different SGE technologies are performed by Desideri et al. [17], Focaccia et al. [18], Emmi et al. [19] and Liu et al. [20]. While Schiel et al. [21] emphasize the importance of heat demand knowledge in their study area to examine SGE suitability, less attention is on the assessment of actual cooling requirements. However, the latter is particularly important for feasibility analyses of SGE in areas with high cooling demand densities, as often found in industrial, commercial or public buildings. At the same time, economic analyses are mostly concerned with the high initial capital costs [22–24] or consider only one particular SGE system [25–27]. However, economic assessments that focus solely on SGE contribute less to its economic feasibility as the costs of competing technologies are not considered. Hence, economic comparisons between SGE systems and their competing heating and cooling technologies are required to emphasize potential annual savings. This applies even more for economic feasibility studies of large-scale SGE technologies associated with particularly high capital costs or still unknown technical variants of SGE, which often accounts for difficulties in market penetration.

Furthermore, Schelenz et al. [28] demonstrate the importance of a coordinated site characterization to substantially increase the reliability of SGE system planning. Hence, collecting and analyzing site-specific data of both building requirements and subsurface properties are re-

quired to conduct a comprehensive techno-economic feasibility study of SGE systems. Addressing these shortcomings of presently available feasibility studies by considering technical and economic aspects of building requirements, SGE systems, as well as competing technologies is the subject of the present thesis.

1.2 Techno-economic feasibility of SGE

Feasibility analyses of SGE applications in the early stages of project planning are more extensive compared to most common heating and cooling technologies, but at the same time, they are essential and represent the central pillar of project development. The Committee of the Associations and Chambers of Engineers and Architect for fee regulations with the German acronym AHO [29] establishes a specific basis for required planning services in the field of shallow geothermal energy.

According to Bücherl and Walker-Hertkorn [30] and AHO [29], SGE system planning consists of eight consecutive and interconnected project phases as illustrated in Figure 1-1.

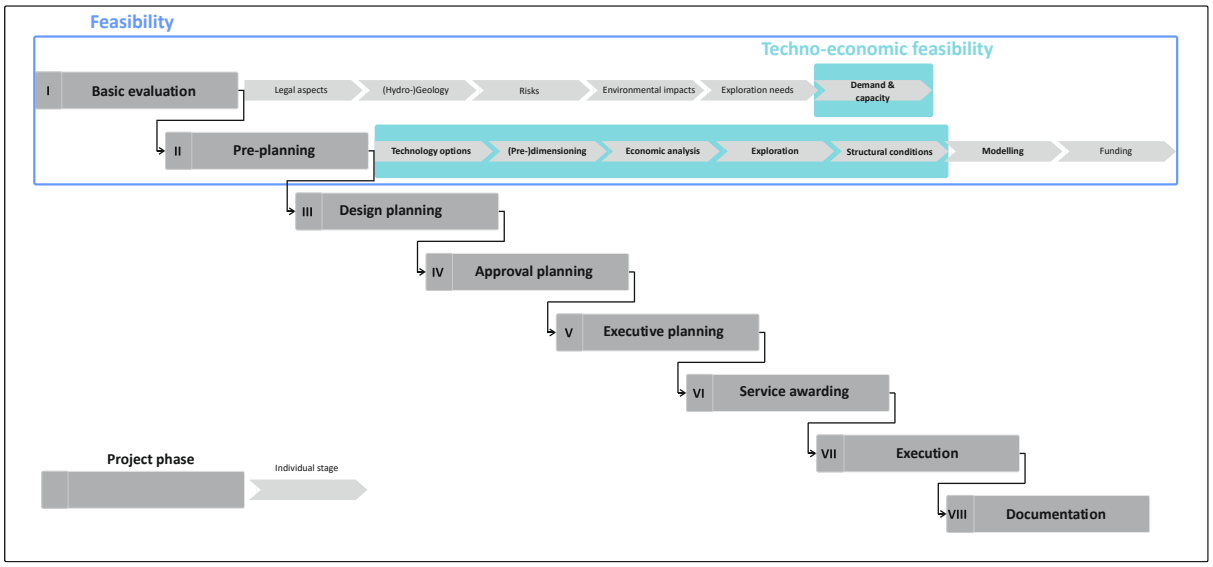

Figure 1-1: The sequence of the planning process of SGE systems including project phases and individual stages as derived from AHO and Bücherl and Walker-Hertkorn [29, 30]. The feasibility study comprises two project phases in the early stage of project planning and can be further specified as techno-economic feasibility. The included stages of the latter are highlighted in green as defined in the present thesis.

The feasibility analysis comprises two project phases, referred to as basis development and pre-planning, which are subdivided into individual stages. Please note that the illustrated order

of individual stages only serves as a basic frame and may deviate in practice depending on the type and size of the considered SGE system and the individual project management. Large-scale systems, in particular, for heating and cooling of industrial and commercial infrastructures require a detailed and thorough feasibility analysis [18]. As technical realization relies on economic viability, several technical investigations form the basis for economic assessments. Consequently, in the present thesis, several stages which are firmly connected with each other are referred to as techno-economic feasibility (TEF) and further specified hereafter as derived from Walker-Hertkorn [30] and AHO [29]:

- **Demand and capacity:** Heating and cooling requirements of a building are the final part of the basic evaluation and are typically derived in collaboration with the building service to form a central pillar for the subsequent phases of pre-planning and design planning. SGE systems are designed based on the heating and/or cooling load profile, which typically consists of monthly values [31]. For new buildings, either standard load profiles as provided by the German technical guideline VDI 4640 [32] are applied or synthetic load profiles are simulated based on the planned building characteristics and the ambient air temperature [33].
- **Technology option:** Based on the findings of the basic evaluation, the type of SGE system that is appropriate is either examined or narrowed considering legal aspects, usage potential, supply reliability, synergetic usage possibilities and building requirements. The preferred solution is pointed out, while others are excluded.
- **(Pre-)dimensioning:** Implies the basic conception of the SGE system mostly depending on the findings of the fundamental (hydro-)geological investigation and the demand and capacity analysis of the basic evaluation phase [31]. This includes, for instance, an assessment of the required number and depth of boreholes or groundwater wells to meet the heating and cooling requirements of the building. In some countries, publicly available tools are utilized for this stage [34, 35].
- **Economic analysis:** In order to decide whether to invest in SGE or not and to complement the discussion on the technology option, the performance of economic analyses is required. Investment costs and annual operating expenses are determined following the German technical guideline VDI 2067 [36]. Cost-benefit analyses to economically compare the SGE system either with competing or replaced heating and cooling systems are proposed to obtain potential annual savings and associated amortization [37].

- **Exploration:** Refers to the determination of thermo-physical, hydro-geochemical and hydraulic properties of the subsurface. Depending on the type and size of the SGE system, the execution of test drillings and monitoring wells is required to perform different types of field tests, which are comprehensively summarized in Witte et al. [38] and Luo et al. [39]. The performance of thermal response tests (TRTs) is considered the most common field investigation to explore subsurface thermal properties for multiple borehole heat exchanger (BHE) [40, 41].
- **Structural conditions:** Refers to the assessment of already existing structural and engineering factors at the site. Aboveground and underground structures due to anthropogenic activities such as buildings, electrical or hydraulic lines, sewers, basements or already existing geothermal systems particularly affect the drilling procedure and the efficiency of operation of SGE systems [42]. Furthermore, the building interface of existing facilities is evaluated to subsequently ensure a smooth integration of SGE.

In order to finalize the feasibility study and to provide a smooth transition to the design planning, analytical or numerical models are performed to characterize the subsurface heat transport of the considered SGE system [43]. These simulations combine the main findings regarding the heating and cooling requirements of buildings and the subsurface properties determined during the exploration of the study site.

1.3 Considered heating and cooling supply technologies

According to Behrens and Hawranek [44], feasibility studies are a prerequisite tool providing all required information for decision-making by considering the predefined objectives. Regarding the heating and cooling supply of a facility, the objectives are related to a considered type of technology, which is either to replace an existing system or to be compared with an alternative option. To address this standard, various SGE systems and conventional technologies for heating and cooling supply are an integral part of this thesis. Each considered system from Chapter 2 to Chapter 5 is illustrated in Figure 1-2 and introduced hereinafter.

Aquifer Thermal Energy Storage

Low-temperature Aquifer Thermal Energy Storage (LT-ATES) is the most frequently applied underground thermal energy storage (UTES) technology to tackle the seasonal gap between

times of the highest demand and periods of the highest energy supply [45]. While a minimum of two open groundwater wells is required to realize the seasonal operating mode, LT-ATES typically consists of multiple well arrays to heat and cool large infrastructures such as airports, hospitals or universities. In winter, warm groundwater stored over the summer is extracted from the warm well for heating supply. HPs are an integral part of the entire system to raise the temperatures to the required level for heating supply of the associated building [46, 47]. In summer, the pumping direction is shifted and cold groundwater stored over the winter is extracted for cooling purposes. Abstraction temperatures below 10 °C are often sufficient for direct cooling supply without HP usage [48]. At the same time, the produced waste heat during cooling supply is injected back into the aquifer via the warm well and stored until the heating season begins. LT-ATES mainly operate to a maximum storage depth of 150 m [45].

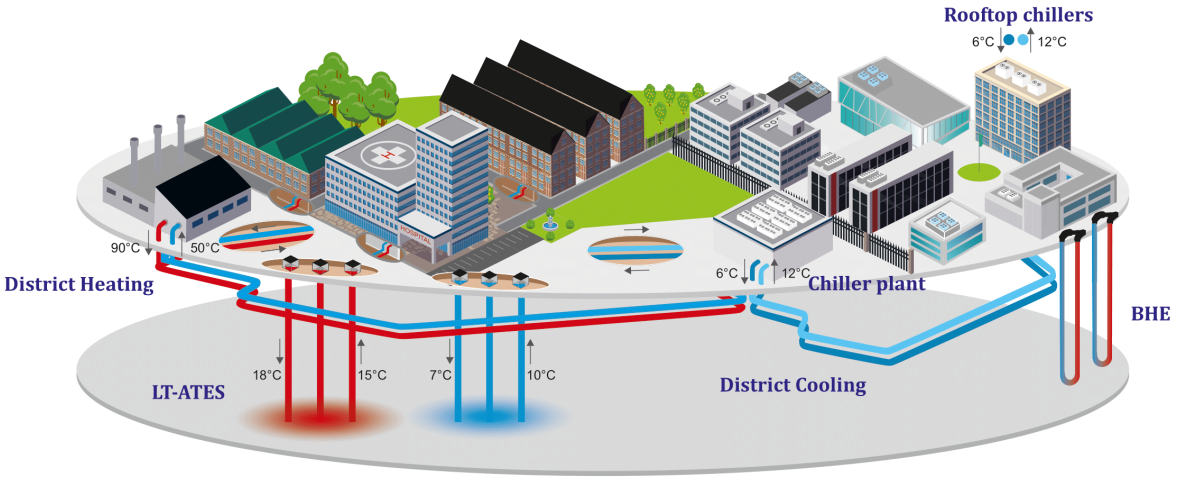

Figure 1-2: Overview and basic principle of heating and cooling technologies discussed in the subsequent Chapters 2 to 5 including low-temperature shallow geothermal energy systems (Aquifer Thermal Energy Storage and borehole heat exchanger), conventional compression chillers as well as large-scale district heating (DH) and cooling (DC) systems.

Even though the vast majority of ATES systems are equally utilized for heating and cooling supply, few installations provide either heat or cold, which is demonstrated in Rostock (heating), Germany and at Stockton college (cooling), USA [49, 50]. Fleuchaus et al. [51] provide a comprehensive analysis of temperature levels of 73 LT-ATES systems currently in operation. Due to the achieved storage effects, average production temperatures of LT-ATES are optimized by about 3 K towards natural groundwater showing warmer (winter) or colder (summer) production temperatures. Hence, average abstraction temperatures for heating and

cooling amount to 15 and 10 °C, respectively. Whereas LT-ATES is well established in the thermal energy market in the Netherlands with almost 3,000 systems installed, Germany is considered more of a blank sheet regarding ATES usage, with only two known systems currently in operation [49]. Further details on LT-ATES are provided in Chapter 4.

Borehole Heat Exchanger

The most commonly applied SGE technology option is a closed-loop vertical borehole heat exchanger combined with a HP also referred to as ground source heat pump (GSHP) system. A circulating heat carrier fluid transports the received thermal energy from the subsurface to the coupled HP [52]. Vertical BHEs are typically plastic tubes (U-pipes) with depths ranging between 50 – 400 m [53]. To prevent borehole collapse and groundwater contamination, and to enhance thermal contact between pipe and ground, the general practice is to backfill the annular space with grout or backfill material [54]. GSHPs achieve average operating efficiencies, quantified by the seasonal performance factor (SPF), of about 4 [55], meaning 1 kWh of electrical input yields approximately 4 kWh of thermal energy. BHEs range from single installations supplying detached family homes to large SGE fields for heating and cooling of commercial and industrial facilities [56–58]. Direct cooling is achieved without mechanical refrigeration by circulating the heat carrier fluid in the U-pipe and bypassing the HPs [59]. With more than 380,000 systems currently in operation and an installed capacity of 4,400 MW, Germany is one of the leading countries in terms of geothermal HP usage [60].

Compression Chillers

At present, there are about two billion air condition (AC) units in operation worldwide with a growing sales figure of ten new AC units for every second passed [61, 62]. The most frequently applied technologies for cooling supply are different types of electricity-driven vapor-compression refrigeration systems, which are grouped under the common term compression chiller [63]. Chillers are considered as turnkey systems sized based on the required cooling capacity of the building indicating the amount of heat the device can remove over time from the space being cooled [64]. In its basic operating principle, a vaporous refrigerant passes through the electrically driven compressor resulting in a rise in temperature and pressure. While transported to the condenser, the vapor turns into fluid associated with heat release. After passing the expansion valve, the evaporator vaporized the liquid under heat absorption and the medium is finally cooled [65, 66]. Chillers used for cooling supply are typically designed for supply temperatures of 6 °C and return temperatures of 12 °C.

The global market size of chillers was estimated at around USD10 billion in 2019, with expected annual growth rates of 4.3 % [67]. The highest share of all chillers sold has a capacity below 500 kW [68], indicating the most frequent use of chillers for individual and decentralized cooling supply. Chillers can be distinguished between water-cooled and air-cooled chillers. The latter are characterized by visible condenser fans installed on the roofs to release heat to the environment (Figure 1-2). They account for 37 % of the global chiller market revenue and are typically used for small to medium sized commercial buildings [67]. Water-cooled chillers typically operate in combination with cooling towers and are mostly applied to cool large-scale infrastructures or to feed district cooling (DC) networks.

District heating and cooling networks

DC systems deliver chilled water from a central production plant through a network of underground pipes to various consumers. The production of chilled water can be driven by different types of technologies such as compression or absorption chillers and large-scale SGE systems or by lakes, rivers or seawater. DC networks operate with one supply and one return pipe each, with common supply temperatures of 6 °C and are installed in areas with high cooling demand densities such as commercial areas or specific districts of cities [69–71]. As a result of higher comfort standards, DC networks are particularly popular in the USA, while recently the largest growth rates are observed in the Middle East [72]. In contrast, DC networks are still a rather undiscovered solution in Europe, with a market share of about 1 % equal to 3 TWh, and about 150 systems currently in operation [73, 74].

Blueprints for successful DC operation are often found at universities, which can be described as melting pots of large-scale cooling supply that combines different types of technologies as shown in Figure 1-3. US universities are considered as pioneers in the implementation of DC networks. In its basic form, the combined heat and power (CHP) station of the university supplies the coupled chiller plant with electricity or heat to power the compression or absorption chiller, which operates in combination with thermal energy storage (TES) [75]. This concept enables, for instance, the installation of occasionally reported cooling capacities above 100 MW [76].

Common DC networks with chiller plants are also applied at universities in Europe, for instance at the University of Stuttgart or the Campus South of the Karlsruhe Institute of Technology (KIT). At the same time, new generations of DC and DH networks fed by renewable energy sources are considered as a promising solution and are slowly gaining popularity in recent years

[77]. Best practice examples of successful integration of ATES in DC networks can be found at Dutch universities such as Radboud University and TU Eindhoven (TU/e). The latter operates the world largest ATES system with 32 wells installed and a cooling capacity of 20 MW distributed over an underground network of 8 km [78, 79]. Please note, that these networks, which are also found at ETH Zürich combined with borehole thermal energy storage (BTES), are characterized by the fact the same distribution system is used for both heating and cooling supply. One of the largest GSHP systems is in operation at Ball State University (BSU) comprising 3,383 boreholes up to a depth of 150 m. Combined with centrifugal chillers producing hot and cold water, the entire system supplies 47 buildings [72, 80].

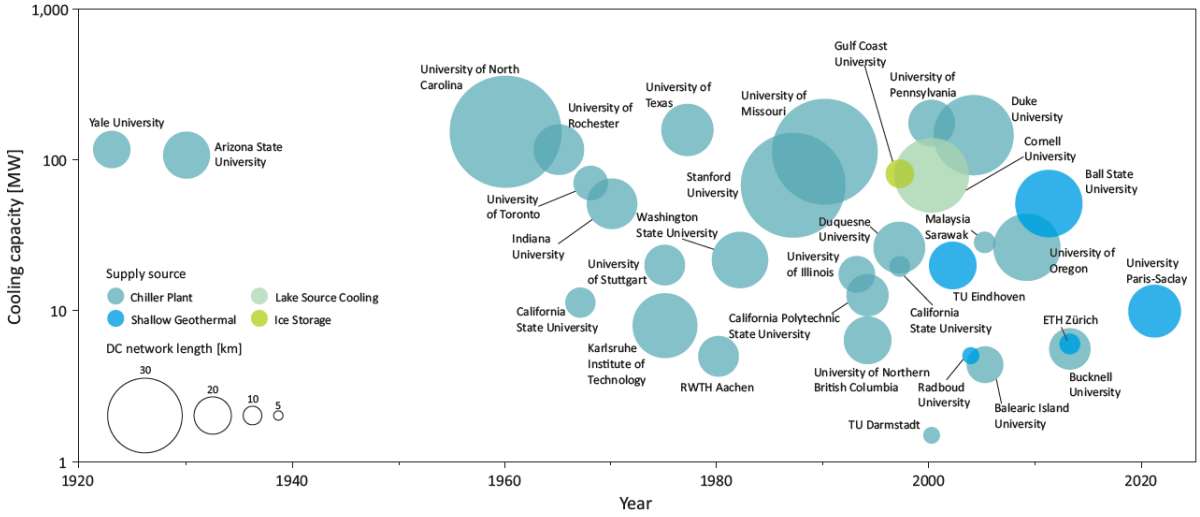

Figure 1-3: Evolution of district cooling networks at university sites over time considering cooling capacity, network length and supply technologies to feed the system, derived from Refs. [50, 76, 78, 81–114].

While the role of future DC networks is still debated in Europe, DH systems are more established in the thermal energy sector with about 6,000 networks in operation and a market share of up to 50 % in northern countries [115, 116]. With growing urbanization and the respective temperature levels required for space heating and cooling in modern or refurbished buildings continue to converge, SGE systems strive to tap into large-scale thermal energy markets. While district heating (DH) technologies were limited to systems producing hot water or steam, new generations of DH networks operate with lower temperatures in the range of 10 to 50 °C and therefore even request the integration of SGE [77, 117, 118]. In Germany, DH is well established and benefits from past subsidy programs contributing 10 % to the current heating supply [119]. However, heat generation for DH in Germany is still dominated by fossil-based energy

sources such as natural gas (42 %) and coal (24 %), while renewable energy sources only contribute with 20 % [120]. Furthermore, the compulsory connection to DH networks, often found at the local level, together with low renovation rates of the current building stock [121, 122], inhibits a fast integration of SGE systems and renewable energy source in general.

Many large-scale heating and cooling solutions are found at research facilities, even consisting of several best practice examples of SGE systems, which is theoretically predestined for knowledge transfers within research and development (R&D). However, information on economics, technical data or operating performance is rarely published and therefore not transferable to similar project goals and related TEF studies. This is explained by Werner [123], who emphasizes that DHC systems at universities are rather considered as grey area since they are mostly part of the customer side of the energy system distributing heat and cold to their own buildings. Most statistics on DHC systems, however, refer to systems that belong to the energy sector providing heat and cold to many customers.

1.4 Study sites

The approach of the TEF analysis of the present thesis, as illustrated in Figure 1-1, is demonstrated at three different sites, namely the Campus North (CN) of the Karlsruhe Institute of Technology (KIT), the municipal hospital Karlsruhe and the University of Applied Sciences Karlsruhe with the German acronym HsKA, which are located near or in the city of Karlsruhe, Germany (Figure 1-4). All sites have the common vision to implement different types of SGE systems, particularly evoked by the fact that the current cooling supply requires sustainable and future-proof solutions.

The CN of the KIT is a large research facility covering an area of about 2 km^2 (Figure 1-4a). Currently, the cooling supply is decentrally organized using air-cooled chillers installed on the roofs of each building. While ambitious climate-neutral goals are already communicated, the CN elaborates the transition to a promising DC system using renewable energy sources. Following some best practice examples in Figure 1-3, the use of LT-ATES as cold storage is considered a promising technology option at the site. However, the planning procedure is inhibited as some of the individual stages of the TEF are not addressed, yet. This includes the determination of capacities and demands of the buildings as well as an economic analysis of the current state, which are consequently addressed in Chapter 2 and 3.

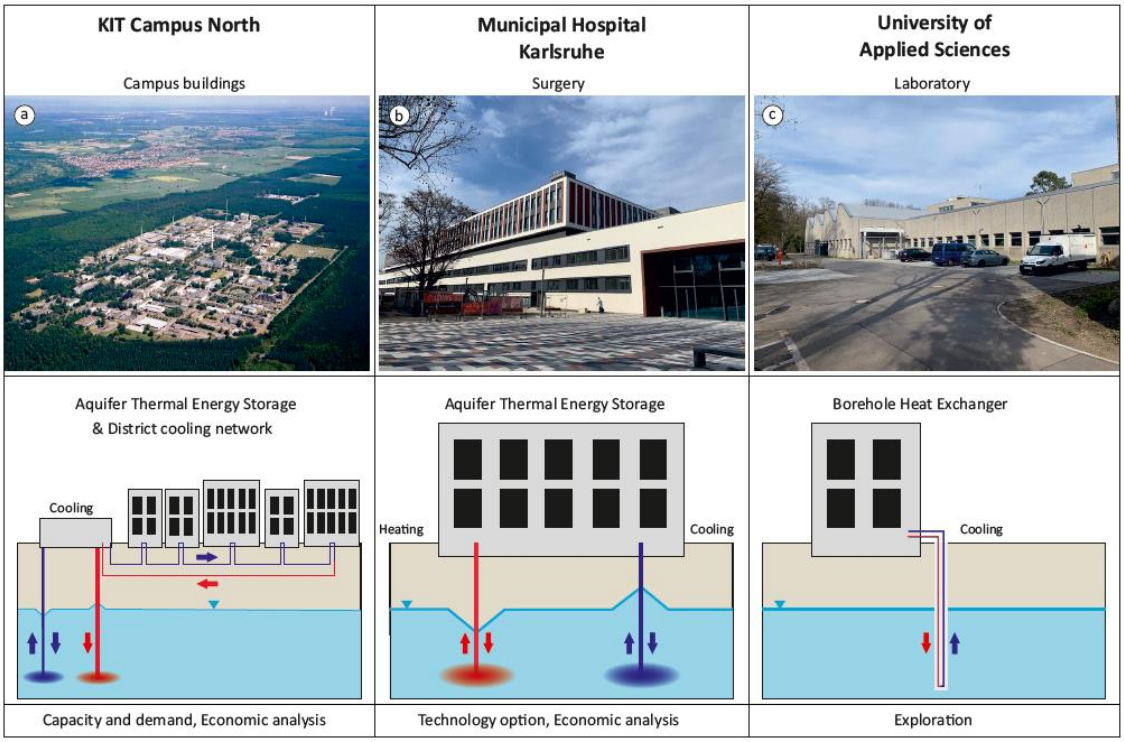

Figure 1-4: Study sites including considered LT-SGE technologies (modified after Bayer et al. [124]) and the applied stages of the techno-economic feasibility as analyzed in the present thesis. ©: (a) KIT; (b), (c) Simon Schüppler.

The municipal hospital in Karlsruhe constructed a new facility, including a surgery with 240 beds, which will be put into operation in 2021 (Figure 1-4b). Initial considerations regarding suitable heating and cooling technologies also included LT-ATES. However, the hospital administration finally decided to use the preexisting connection to the DH network of the municipal utility and compression chillers for cooling supply. Despite this decision, further feasibility studies on the use of ATES at the site are required, as the current heating and cooling supply of the entire hospital area is considered rather unsustainable. While the hospital operates its own DC network fed by a chiller plant of 6.5 MW, most of the heating demand is met by the DH network of the city. In order to raise awareness of ATES technology and its economic viability towards the hospital administration, Chapter 4 provides a cost-benefit analysis of LT-ATES and the current heating and cooling supply for the new building.

The University of Applied Sciences has a BHE field consisting of nine individual U-pipes. The BHEs were installed to a depth of 36 m without backfilling as part of a ZIM research project in 2015. While the focus of the project was more on the development of monitoring technologies for BHEs, less attention was on the actual usage of the BHE field and a feasibility

study was not prepared. Consequently, the BHE field was not further used for heating or cooling supply. However, as research activities in the adjacent laboratory (Figure 1-4c) produce waste heat, different concepts for removing the heat using the existing BHEs are currently being examined [125]. This requires a subsequent feasibility analysis with a focus on the subsurface properties as the university aims to use the existing BHE field for direct cooling. Therefore, the site is representatively used for the exploration stage of TEF studies, which is addressed in Chapter 5.

1.5 Objectives

Techno-economic feasibility (TEF) studies in the early stages of project development play a key role in the successful implementation of SGE systems. As system size increases, TEF studies of SGE become more comprehensive and consist of several multidisciplinary approaches. At the same time, there is limited available information on holistic TEF studies that consider each of the individual stages shown in Figure 1-1. Thus, the objective of this thesis is to emphasize and improve the scope and reliability of TEF studies for large-scale SGE systems with focus on the thermal energy demands, economic analyses and the exploration stage. To address this, three specific study sites (Figure 1-4) are considered for applying different approaches, each associated with specific goals:

- The first step considers the initial stage and aims to determine cooling capacities and demands of buildings by applying two different approaches. As there is only little focus on the actual cooling requirements of buildings in general, the aim is to raise awareness for and to demonstrate the quantification of demands, capacities and spatial distribution of the latter. These investigations are considered a cornerstone not only for TEF analyses but also for sound planning of SGE utilization to supply large-scale facilities or urban districts.

- Another objective is to address the stage of the economic analysis by examining the current cooling supply at a site with focus on the related supply costs. In this context, potential shortcomings of the cooling supply using compression chillers can be derived to underline the need for developing sustainable cooling solutions.

- Since lack of awareness about the economic benefits of large-scale SGE systems is considered a key barrier to thermal energy market penetration, a further goal is to demonstrate the approach of cost-benefit analyses of SGE by considering LT-ATES and conventional heating and cooling technologies.

- The final part addresses the exploration stage dealing with advanced measurement technologies to determine subsurface thermal properties. As proper TEF analyses of SGE systems rely on profound information and data, it is aimed to emphasize the importance of detailed on-site measurements. For this purpose, a holistic analysis of measurement uncertainties associated with vertical temperature profiles using wireless measurement technology is provided.

1.6 Structure of the thesis

The present work is prepared as a cumulative thesis and consists of four individual studies, which are enclosed in Chapters 2 - 5. All studies were submitted to ISI-listed journals. The studies in Chapter 3, 4 and 5 were submitted as peer-reviewed studies, whereas the study in Chapter 2 is classified as News Item. Three studies have already been published, while the study in Chapter 3 is currently under review. The arranged order of the studies is derived from the chronological sequence of the aforementioned individual stages of the TEF analysis as illustrated in Figure 1-1.

Chapter 2 contains the third study entitled "*Quantifying installed cooling capacities using aerial images",* which was published in the *Journal of Photogrammetry, Remote Sensing and Geoinformation Science* as News Item. This study introduces a practical approach to estimate the installed cooling capacities and determine the spatial distribution of air-cooled chillers using aerial images. The approach is performed at the Campus North of the KIT and considers 47 compression chillers identified by using aerial images. Access to the actual installed cooling capacities enables validation and reliability assessment of the novel method.

Chapter 3 presents the fourth study entitled "*Cooling supply costs of a university campus*", which is submitted to *Energy*. This study is directly linked to Chapter 2 and deals with the current cooling supply of the Campus North of the KIT. The study is performed on the basis of the forthcoming transition from the decentrally organized cooling supply to future-proof cooling solutions. In order to provide a sound basis for further process development and future investment decisions, the arising cooling costs of 23 considered buildings are investigated. To compensate for the uncertainties of the input parameters provided by the facility management (FM), a Monte Carlo simulation with defined parameter ranges is performed. Comprehensive data from two reference buildings enable the subsequent validation of the simulation. The holistic analysis enables the discussion on further optimization measures and benchmarking with other universities where DC systems are already implemented.

Chapter 4 includes the first study "*Techno-economic analysis of an Aquifer Thermal Energy Storage (ATES) in Germany*", which was published in *Geothermal Energy*. It contains the investment cost and operating expenses of a potential LT-ATES for the heating and cooling supply of a recently installed building of the municipal hospital of Karlsruhe. Due to the uncertainties of the input parameters of the investment costs, a Monte Carlo simulation with assigned parameter ranges is carried out. On this basis, a cost-benefit analysis is performed to

compare the potential LT-ATES with the current supply technologies consisting of district heating and chillers for cooling. Furthermore, the considered individual systems are compared by determining operational CO_2-emissions. Finally, the results of the potential ATES are compared with economic data of current or former ATES systems.

Chapter 5 contains the second study "*Uncertainty analysis of wireless temperature measurement (WTM) in borehole heat exchangers*" published in *Geothermics* and focuses on the exploration stage. This study examines uncertainties and errors associated with the measurement of vertical temperature profiles in shallow U-pipe borehole heat exchanger (BHE) at the HsKA using wireless probes. The GEOsniff probe, which is a representative device for initial wireless measurements and long-term temperature monitoring of BHEs, is used for the analysis. First, the measurement procedure is explained using basic analytical equations. The errors due to the measurement technology are quantified in the laboratory with focus on the accurate calibration procedure, the descent velocity and the thermal time constant τ. These results are finally applied to measured values at a BHE test site, allowing the visualization of expanded measurement uncertainties of the recorded temperature profiles. In addition, distributed temperature sensing (DTS) measurements using common fiber optic cables and punctual Pt100-sensors serve as a qualitative comparison.

Finally, Chapter 6 summarizes and evaluates the main results of the four presented studies considering important issues for future techno-economic studies and planning of LT-SGE systems. Beyond that, pending research questions and proposals are compiled based on the major findings of this thesis.

Chapter 2

Quantifying installed cooling capacities using aerial images

Reproduced from: Schüppler S, Fleuchaus P, Zorn R, Salomon R and Blum P (2021) Quantifying Installed Cooling Capacities Using Aerial Images. Journal of Photogrammetry, Remote Sensing and Geoinformation Science (PFG). News item. doi: 10.1007/s41064-021-00137-0.

Abstract

Cooling supply is expected to be the fastest growing energy consumer of buildings. However, the majority of both comfort and industrial cooling supply is still based on costly and CO_2-intensive supply technologies such as compression chillers (CCs). At the same time, only sparse information exists on the spatial distribution and installed capacities of cooling installations worldwide. The aim of this study is, therefore, to introduce a novel approach to identify and quantify installed cooling capacities of CCs by aerial image analysis. We demonstrate this easily applicable method at a university campus in Germany, where 36 air-cooled CCs with a total installed cooling capacity of 16 MW are considered. The installed cooling capacities of all detected CCs are estimated based on the number of identified fans by considering the performance specifications of the respective CC manufactures. The comparison with the actual installed cooling capacities revealed an average deviation of 36 %. With increasing installed cooling capacity (> 350 kW) the relative accuracy of the method improves indicating a higher suitability of the applied method for larger installations. The proposed method can significantly contribute to an improved understanding of location and quantity of cooling capacities and facilitates sustainable urban planning and the transition from decentralized cooling machines to renewable and sustainable supply solutions.

2.1 Introduction

Air conditioning accounts for around 20 % of the total electricity used in buildings worldwide [126]. With population growth, global climate change and increasing incomes particularly in the world's hottest regions, power consumption for air conditioning is expected to rise up to 33-fold by the year 2100 [127, 128] and on average up to 750 % in the residential and commercial building sector until the year 2050 [128]. Hence, cooling is the fastest growing use of energy in buildings [129]. While rising demand for space cooling is already putting enormous strain on electricity systems [126], it is crucial to foster the transformation of the cooling sector towards sustainable technologies. To develop strategies for rapid integration of renewable solutions and to optimize the existing cooling supply, more information is required on the location and capacities of currently installed fossil-based cooling systems.

In recent years, different methods were developed to estimate the heating and cooling demand from district to global scale. These methods can be generally subdivided into top-down and bottom-up approaches [130, 131]. Top-down models analyze the model area as an entity, considering its general characteristics. The heating and cooling demand is assessed based on parameters such as population density, income, usage, climate or urban morphology [132]. In contrast, bottom-up models calculate the urban heating and cooling demand by the sum of the thermal energy demand of each building [132]. While bottom-up models are mainly considered on district or urban scale, top-down approaches can be also used for large-scale analyses. Considering the literature in the field of thermal energy modelling, it is apparent that most top-down and bottom-up analyses mainly focus on assessing the heating demand [16, 21, 133]. One reason is the fact that heating demand is easier to predict as it is assumed that the majority of buildings require thermal energy for space or tap water heating. In contrast, comfort cooling is often still a luxury and only rarely utilized particularly in residential buildings [134]. Hence, it is difficult to estimate not only the theoretical but also the actual cooling demands and installed cooling capacities.

At the same time, energy for cooling is mainly produced individually using fossil-based technologies. The decarbonization of the cooling sector, however, requires centralized cooling solutions in combination with renewable technologies. To facilitate potential analyses and demand models as well as efficient planning and implementation of cooling grids, comprehensive information on the location and quantity of installed cooling capacities is essential. Despite the importance of this, cooling demands of buildings are rarely assessed and

the measurement of cooling supply is to date uncommon [135]. In addition, there is still no approach to identify cooling infrastructure on a large-scale and only a few studies site-specifically analyze the required cooling capacities and demands [136]. Hence, the study aims to introduce a novel approach enabling the detection of installed compression chillers and the quantification of their related cooling capacity using aerial images. To demonstrate and validate our approach we used 36 air-cooled compression chillers at the Karlsruhe Institute of Technology (KIT), Germany.

2.2 Material and methods

2.2.1 General approach

Compression chillers (CCs) are the most frequently used air conditioning technology for space and process cooling of residential and industrial buildings [63, 137]. The operating principle of a compression refrigeration system is comprehensively described in the literature [e.g. 138–140]. The most visible characteristic feature of air-cooled systems is the condenser and associated fan unit, which is used to extract heat from the system by means of the ambient temperature [141]. Studying data sheets of these chillers reveal a correlation between the number of integrated fan units and the installed cooling capacity. Thus, in this study, we apply this relation estimating the installed cooling capacities of air-cooled CCs currently in operation using aerial images.

The applied method is subdivided into four consecutive worksteps, which are summarized in Figure 2-1. Aerial images are used to identify the existing CCs and to quantify their installed cooling capacities. To demonstrate the straightforward application of the method, we decide to use common satellite images from Google Maps instead of high-resolution images. First, we detect respective CCs installed on the roof or in the immediate vicinity of the supplied building in the study area (Figure 2-1a). As a representative study site for the aerial image analysis, we choose the Campus North (CN) of the KIT. The detected CCs are subsequently analyzed in more detail by counting the number of integrated fans (Figure 2-1b). The determined number of fans enables the quantification of the installed cooling capacity by using the aforementioned relation derived from the respective datasheets of the installed CCs (Figure 2-1c).

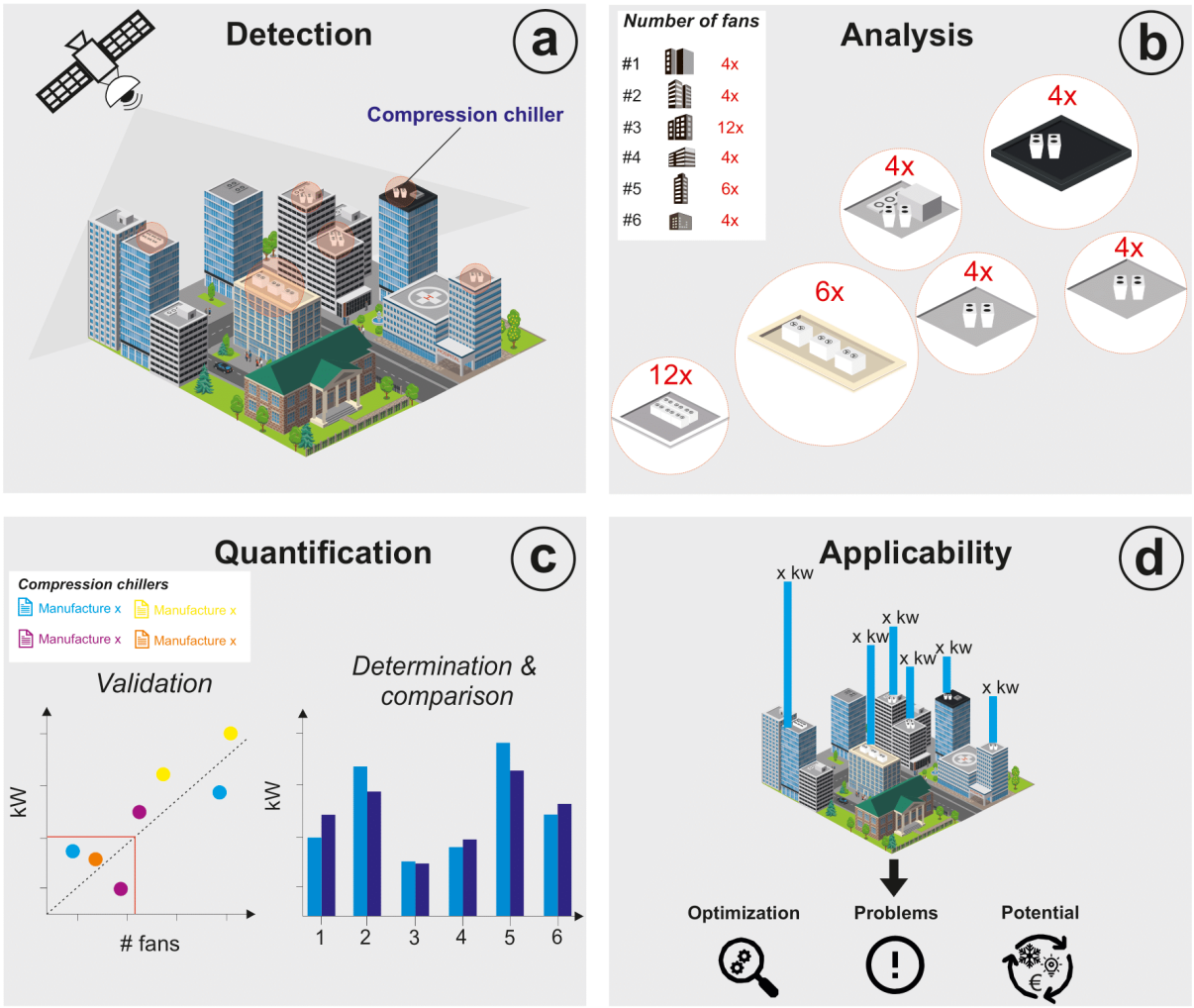

Figure 2-1: Workflow of the presented and validated method.

Furthermore, we validate the practical applicability of this method by comparing our estimated values with the actual installed cooling capacity of the observed CCs (Figure 2-1d). Finally, we discuss the practical implementation of this method for different fields of application. We address current obstacles that occurred while applying the method and provide further suggestions for improvements (Figure 2-1d).

2.2.2 Study site

The CN is a large research facility of the KIT located in the temperate climate zone, approximately 12 km north of Karlsruhe, Germany. A heterogeneous building stock mainly used for academic research, administration and external companies characterizes the study site. We select this particular area for applying our method as almost every building at the campus requires space or process cooling to supply laboratories, experimental facilities, data centres or

production plants. Cooling of each building is decentralized and frequently supplied by visible air-cooled compression chillers. The observed and analyzed systems (Figure 2-2) are defined as split devices after Bohne [142].

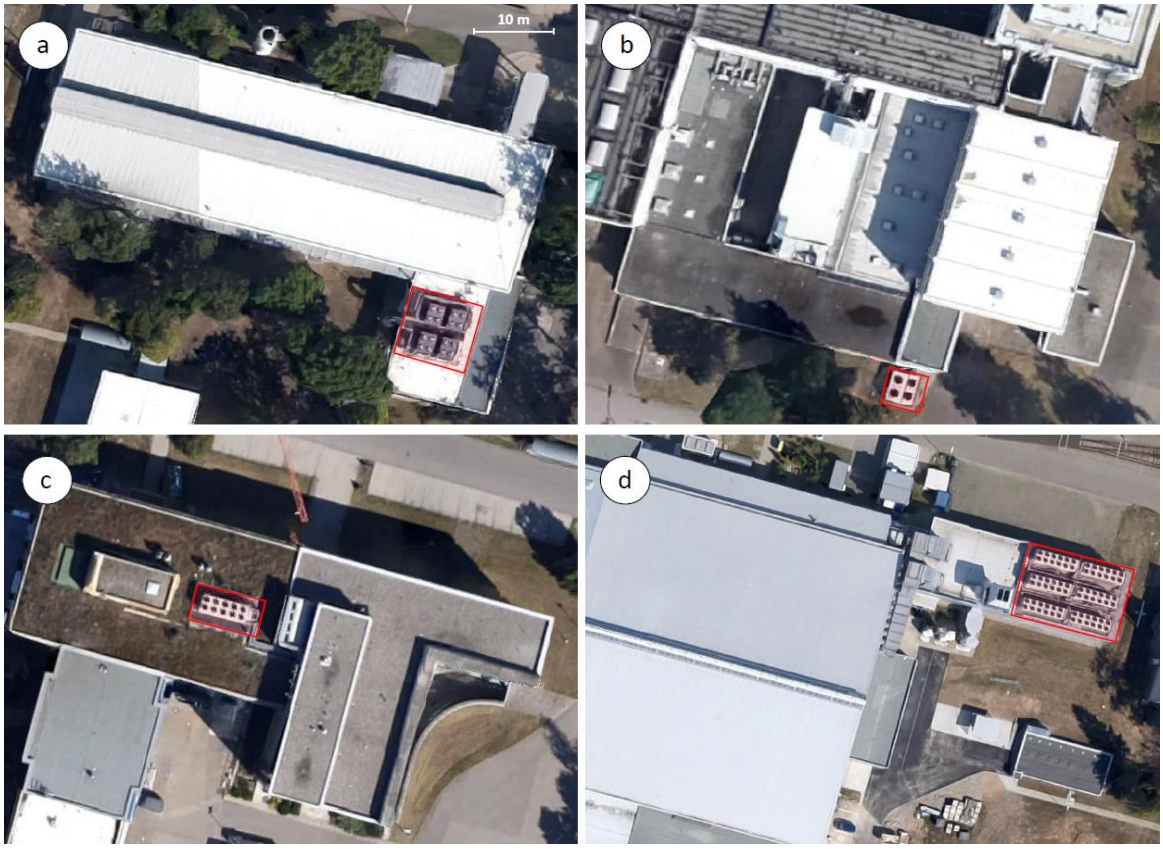

Figure 2-2: Examples of analyzed aerial images showing the outer part and fans of the installed compression chillers, highlighted in red, and the supplied campus building.

The visible cooling part, consisting of condenser and fan unit is installed outside, while the components for space cooling are inside the building. The actual installed cooling capacities of the installed CCs were provided by the KIT facility management (FM) enabling the validation and further optimization of the applied methodology. As a result of the building heterogeneity, the aerial image analysis is carried out for a large range of cooling capacities and is therefore representative for small and large commercial and industrial buildings typically ranging between less than 200 kW [143] to more than 7,000 kW [144]. In total, we observe and analyze 36 CCs, which supply 18 buildings of the university campus with energy for cooling. Overall, 340 single fans are considered in the present study. Figure 2-2 exemplarily shows aerial images of four different buildings and their related CCs, which are representative of all observed CCs.

The observed systems are all clearly assigned for each supplied building. The number of installed fan units for each building ranges from a minimum of three to a maximum of 72 fans, i.e. six units with 12 fans each (Figure 2-1d). Specific types of CCs manufactured from the two companies Emicon and Trane are installed in the study area.

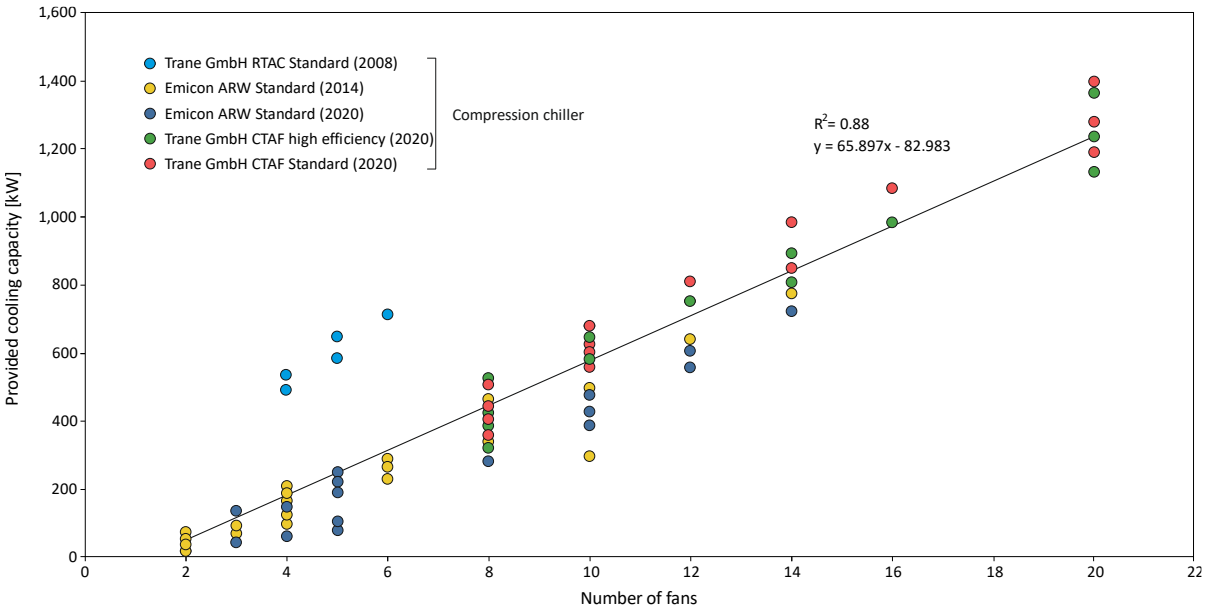

Figure 2-3: Provided capacities for space and process cooling and the related number of fans of the different types of installed air-cooled compression chillers at the study area. The information is collected from the datasheets of the respective manufacturers. The determined regression line enables the estimation of the installed cooling capacities using aerial images.

Due to the given quality and resolution of the aerial images (Figure 2-2), the specific producer and type of the installed CCs could not be identified. Thus, we use the required information of the accessible data sheets of five different types of CCs [145–147]. Figure 2-3 illustrates the positive correlation between the installed cooling capacity and the number of fans derived from each data sheet resulting in the following regression equation (Eq. 2-1):

$$y = 65.897 \cdot x - 82.983 \qquad \text{(Eq. 2-1)}$$

where y is the cooling capacity (kW) and y is the number of fans. The resulting linear equation of the determined regression line in Figure 2-3 and the number of counted fans by means of the aerial images enable the calculation of the installed cooling capacities, referred to as estimated cooling capacity, of each observed CC unit. The estimated values are finally

validated with the actual data of the installed cooling capacities, which are provided by the facility management and building operators of the campus. The CCs predominantly have an even number of installed fans, the exception being systems with three fans.

2.3 Results and discussion

2.3.1 Data evaluation

Figure 2-4 shows the amount of actual and estimated installed cooling capacities of all 36 observed CCs of the university campus. The closer a scatter is to the black dashed line, the higher the accuracy of the applied method.

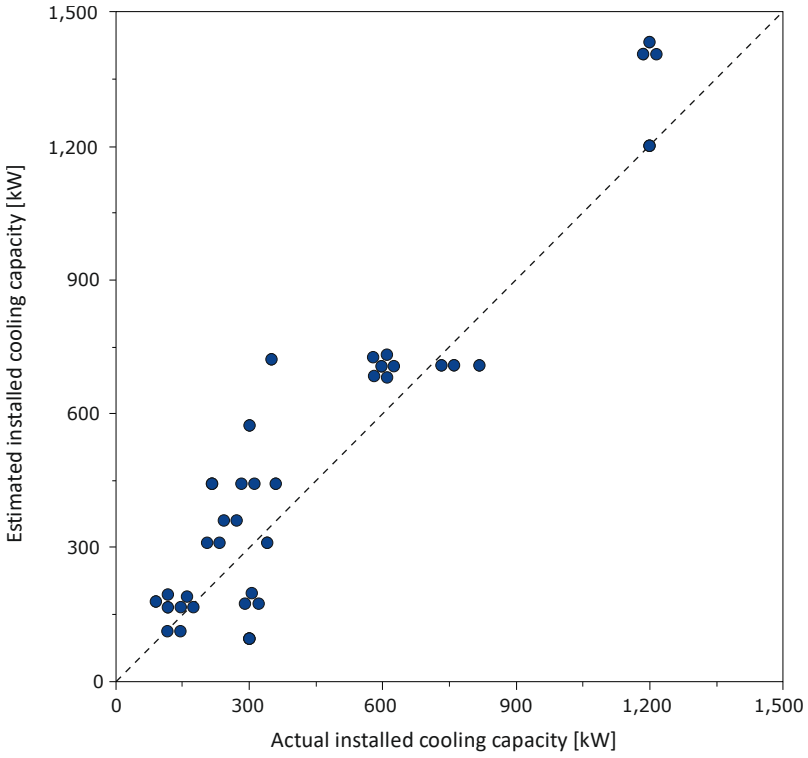

Figure 2-4: Comparison of installed cooling capacities of the analyzed compression chillers at the university campus. Each scatter represents a single compression chiller observed by means of aerial images.

The aerial image analysis yields an overestimation of the installed cooling capacity for 26 out of the 36 observed CC systems. The maximum actual installed capacity amounts to 1,200 kW, while 64 % of all observed CCs have a capacity of less than 400 kW. The total installed cooling capacity of all analyzed CCs is estimated at 18.5 MW and is about 13 % larger than the total

actual installed cooling capacity. Thus, the cumulative absolute amount of the actual installed cooling capacity is approximately 2.4 MW smaller than the estimate.

Figure 2-5 compares the estimated with the actual installed cooling capacities of each observed CCs in more detail. The average deviation between the two values for each CCs corresponds to 36 %.

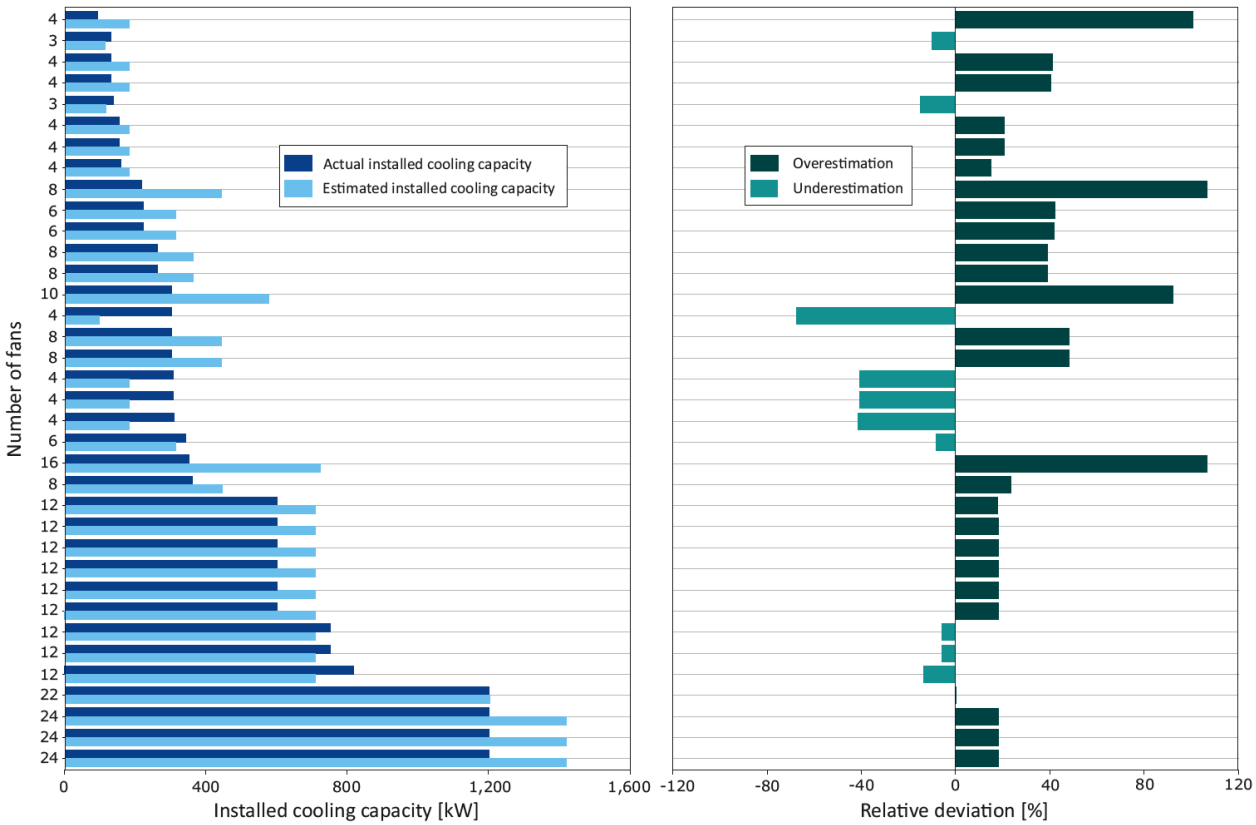

Figure 2-5: Comparison of actual and estimated values for the installed cooling capacity and the relative deviation between the two values for each observed compression chiller. The values are sorted in ascending order by the actual installed cooling capacities and contrasted with the number of installed fans.

The comparison clearly shows a decrease in deviation with increasing installed cooling capacity. Even though the larger deviation arising for the estimation of smaller cooling capacities negatively affects the accuracy of the approach, the practical application of the method in urban areas is expected to be less affected by this deviation. Currently, mainly commercial and industrial buildings require space and process cooling with expected larger installed cooling capacities, while air conditioning of residential buildings with lower installed cooling capacities currently only accounts for 8 % in Europe [128]. The relative accuracy above

350 kW of installed cooling capacity improves to 85 % indicating higher suitability of the presented method for CCs with large installed cooling capacities.

The described deviation arising from our method is partially attributed to the technical properties of the CCs. The provided cooling capacities of the observed CCs is not exclusively dependent on the number of fans. The fine adjustment is additionally realized by modifying the rotation speed and diameter of the installed fans, which in particular applies to smaller cooling capacities and, therefore, lower number of fans. Consequently, the number of fans and actual installed cooling capacity show a much better correlation for the capacity range of 350 – 1,200 kW and from 8 fans, respectively (Figure 2-5). In addition, the apparent spread of the different CC providers illustrated in Figure 2-3 resulting from the different performance strength of the fans, has a negative impact on the accuracy of the aerial image analysis. The determined linear regression in Figure 2-3, which is the basis of our cooling capacity estimation, is above the majority of the single scatters representing each installed CCs. This explains the tendency of overestimating the installed cooling capacity as illustrated in Figure 2-5. However, further analyses and applications of the method at different sites are crucial to validate if this result is a general characteristic of the applied method or rather a site-specific issue of the considered CCs at the Campus North.

2.3.2 Potential and optimization requirements

Figure 2-6 shows the reverse chronological development of Google Maps aerial images. The resolution of the images has significantly improved over time. The detection of the installed CCs and the determination of installed fans is feasible since the year 2009. However, the resolution during the last four years remains mostly unchanged, while the improvement between 2005 and 2009 finally enabled the detection of the CCs. Based on the chronological analysis of the aerial images, the detection of the installation date of the CCs is possible in some cases. This allows early estimations of the remaining lifetime of the CC unit, which therefore enables the timely discussion on the following supply technology. In addition, the subsequent installation of additional CCs as a result of increased cooling demand is recognizable.

Based on our analysis, we discuss encountered limits and provide some general suggestions to further improve our presented method and its accuracy. The used aerial images currently only

allow the detection and allocation of the CCs as well as the quantification of their number of fans.

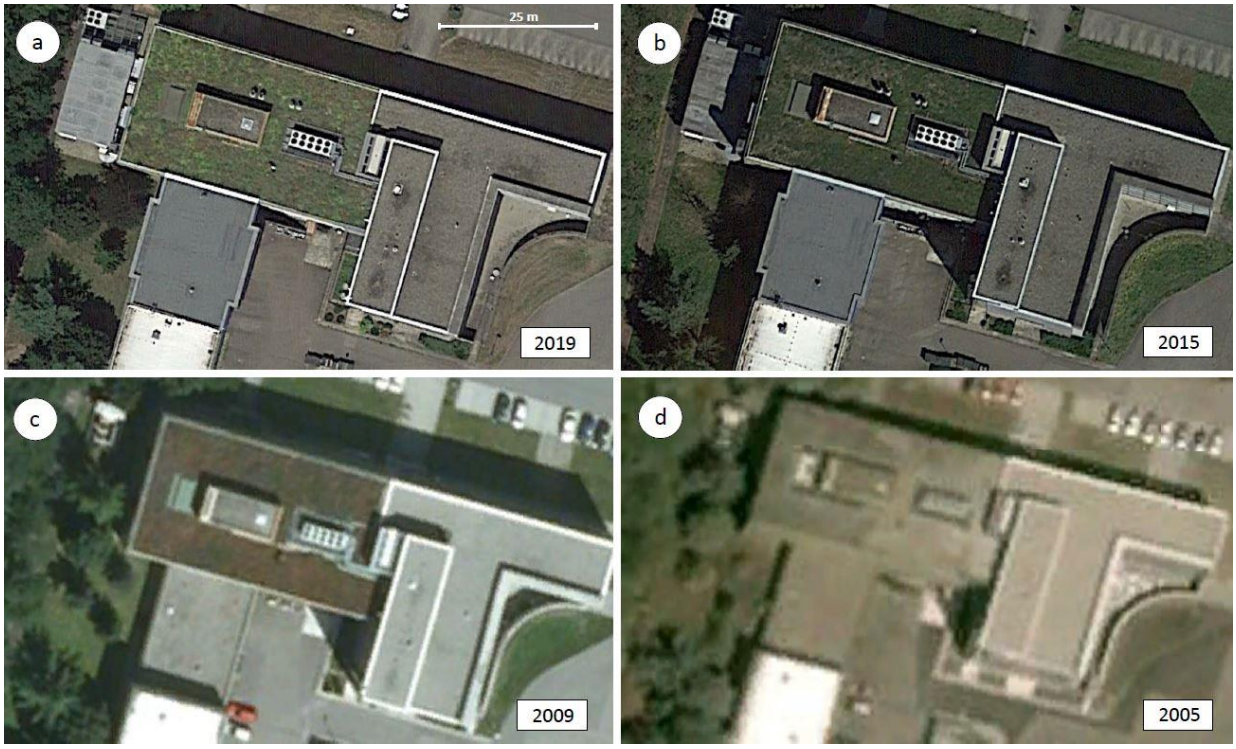

Figure 2-6: Reverse chronological order of aerial images exemplarily showing one compression chiller unit equipped with ten fans and installed on the roof of the supplied building.

A higher resolution of the aerial images would enable the recognition of the fan dimension and the detection of the specific manufacturer. Knowledge of the dimension of each detected fan and the CC unit could be additionally considered in the relation of Figure 2-3 and further improve the applied correlation, particularly for smaller systems. Since the specific manufacturer of the CC is not detectable by means of the aerial images yet, we currently adopt a general approach by using the required information of all used producers considering Figure 2-3. The same approach only adopted for the actual manufacturer of the observed CCs would improve the coefficient of determination and therefore the accuracy of the estimation of the installed cooling capacities. If the introduced method is used more frequently in the future, it would also be conceivable that the manufacturers provide exemplary aerial images of their CC units as part of their data sheet to simplify the classification. Furthermore, the improvement of the image resolution facilitates conclusions on the installation age of the respective CCs by analyzing signs of wear or discoloration as a result of weathering processes. This information

is valuable for the evaluation of potential replacements of the CCs or early planning of alternative renewable cooling solutions.

As a next step, we recommend applying the methodology on a district or urban scale to examine the practicability of the analysis beyond the studied university campus. It can be assumed that in densely populated areas the visibility of the installed CCs is partially limited, for instance by additional building developments. In addition, it is more difficult to assign the detected CCs to the supplied building. The similarity in appearance between the observed fans of CCs and other technologies can lead to potential confusions for the aerial image analysis. Without any prior knowledge of the study area, it may be difficult to distinguish CC fans from free cooling units and recooling plants, respectively, which can result in a larger deviation between the estimation and the actual cooling capacity. A clear identification of the installed assemblies requires accessible documentations of the producers and again a higher resolution of the used images. Extensive study areas require a larger amount of data from different producers of CCs since the diversity of the installed CCs is expected to be much larger compared to the studied campus. A large data set of estimated and actual installed cooling capacities could lead to a determination of a significant correction factor for the applied method, which leads to an increase in accuracy of the estimation. This can ideally be adapted for different amounts of cooling capacities and for example applied on an urban scale. With a predicted increase of installed cooling capacities of up to 60 % until 2025 [148], this knowledge becomes even more important in the future. After gaining more experience, a conceivable aim is to facilitate the approach by transferring the manually conducted analysis to automated image recognition. This would enable a faster and more extensive estimation of the installed cooling capacities and is, for example, already applied for the identification of solar panels [149, 150].

2.4 Conclusion

In this study, we introduce an easily applicable method to detect and quantify the installed cooling capacities of compression chillers (CCs) by means of aerial images. The novel approach is demonstrated at a university campus in Germany, where 36 CCs with an overall cooling capacity of 16.5 MW are considered. The estimation of the installed cooling capacities of each detected CC is validated by the actual values. We demonstrate the option to clearly identify air-cooled CC units and to accurately estimate their related cooling capacity with an average deviation of only one third. With installed capacities above 350 kW, the accuracy of

the estimation significantly improves. This concludes an improved suitability of the method for commercial and industrial buildings with typically larger cooling demands. Even though we are aware that further optimization is required, the method bears a large potential, as currently, according to our knowledge, there is no other method that enables the identification of cooling systems so far. There are still some limitations that are related to possible mistakes due to other installed applications which look similar in appearance to CC or due to low resolution of the aerial images. Hence, a widespread application and further validation of the presented approach at different sites and for a large range of installed cooling capacities are required to comprehensively detect occurring limitations in practice and to further improve this method. Nevertheless, we anticipate that this tool can significantly assist with urban energy planning or energy agencies to identify cooling consumers and to estimate their cooling demands. These are very valuable information for the planning of renewable cooling solutions and the design of district cooling (DC) networks.

Acknowledgments

We acknowledge funding support from the Ministry of the Environment, Climate Protection and the Energy Sector Baden-Württemberg for the project Geospeicher.bw in the context of BWPLUS. We also would like to thank the facility management (FM) of the Campus North of the Karlsruhe Institute of Technology (KIT) and in particular Christian Schnurr, Sebastian Sauer and Frank Eißenhardt for providing us with data and information on the current cooling supply.

Chapter 3

Cooling supply costs of a university campus

Reproduced from: Schüppler S, Fleuchaus P, Duchesne A and Blum P: Cooling supply costs of a university campus. Energy [submitted manuscript].

Abstract

Global climate change and growing research activities lead to increasing cooling demands and related supply costs at universities, while at the same time ambitious goals towards carbon neutral campuses are established. Hence, universities are facing the challenge to develop large-scale future-proof cooling solutions. This also applies to the Campus North of the Karlsruhe Institute of Technology (KIT), where the current cooling supply consisting of decentralized rooftop compression chillers is insufficiently monitored resulting in a lack of knowledge on supply costs and cooling needs of each facility. Hence, the objective of this study is to examine the current cooling supply and related costs by the analysis of 47 compression chillers supplying 23 buildings at the campus. To compensate for the given uncertainties of the provided input parameters, a Monte Carlo simulation is performed revealing cooling costs ranging between 5.4 and 11.4 euro cents kWh^{-1}. The overall supplied energy and installed cooling capacity amount to 70 GWh and 20 MW, respectively. Cumulative annual costs of €4.5 million, mainly resulting from the electricity costs to power the chillers, request for a transition to a decentralized and more efficient cooling supply by integrating renewable cooling supply solutions.

3.1 Introduction

Worldwide air conditioning of buildings accounts for almost 20 % of the total electricity demand while the energy consumption for space cooling amounts to 140 TWh/y in the European Union (EU) alone [126, 151]. In the last 40 years, cooling degree days (CDD) in Europe already rose by 70 % [152]. With population growth and global climate change cooling needs will substantially increase and grow faster than all other end-uses of buildings [129, 153, 154]. Hence, comfort cooling is predicted to increase up to 750 % until the year 2050 [128]. The cooling sector is strongly dominated by electric driven technologies, which potentially leads to a doubling of CO_2 emissions of the electrical supply for cooling by the end of the century [155, 156]. While southern Europe is characterized by high demands for space cooling, Germany has the largest need for process cooling in the EU [157, 158].

The European service sector, consisting of infrastructure for offices, hotels, health care or education, requires the largest amounts of cooling energy with current demands approximately 60 % higher than for the residential sector [159, 160]. The education sector in the UK for instance contributes 13 % to the total energy consumption. Within education facilities, university campuses have the largest energy consumption and are considered as small cities with regard to their energy demand and environmental impact [161, 162]. Thus, sustainability and carbon reduction targets, along with efficiency increase and cost reduction of universities became an important issue for policymakers and energy planners [161, 163–166]. Recent studies predict a large energy saving potential for universities ranging between 30 – 60 % [167, 168]. To reduce primary energy consumption, centralized district heating and cooling networks (DHC) are considered as a promising solution [77, 169]. Whereas the majority of these networks are solely applied for heating, district cooling (DC) grids currently have a market share in Europe of only 2 % [170].

Due to higher comfort standards, the vast majority of DC networks at universities are installed in the US. In most cases, DC is applied in combination with chiller plants and cold thermal energy storage tanks (TES) providing large cooling capacities of up to over 100 MW. Nevertheless, few universities have successfully implemented DHC networks fed by renewable heating and cooling sources. The ETH Zürich, for instance, operates an anergy network with a length of 1.5 km covering 65 % (1,816 MWh) of the cooling demand of the Hönggerberg campus. Seasonal borehole thermal energy storage (BTES) consisting of 431 probes is used as a cold source to extract temperatures suitable for cooling of laboratories (12 °C) [105, 106].

Heating and cooling supply of the Technical University of Eindhoven (TU/e) often serves as a technical blueprint for Aquifer Thermal Energy Storage (ATES) and is considered as the world's largest system with a cooling capacity of 20 MW and 32 installed wells. Up to 32 GWh per year of cooling energy are distributed over 8 km enabling the cooling supply of 20 university buildings [50]. Further low-carbon technologies for cooling supply of universities were considered in the past and are occasionally applied including ice storage [108], river and lake source cooling [110, 171] or more common ground source heat pump (GSHP) systems [57, 172]. However, the current cooling market is strongly dominated by vapour compression refrigeration systems, supplying more than 90 % of the current cooling demand [63, 66].

This is also the case at the Campus North (CN) of the Karlsruhe Institute of Technology (KIT), Germany, where almost the entire campus is supplied by decentralized compression chillers installed at the roofs or in close vicinity to the related facilities [173]. However, the CN pursues the ambitious goal to become climate-neutral by the year 2030. Hence, the facility management (FM) and administration of the CN work closely together with research institutes and have ongoing research projects for the implementation of future-proof energy supply technologies. This also includes the transition from the decentrally installed rooftop compression chillers, further named as chillers, to a DC system. According to Calderoni et al. 2019 [174], the development process of a DC system consists of five consecutive phases summarized in Figure 3-1. At present, the CN is in the early stage of process development favoring the use of groundwater to feed the desired DC network. However, the first process phase lacks current financial figures and market assessment. Installed cooling capacities, required cooling demands and most important occurring costs of the current cooling supply are barely covered and therefore mostly unknown. Consequently, this lack of knowledge in combination with a non-existent master plan strongly impedes a constructive development process and therefore a rapid realization of a future DC system. A comprehensive data analysis on the current energy use is, however, a crucial starting point for the development of promising energy optimization strategies and investment decisions [175].

In order to finalize the first phase and to form a sound baseline for further process development of the DC system, we provide an initial analysis of the current cooling supply with focus on the arising cost for each considered chiller and related building. Due to the poor data availability at the site, we perform a Monte Carlo simulation covering the uncertainties of the given data. The required input parameters are based on a survey among the operational agents and from operational data of two representative buildings at the site. Our work does not intend

to specifically contribute to the project development of a DC system at the CN, but rather serves as a guide for how to analyze the current state of cooling supply and related costs for universities or large facilities in general. This will become particularly important as many research and business facilities in temperate climates face the challenge to adjust their cooling infrastructure in accordance with future demands and carbon emission targets.

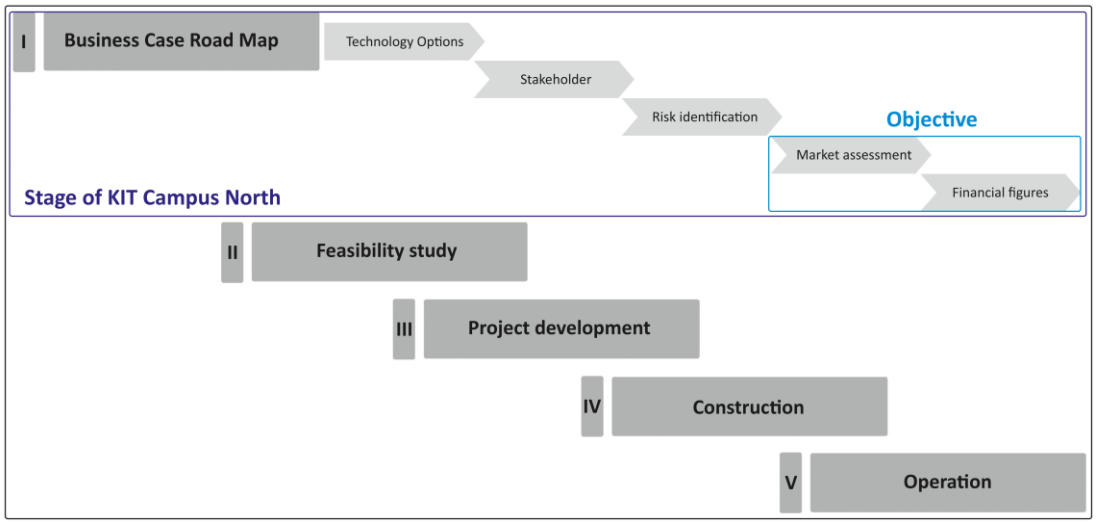

Figure 3-1: Development process of DC systems derived and modified from Calderoni et al. (2019) [174].

3.2 Material and methods

3.2.1 Workflow

The approach of the present study consists of four coherent work steps which are illustrated in Figure 3-2:

1. **Data collection:** as part of the market assessment at the site, a survey among the facility management of the considered buildings of the CN is carried out to examine installation age, electrical power input and in particular installed cooling capacities of each considered chiller unit. In addition, access to the operational data of two representative buildings equipped with electric meter serves as further data basis.
2. **Cost evaluation:** the analyzed financial figures at the site are restricted to those directly related to the considered chillers. We distinguish between investment costs *IC*, demand-related costs *DC* and operation-related costs *OC* of the installed chillers in accordance

with the German technical guideline VDI 2067 [36]. The economic analysis refers to the year 2018 as the required input data are mainly based on the monitoring data of this year.

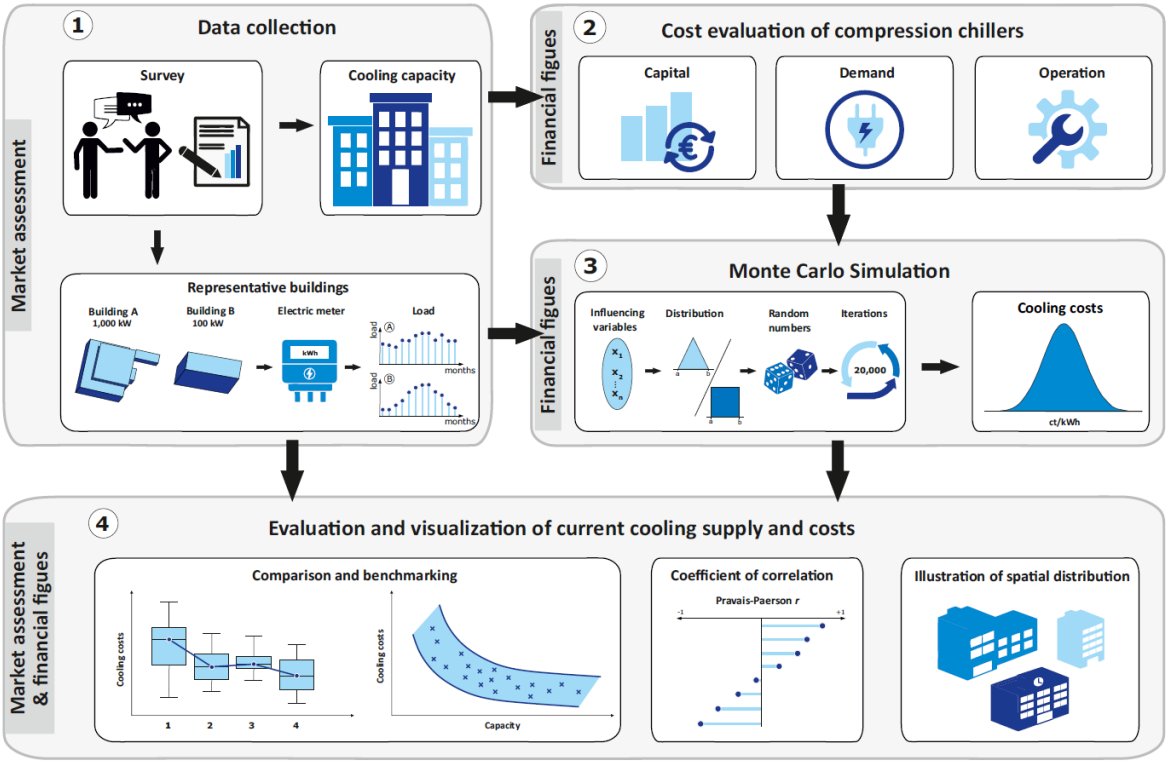

Figure 3-2: Workflow of the presented study.

3. **Monte Carlo simulation:** considering the data availability at the study site, a Monte Carlo simulation is performed to cover the uncertainties of the influencing variables. The simulation delivers the final costs of the cooling supply in euro cents per kWh of each considered chiller. The approach is described in more detail in Chapter 3.2.4

4. **Evaluation and visualization:** as final step, the results of the Monte Carlo approach are analyzed, visualized and compared with the determined cooling costs *CC* of each chiller and related building. In addition, optimization strategies, as well as further steps to successfully proceed with the process development of the DC, are discussed and compared with current cooling supply solutions at other universities.

3.2.2 Study site

The CN is a large research facility of the KIT located 12 km north of Karlsruhe, Germany (Figure 3-3a) and covers an area of about 2 km^2 (Figure 3-3b). The site is characterized by a

heterogeneous building stock consisting of institutions for academic research, administration and external companies. Almost every campus building requires space or process cooling to supply laboratories, experimental facilities, data centers or productions plants.

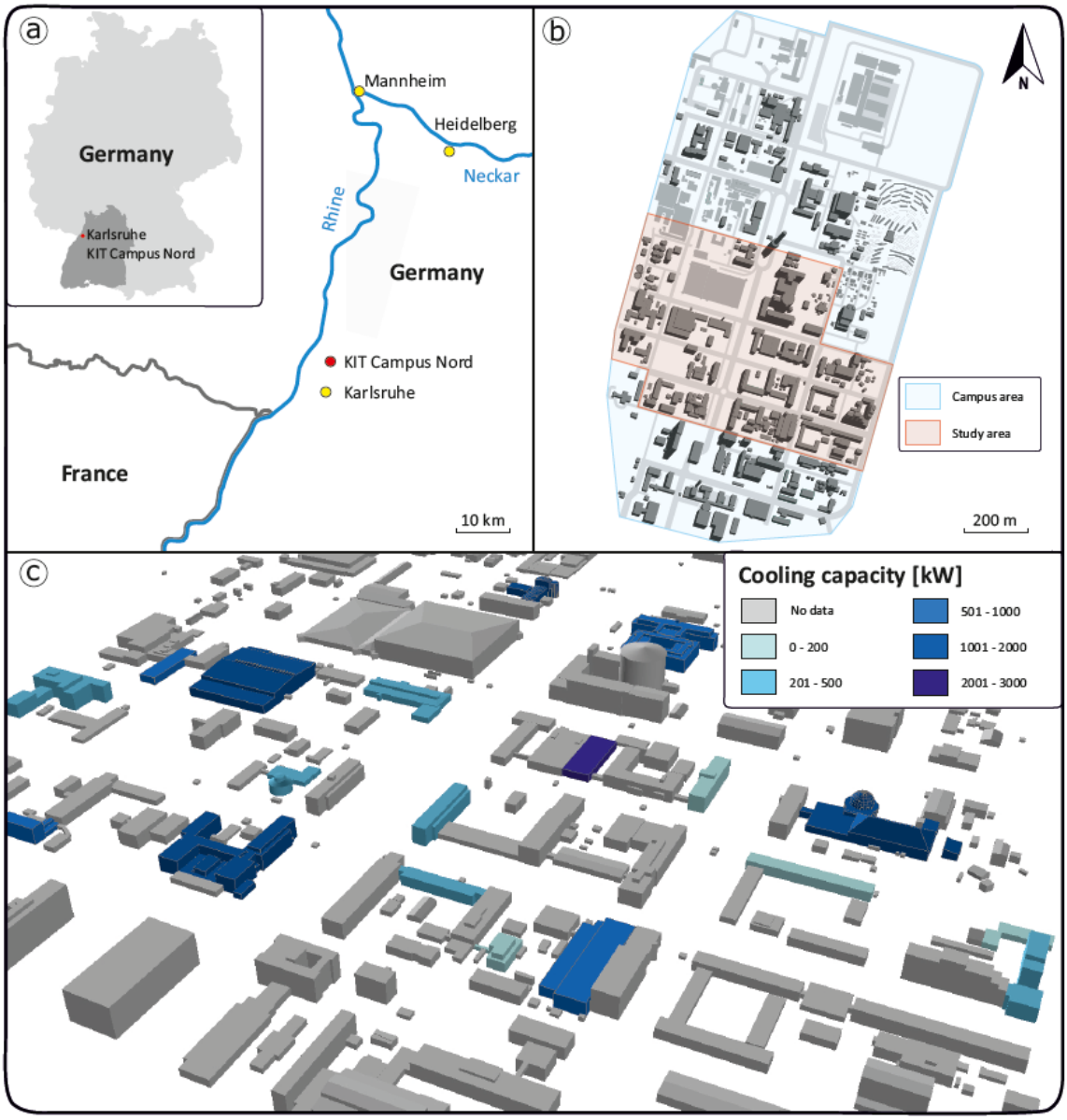

Figure 3-3: Location of the study site (a), main area of interest (b) and installed cooling capacities of the considered buildings of the selected area (c).

The cooling supply of the buildings is decentralized and mainly provided by chilled water compression chillers installed at the roofs or in close vicinity to the supplied buildings operating with typical supply temperatures of 6 °C and return flow temperatures of 12 °C. The chillers are defined as split devices after Bohne 2014 [142] as they have separate components

consisting of a cooling water circuit, often connected to an integrated re-cooling plant outside the building and combined with the condenser, a chilled water circuit connected to the evaporator and a refrigerant circuit. Compared to commercially available systems, some chillers at the CN are installed to meet special requirements, for instance providing process cooling for the particle accelerator named Karlsruhe Research Accelerator (KARA) [176]. The supply management (SM) [177] supplies the research facility with electricity and operates its own cable network connected to an upstream network of the regional energy company [178].

Since most buildings outside the red colored portion of Figure 3-3b comprise of external companies or less relevant buildings with cooling capacities below 100 kW, we narrowed the study area within the CN for our analysis. Overall, 47 air-cooled chillers supplying 23 campus buildings with cooling energy are considered. The main barrier in the determination of the overall arising costs of each chiller for the cooling supply is the insufficient data basis at the site. Cooling supply and related electricity consumption at the campus is presently only monitored for two facilities. To compensate for the lack of data, we first query the installed cooling capacity of each considered chiller and building using a survey within the campus. Since the installed cooling capacities are an important input parameter to determine the cooling costs at the site, we decide to present the values already in the present chapter. The installed capacities of the considered chiller range between 75 and 1,200 kW, while the cumulative installed capacities of each included campus building vary between 90 kW and up to 2,400 kW (Figure 3-3c). Multiple installed chillers for a single building are occasionally required for redundancy ensuring operational safety, but are more often used to split the required loads in particular at high demands to reduce the wear on the systems. The installation age at the date of investigation of the chiller is between 2 and 40 years with an average value of 18 years.

Table 3-1: Technical data and relevant parameters of the two selected reference buildings A and B. The data are queried by means of the survey and after additional consultation with the facility management of the Campus North.

Parameter	Unit	Building A	Building B
Cooling supply		3 chillers	1 chiller
Operating time *t*	a	2; 21	19
Electrical power input	kW	739 (1 x 239; 2 x 250)	40
Installed cooling capacity *C*	kW	3,004 (2 x 965; 1 x 1074*)	128
Investment cost *IC*	€	650,000*	300,000
Electricity consumption *EC*	kWh	2,050,549	120,832
Seasonal energy efficiency ratio *SEER*		4.49	4.79
Cooling demand *CD*	kWh	9,206,965	578,785

* Investment cost *IC* only provided for the chiller with the operating time of 2 years and installed cooling capacity of 1,074 kW.

In addition to the queried cooling capacities of 47 chillers, a comprehensive data set of the aforementioned two representative campus buildings was provided serving as initial basis for the present approach. We chose these two facilities, hereinafter anonymously referred to as building A and B, as representative infrastructure due to the good data availability from an installed electric meter which records the power consumption of the chillers on an hourly basis. Furthermore, important parameters such as investment costs and efficiency of the chillers, here quantified with the seasonal energy efficiency ratio (SEER) of the two building are available. The SEER is defined as the ratio of the total seasonal cooling output of the chiller and the electrical energy input and is further described in Refs. [179–181]. This data set of the two buildings enables the validation of the subsequently conducted Monte Carlo simulation. The provided data of both facilities are summarized in Table 3-1.

3.2.3 Economic analysis

Cost evaluation

Three cost groups are considered including upfront investment, demand-related costs *DC* and operational-related costs *OC* based on the German technical guideline VDI 2067 [36]. *DC* and *OC* are annual expenses, here representatively determined for the year 2018. The sum of the

cost categories is considered as total cost expenditure *CE*. The parameter values to calculate each cost group are determined in close cooperation with the facility management of the campus. Thus, our approach relies less on literature value estimations, but is instead characterized by on-site experiences. The required input parameters to determine the cooling costs (CC) are summarized in Table 3-1.

Investment costs

The upfront investment of each chiller includes costs for the machine and integration in the existing building technology. These costs are typically a function of the system size and are therefore included as specific investment costs *IC* € kW^{-1} in the calculation. As the installed machines are adapted to the specific requirements at the site, estimations based on literature values are not appropriate. In addition, the system boundaries in the literature are rarely defined, which can easily result in misleading assessments. Thus, the provided investment costs of building A and B (Table 3-1), are the basis of the present approach, while the facility management (FM) additionally supplied specific investment costs *IC* of two additional buildings which amount to 1,375 and 460 € kW^{-1} for installed cooling capacities of 300 and 1,200 kW, respectively. Based on these values and the consultancy of the FM, we define a range of the specific investment costs for related cooling capacity intervals serving as input parameter for the Monte Carlo simulation (Table 3-2).

Demand-related costs

The demand-related costs *DC* compose of the costs for electricity, comprising of commodity price *CP* in euro cents kWh^{-1} and capacity charge *Ch* € kW^{-1}, to power the cooling machines. As we consider the installed cooling capacity *CC* of each chiller as a deterministic value, the defined range of the produced energy for cooling Q_c depends on the annual hours of operation *HO*. Here, we distinguish between system size and cooling supply in summer and winter. In the latter, process cooling for laboratories or research infrastructure is mostly required. At the site, larger installations (> 600 kW) typically show smaller utilizations. The average considered *HO* of chillers with cooling capacities above 600 kW are therefore lower. The electricity consumption *EC* of the chiller is associated with the aforementioned SEER. The amount of *Ch* depends on the installed cooling capacity of the respective chillers. Capacities below 600 kW are provided with electricity from the low voltage grid, while capacities above 600 kW are connected to the medium voltage grid. In general, costs for water or other refrigerants are considered for cooling machines. However, it is not required to refill or replace the operating

liquid of the chiller during the lifetime of the systems at the site. Thus, the considered *DC* are calculated as follows:

$$DC = EC + CP + C \cdot C_h = \frac{C \cdot HO}{SEER} \cdot CP + CC \cdot C_h \quad \text{(Eq. 3-1)}$$

Operation-related costs

Operation-related costs *OC* are costs for maintenance and service of the chillers. Typically, *OC* are estimated with a maintenance factor *f*, defined as a certain percentage of the initial investment [36]. As the individual design of the chiller is associated with larger maintenance effort, *f* is consequently larger than commonly assumed values of around 2.0 %. For this reason and considering that chillers with longer operational time require more intensive maintenance, we grade *f* in accordance with the installation age of the chillers between 3.5 and 10 %.

Cost calculation

The aforementioned cost elements are summarized as total cost expenditures *CE* for each chiller during the observation time *T* and discounted with the interest rate *i* to the present value, also referred to as capital-related costs *CR*:

$$CR = \sum_{t=0}^{T} CE \cdot \frac{1}{(1+i)^t} = \sum_{t=0}^{T} (IC + DC + OC) \cdot \frac{1}{(1+i)^t} \quad \text{(Eq. 3-2)}$$

where *t* is the year in which the expenses arise. To define the average annual expenses, we determine the annuity *A* by multiplying the *CR* with the annuity factor *a*:

$$A = CR \cdot \frac{i-1}{1-i^{-T}} = CR \cdot a \quad \text{(Eq. 3-3)}$$

To simplify the approach, the potentially arising residual value R_w is not considered as the cooling machines are entirely depreciated after the operating lifetime and additionally customized to the specific requirements of the site impeding further sale.

3.2.4 Monte Carlo simulation

As a result of the aforementioned insufficient data basis, some of the chosen input parameters to determine the cooling costs of the chillers carry uncertainties. This includes the specific investment costs *IC*, supplied cooling energy Q_c, which is defined as the product of capacity *C* and hours of operation *HO*, SEER and interest rate *i*. To account for these uncertainties and to identify the related processes, a Monte Carlo simulation for each of the 47 considered chillers and a related sensitivity analysis is performed. The objective is to determine the cooling costs *CC* in euro cents per kWh arising in the year of observation. By applying and combining Eq. 3-1 and Eq. 3-2 the simulation calculates *CC* based on Eq. 3-4 for each iteration:

$$CC = \frac{I \cdot \frac{i-1}{1-i^{-T}} + CP \cdot \frac{C \cdot HO}{SEER} + Ch \cdot C + I \cdot f}{Q_c} \qquad \text{(Eq. 3-4)}$$

Since the objective is to determine the *CC* from the perspective of the year of observation, which is the year 2018, we only discount the up-front investment which is related to the year of installation. *T* is set to 15 years which is the commonly suggested depreciation time of chillers [36]. Please note that therefore, this approach slightly differs from the common calculation of the levelized cost of energy (LCOE), which is, for instance, discussed by Hansen, 2019 [182]. However, we intentionally decided to perform the Monte Carlo simulation on the basis of Eq. 3-4, as this approach better represents the current state of the cooling costs of the chillers, while the LCOE would unnecessarily complicate this approach. The number of Monte Carlo iterations is set to 20,000. However, some input parameters can be assessed with a deterministic value, as they were recorded during the survey or provided by the facility management of the campus, respectively. This implies the installed cooling capacity, installation age *a*, commodity price *Cp* and maintenance factor *f*.

Table 3-2: Input parameters, defined ranges and related distributions for the Monte Carlo simulation of the cooling costs CC.

Parameter	Unit	Dependency	Minimum	Mode	Maximum	Source	Distribution	Classification
Installed cooling capacity	kW			75 – 1,200 (Figure 3-3)		survey		
Operating time *t*	a			2 - 40		survey		
Observation period *T*	a			15		[32]		
Measurement	€ a^{-1}			81		FM		deterministic
Commodity price CP	euro cents per kWh	P > 600 kW P ≥ 600 kW		15.72 11.42		FM		
Capacity charge C_h	€ kW^{-1}	P ≥ 600 kW		74,76		FM		
Maintenance factor *f*	%	t ≤ 5 a 5 a < t ≤ 15 a t > 15 a = 10.0		3.5 7.0 10.0		FM		
Investment cost *IC*	€ kW^{-1}	P < 150 kW 150 kW ≤ P < 300 kW P ≥ 300 kW	1,000 900 450	2,250 1,000 750	2,500 2,350 1,000		triangular	
Operating time summer OT_s	h	P < 600 kW P ≥ 600 kW	1,600 1,200	2,400 2,000	3,600 3,200		triangular	
Operating time winter OT_w	h	P < 600 kW P ≥ 600 kW	800 400	1,600 800	2,800 2,000		triangular	stochastic
SEER			3,50	4.15	4.80		rectangular	
Interest rate *i*	%		1	3	5		rectangular	

The required input parameter to calculate *CC* on the basis of the Monte Carlo simulation are summarized in Table 3-2. To analyze the linear relationship between *CC* and each of the parameters in Eq. 3-4, we determine the Pearson correlation coefficient (PCC) as described by Yang 2008 [183]. The PCC takes values ranging between 1 and –1 [184] and is estimated as follows:

$$\rho(X,Y) = \frac{\sum_{i=1}^{n} x_i y_i - n\bar{x}\bar{y}}{\sqrt{\sum_{i=1}^{n} x_i^2 - n\bar{x}^2} \cdot \sqrt{\sum_{i=1}^{n} y_i^2 - n\bar{y}^2}} \qquad \text{(Eq. 3-5)}$$

where *n* is the amount of data of each chiller, here equal to the iterations of the Monte Carlo simulation, x_i and y_i are the values of the applied variables and $\bar{x}$ and $\bar{y}$ are their respective mean values.

3.3 Results and discussion

3.3.1 Reference buildings

Figure 3-4 exemplarily shows the load curves of the two reference buildings A and B for the year 2018. Building A is supplied by three chillers with a total cooling capacity of 3,000 kW and has the largest installed cooling capacity of all considered campus buildings in this study. This particular building mostly requires process cooling depending on the utilization of the instruments and is less related to the ambient temperature variation. The base load of building A amounts to 100 kW, while the peak loads of up to 400 kW arise from the conducted experiments on workdays. On the other hand, building B requires space cooling for offices and laboratories supplied by one single chiller with a capacity of 128 kW. Thus, the load curve of building B stronger correlates with the ambient air temperature at the site ($R^2 = 0.874$). The annual operation time of building B is almost 50 % longer compared to building A confirming the lower utilization for chillers with larger capacities.

Eq. 3-4 and the deterministic input parameters of Table 3-1 enable the calculation of CC of both buildings which furthermore serve as validation for the subsequent Monte Carlo simulation. Using an interest factor *i* of 1.4, building B has *CC* of 8.5 euro cents kWh^{-1}, whereas building A with three chillers in operation shows *CC*of 6.0 euro cents kWh^{-1}. For the

latter, only the annuity of the chiller with an operation age of two years is considered as the other two chillers are already depreciated exceeding the age of 15 years.

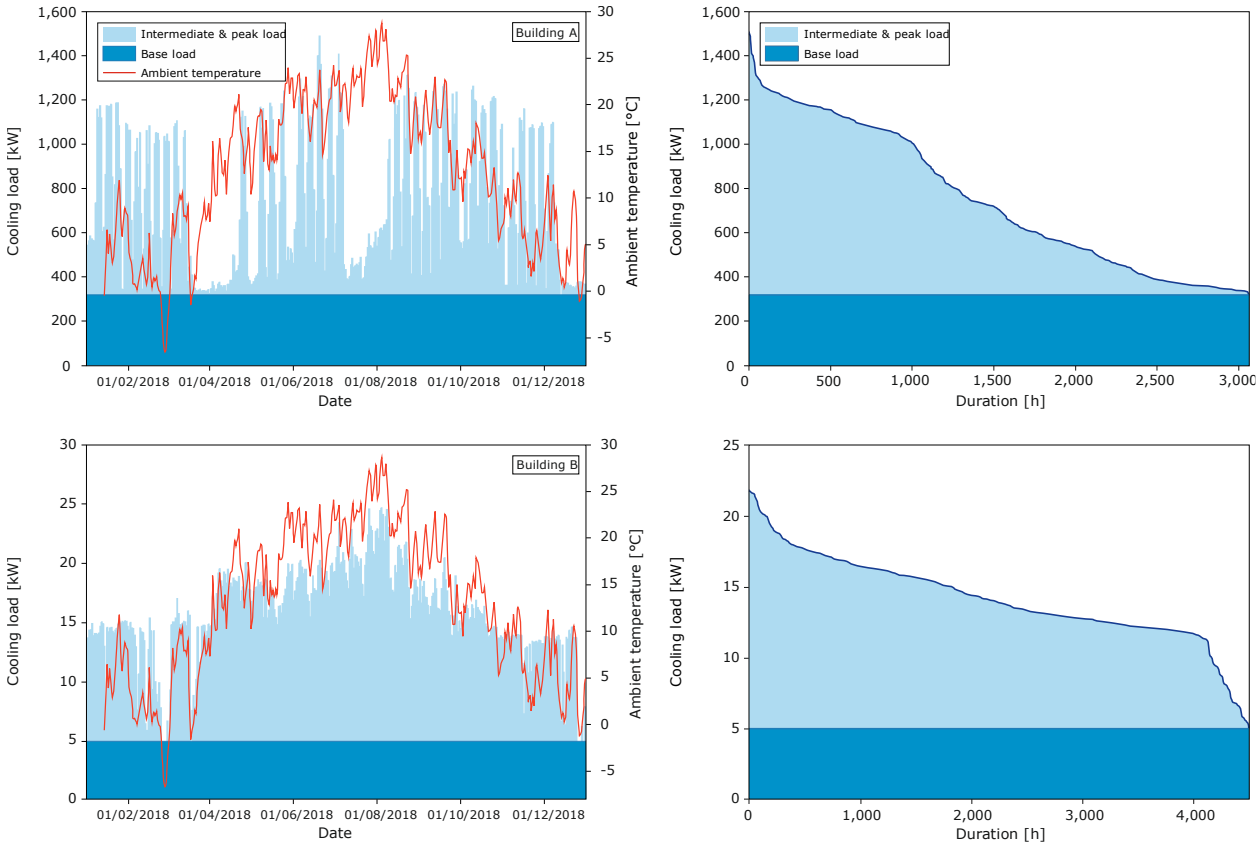

Figure 3-4: Load curves and cumulative load curves of the two reference buildings A and B and ambient air temperature [185] at the site for the year 2018.

3.3.2 Monte Carlo simulation

Figure 3-5a shows the results of the Monte Carlo Simulation in form of a unimodal probability distribution of *CC* for both reference buildings A and B. Building B uses a single chiller for space cooling with a simulated median value of 8.4 euro cents kWh^{-1} and an average value of 8.37 (± 0.96) euro cents kWh^{-1}. For building A, two chillers with an installed cooling capacity of 965 kW and another chiller with a capacity of 1,074 kW are used. As the two chillers also show the same installation age, their probability distributions are congruent with median values of 5.7 euro cents kWh^{-1}. The third chiller with the larger cooling capacity has a median value of 6.1 euro cents kWh^{-1}. The average cooling costs of building B amount to 5.79 (± 1.30) euro cents kWh^{-1}. The calculated values of Chapter 3.3.1 only show a small deviation of 1.2 and 5.0 % compared to the simulated median values of *CC* and are within the

standard deviation of the respective average values. Thus, it can be stated that the simulated results provide a good match with values calculated based on actual data and are appropriate for a first assessment of the *CC* of the Campus North.

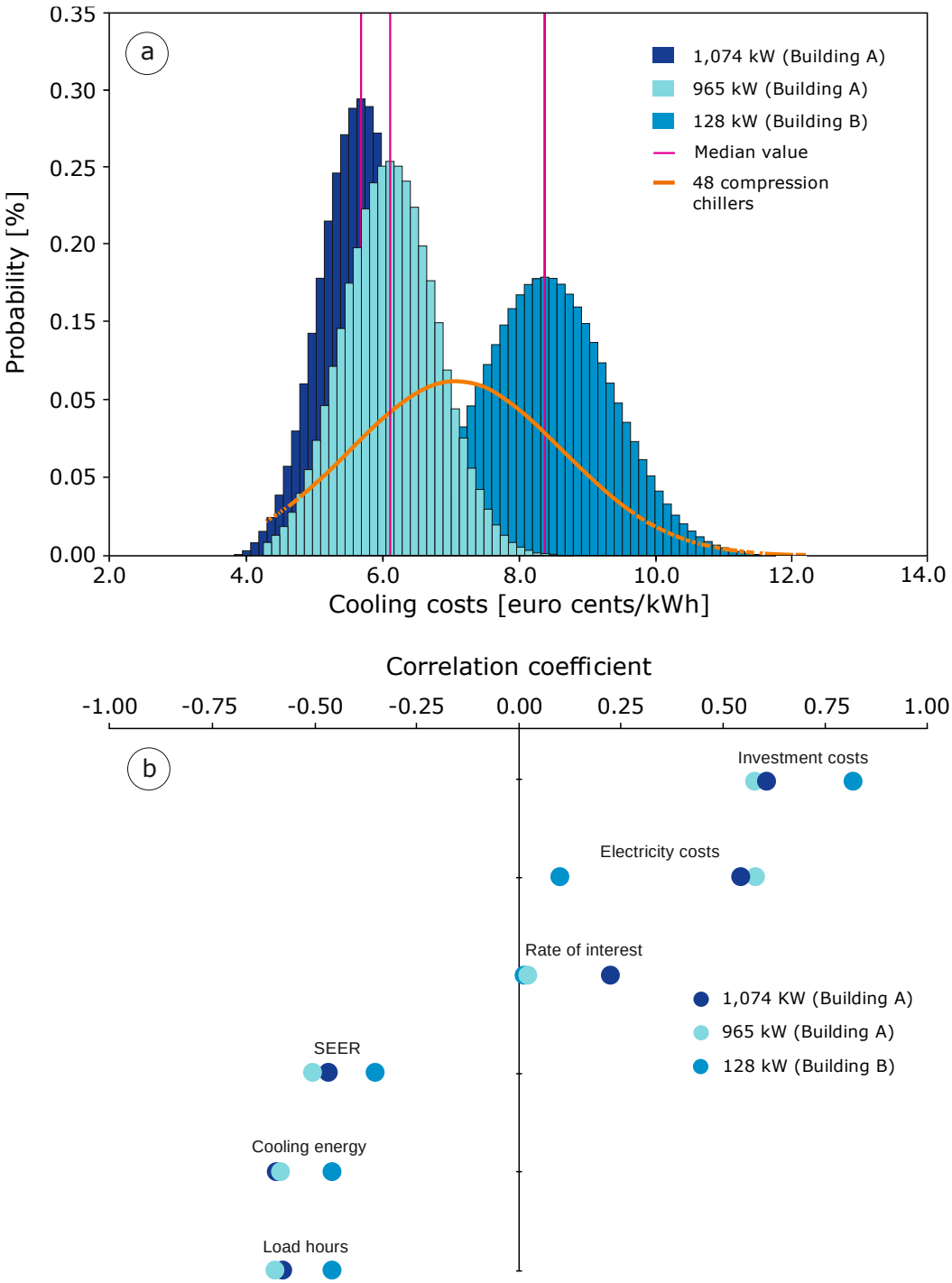

Figure 3-5: Probability distribution of the Monte Carlo simulation exemplary for the two reference buildings (a) and related Pearson correlation coefficient PCC (b) between the cooling costs and the individual parameters of Eq. 3-4.

Figure 3-5b reveals the Pearson correlation coefficients PCCs between *CC* and the uncertainties of the input parameters of Eq. 3-4 for the two chillers of building A and the 128 kW chiller of building B. As capacity, age and maintenance factor are set as fixed values for each chiller (Table 3-2), we calculated PCC for the remaining six parameters using Eq. 3-5. Specific investment costs *IC* and electricity price *EC* show the highest positive linear correlation to *CC*. As most of the currently applied heating and cooling supply technologies of buildings are scalable regarding system size [45, 186–188], the specific investment costs typically decrease with increasing capacity. Hence, the correlation coefficient of building B (0.80) is significantly higher than for both chillers of building B, which has the largest cumulative installed cooling capacity (3,000 kW) of all considered campus buildings. Even though the CN is a large energy consumer related to a lower special charge, the costs for electricity still have a relatively large linear correlation with *CC*. A previous sensitivity analysis confirms the strong linear dependency of EC and cooling cost of compression chillers in particular [189]. The larger the power consumption of the chillers, which is related to SEER and supplied cooling energy Q_c, the higher the correlation factor of the electricity costs. Please note that *EC* are a rather site specific parameter and therefore its correlation coefficient can regionally vary strongly, in particular when considering that Germany currently has the highest electricity costs in Europe [190, 191]. The highest negative linear correlation is observed for the supplied cooling energy Q_c and the load hours, which are connected to each other over the installed cooling capacity of the chillers. Please note that the PCC only describes the linear relationship of two (co-)varying variables. Thus, the negative exponential relation, for instance, between the supplied cooling energy and *CC* as in the present study is not shown.

3.3.3 Cooling costs of the university campus

In addition to the simulated values of the chillers of the two representative buildings, Figure 3-6 illustrates the simulated *CC* of all 47 considered chillers of the Campus North as a function of their cooling capacity. The Monte Carlo simulation reveals a large range of *CC* between 5.4 and 11.4 euro cents kWh^{-1} with an average value of 6.7 (± 1.4) euro cents kWh^{-1}. Even though specific cooling costs are not fully described by the regression, the relation between decreasing cooling costs with increasing capacity is shown emphasizing the economy of scale. This relationship is particularly evident for installed cooling capacities between 75 and 300 kW where the *CC* decrease by up to 50 %.

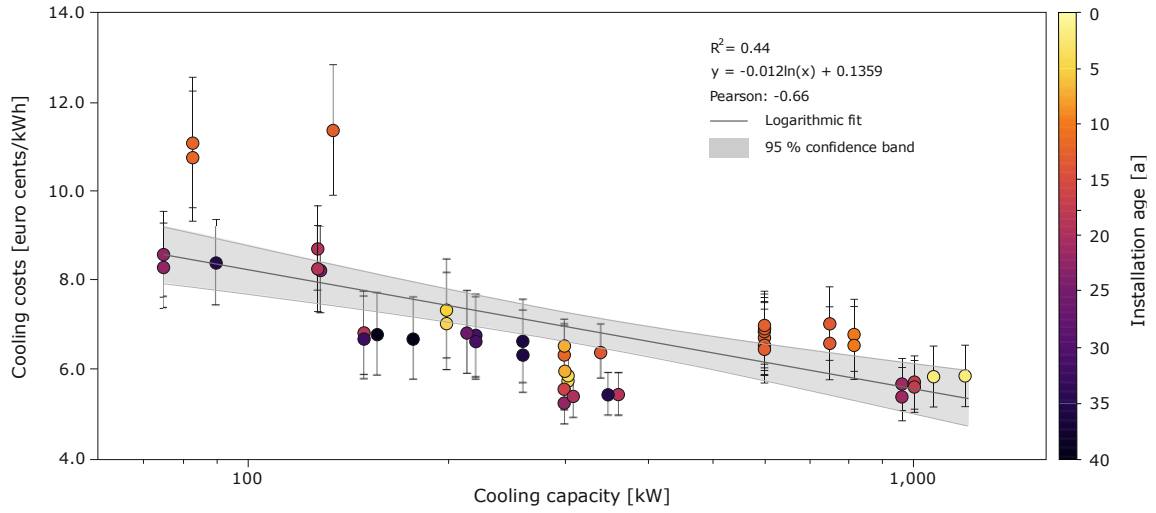

Figure 3-6: Cooling capacity and costs including standard deviation, logarithmic regression and 95 % confidence interval of all considered chillers of the campus in dependency of their installed cooling capacity. The installation age of each chiller is also expressed by the color range, illustrated in the right color bar.

However, in the capacity range between 500 and 1,000 kW *CC* are 12 % higher on average compared to chillers with capacities between 250 and 500 kW. This is due to the fact that most of the chillers with larger capacities have lower installation ages and are therefore not depreciated yet, resulting in an annual amount of annuity. Furthermore, operating chillers with sizes > 600 kW are associated with an additional charge for the installed capacity. Expenses above 10 euro cents kWh^{-1} are not only explained through depreciation costs, but also result due to the high demands of process cooling supply.

However, a low R^2 value of around 0.44 substantiates the results of Figure 3-5, indicating that *CC* is also affected by several other parameters. Investment costs *IC* for installations older than 15 years are already depreciated and are, therefore, not considered as arising expenses for the year 2018. This applies to 24 and approximately 51 % of all analyzed installations. Please note that the cooling costs are simulated results while the cooling capacity and installation age are actual values collected by the survey. With increasing capacities, the absolute value of the standard deviation of the *CC* decreases. For instance, the standard deviation of the *CC* for installed capacities of 100 kW is approximately 30 % larger compared to chillers with 1,000 kW of cooling capacity resulting from the relatively larger value range of stochastic parameters for smaller installations in particular, which is especially the case for the specific investment costs *IC* (Table 3-2).

As some campus buildings are supplied by up to six chillers, Figure 3-7 additionally provides the spatial distribution of the considered campus buildings and related average values of the simulated cooling costs. Furthermore, the total costs of the cooling supply for each building are illustrated as absolute values and subdivided by their cost groups as introduced in Figure 3-2. As utility maps are essential for planning the distribution systems of DC networks [192], the facility management can use the information of Figure 3-7 in the frame of the subsequent feasibility study and project development. Preferential integration of buildings with the highest overall costs, directly related to the cooling demand, in the course of the DC network is proposed. The supplied cooling energy and related total costs for one year of all considered buildings amount to 70 GWh and €4.5 million in total, respectively. The total costs are directly related to the demand and range between €45,000 and €606,000. While buildings with large cooling demands have at least two chillers installed enabling the split of the required loads, individual chillers often operate at maximum load which occasionally leads to breakdowns of the machines, particularly on warm days. This significantly reducing operational safety of the supplied building can impede a smooth cooling supply by means of individual chillers and allow for potential supply shortfalls.

Compared to the actual supplied cooling energy for building B of 9.2 GWh, the simulation yields cooling energy of 9.61 (± 0.66) GWh, which is an overestimation of 4 %, and total annual costs of €556,000 (± 33,000). The presently non-existent monitoring infrastructure of the cooling supply at the campus, however, impedes a more accurate and reliable data acquisition. The vast majority of chillers at the study site are connected to the main electric meter of the entire building together with other electric consumers. Thus, separate information about the electricity consumption, with the exception of buildings A and B, of each chiller is not available. Furthermore, data about current and historical investment costs of chillers are not only superficially documented but also difficult to access even for employees of the facility management.

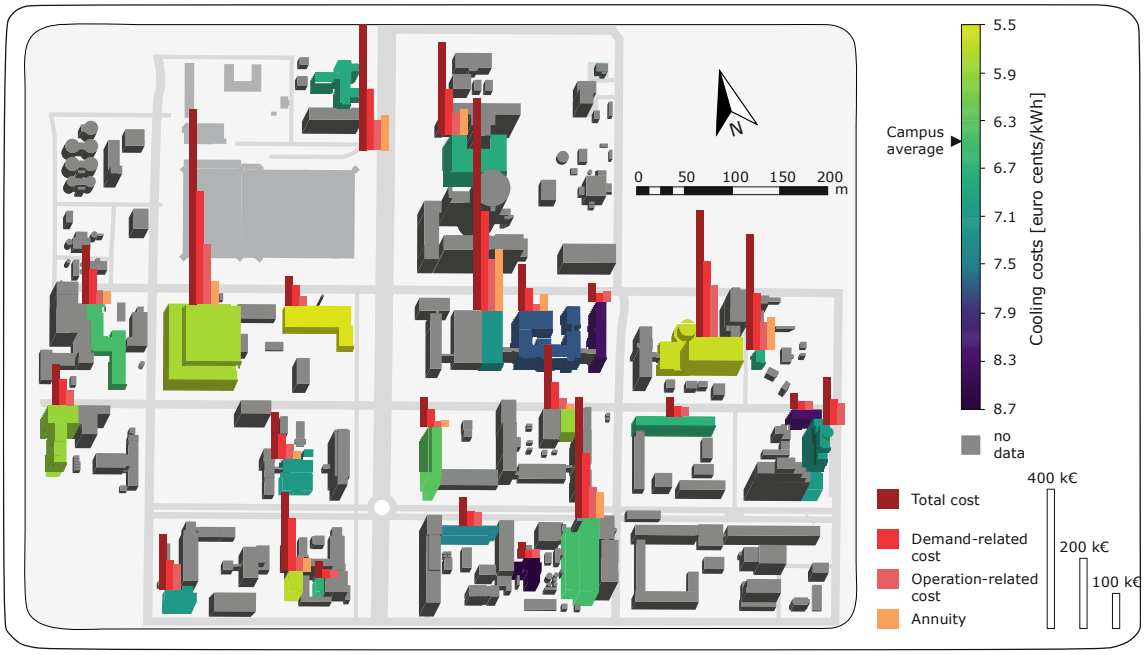

Figure 3-7: Spatial distribution of the considered 23 buildings of the Campus North of the KIT and related cooling costs. The total costs including subcategories are illustrated with colored bars.

3.3.4 Optimization and benchmarking

The performed evaluation of the market assessment in the present study is based on the installed cooling capacities of each building. However, actual cooling loads, which are considered as foundation for designing a DC system directly affecting the performance and cost-effectiveness [193], are currently only recorded for the two reference buildings (Figure 3-4). Hence, cooling loads should be comprehensively established at the campus, at least for a representative amount of buildings, and further distinguished between base and peak loads. The installation of energy meters explicitly for the cooling supply in combination with the development of an energy monitoring system (EMS) should be considered not only to facilitate the process development but also in the perspective of a reliable operation of a future DC system [70, 194]. In addition to a DC system, already installed rooftop chillers can either serve as redundancy to improve supply reliability or provide relief during times of peak loads in summer. This concept is implemented at the Campus South CS of the KIT. Here, three centrally installed cooling machines supply 150 campus buildings by means of an extensive DC network with a total cooling capacity of 8.0 MW and a length of 15 km [81, 195]. Facilities with large cooling capacities such as the data center receive further energy for cooling from additionally installed rooftop chillers which are equal to the systems of the CN. However, operational and economic

data of this DC network are not published and a comparison of the cooling solutions of both campus of the KIT has not yet been carried out.

Thinking in terms of a holistic optimization strategy of the cooling supply of the entire campus, the transition from decentralized chillers to a centralized DC network combining renewable cooling solutions is crucial to reduce the environmental impact, demand-related costs and overall cooling demand by increasing reliability, flexibility and redundancy as already emphasized by Refs. [70, 155, 179]. Hence, the CN should strive to accelerate the development process of the desired DC system based on the finding of the business case road map as illustrated in Figure 3-1. To meet the ambitious goal of a sustainable and climate neutral campus, current discussions on technology options promote the implementation of an anergy or low-temperature DC network [77], in combination with low-temperature Aquifer Thermal Energy Storage (LT-ATES). The latter is a shallow geothermal energy (SGE) application using open groundwater wells to seasonally store and extract thermal energy for heating and cooling of buildings [45]. For cooling supply, groundwater stored in winter with typical extraction temperatures of 10 °C [51] is used to cool the building or to feed a DC network [196, 197]. Depending on the subsurface properties and the building requirements the groundwater can be used directly or in combination with a heat pump to cool the building [48].

The study of Schüppler et al. 2019 [197] examines the economics of a potential LT-ATES for heating and cooling supply of a hospital with the same cooling capacity as building B in the present work of 3,000 kW. By applying Eq. 3-4 *CC* of the ATES only for cooling amount to 3.3 euro cents kWh^{-1} which is equal to cost reductions of 42.7 % compared to the chiller system of building B. However, while decisions on electricity supply technologies are often based on standardized calculations such as levelized costs of energy (LCOE) [182], less focus is on the consistent determination of cooling costs. Hence, first market assessments on currently suitable technology alternatives are rather based on the achieved efficiencies of cooling supply of comparable sites as illustrated in Figure 3-8.

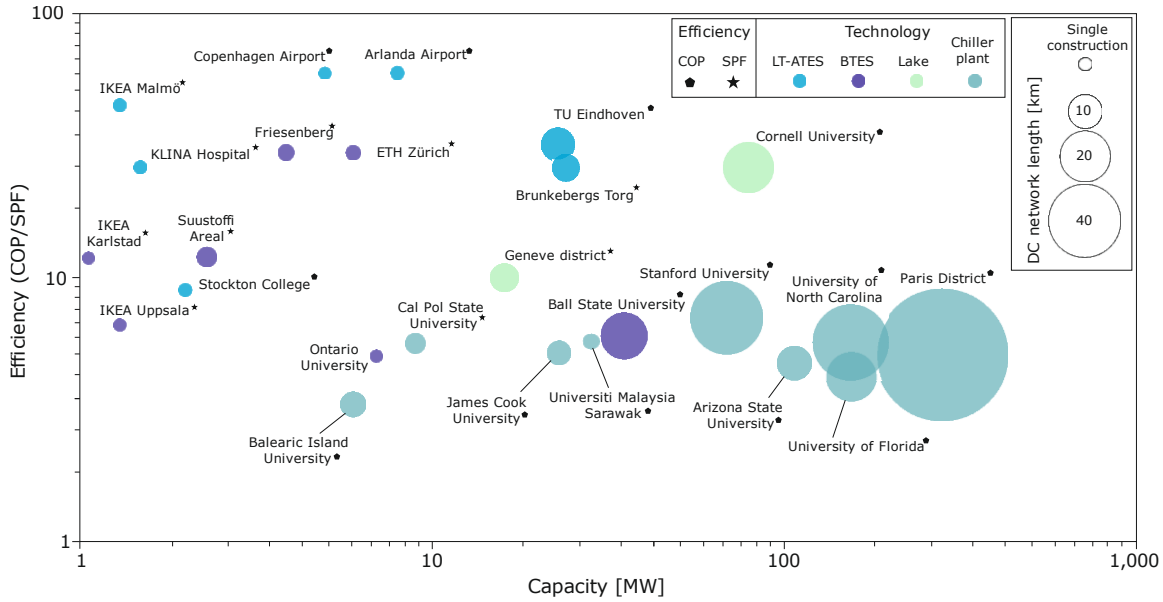

Figure 3-8: Market assessment of various types of cooling technologies based on the supply efficiency using the coefficient of performance (COP) or the seasonal performance factor (SPF) as derived from the following references [50, 76, 94, 97, 106, 108–111, 198–211].

Even though water cooled chiller plants are limited in terms of efficiency, they are continuously considered as state-of-the-art technology, in particular for large-scale DC systems (> 40 MW). However, technological progress regarding underground thermal energy storage (UTES) systems along with energy efficient buildings, facilitates the integration of shallow geothermal energy (SGE) yielding significant operational benefits. As subsurface temperatures are close to building conditions, cooling supply requires less exergy input and SGE systems can occasionally serve as natural sink [212]. This is particularly the case when SGE systems are further optimized due to beneficial storage effects demonstrated at airports in Arlanda and Copenhagen, or at the Technical University Eindhoven (TU/e) [50]. Hence, efficiencies quantified by seasonal performance factors (SPF) or coefficient of performance (COP) above 20 for several considered SGE systems are achieved. In these cases, the extracted temperature levels are suitable for direct usage without the additional utilization of heat pump systems and therefore only require electricity input to power the pumps for groundwater or brine extraction. Furthermore, Figure 3-8 shows, that direct usage of SGE systems for cooling is particularly efficient in regions with cold to moderate climates such as Denmark (e.g. Copenhagen airport) or Sweden (e.g. Arlanda Airport, IKEA), which is also emphasized by Arghand 2021 [213]. Here, subsurface temperatures are considerably lower and required cooling loads of buildings are smaller, which is particularly suitable for direct cooling throughout the whole cooling

period. While access to surface water, as shown at Cornell University, is mostly limited, SGE technologies, can achieve efficiencies unreachable for conventional chiller plants. Compared to the chiller efficiencies of the present study (e.g. SEER of 4.5 of building A), only a fraction of electricity demand to power the cooling system is required due to the installation of DC systems in combination with renewable energy sources. This not only leads to lower demand-related costs, but also to a significant reduction of carbon emissions. The DC system fed by an ATES system of TU Eindhoven additionally enables the annual saving of 13,000 tCO_2, which significantly contributes to the climate-neutrality of the university [214].

While little is known about the overall arising costs of DC in general and ATES systems in particular, comprehensive economic analyses of key projects as encountered at TU Eindhoven are crucial to foster technology adoption. Furthermore, knowledge transfers in terms of master plan developments of successfully implemented projects should be therefore pursued. Hence, we propose regular benchmarking opportunities consisting of roundtable meetings for university stakeholders, which is already established for hospitals [215] or hotels [216].

3.4 Conclusion

The analysis of the cooling supply of 23 campus buildings using 47 air-cooled chillers as part of the development process of a DC system, provided insights into the cooling costs of the decentrally organized cooling of a university. The simulation reveals positive economies of scale with cooling costs ranging between 5.4 and 11.4 euro cents kWh^{-1}. Large cooling capacities, particularly for process cooling of up to 3,000 kW for a single building, and a high share of electricity costs of 54 % to power the machines lead to annual costs of €4.5 million. Thus, the university is forced to significantly reduce cooling costs and cooling loads along with CO_2 emissions by simultaneously increasing the reliability of the cooling supply of each faculty by implementing a DC system. While this work mainly focuses on the current state of the cooling supply to finalize the first phase of process development of a DC system at the Campus North (Figure 3-1), further work should apply these findings in order to advance the installation of a DC system involving the following major steps:

- Development of a global master plan covering all levels of planning (business case road map, feasibility, project development, construction and operation) including all identified stakeholders as described by ASHRAE (2013) [192]. Potential stakeholders

of the project development are facility management, building service, research facilities, local authorities, consultants or the committee of the university.

- Strategy to integrate the DC network into the current building stock considering the cooling conditions as derived in the present study by emphasizing the specific requirements of ATES. Special attention is also required on the synergetic combination with existing rooftop chillers and the proper integration of the DC system into the current cooling distribution network of the campus buildings [174].

- Preparation of a techno-economic feasibility study of the proposed DC system considering the renewable energy source consisting of capital (CAPEX) and operational expenditures (OPEX) and subsequent performance of a profitability analysis. For the latter, we propose to use the financial figures of the present work as a base case for a dynamic investment calculation to receive the expected net present value (NPV) and amortization time of the considered DC system.

To globally develop future-proof cooling solutions at universities with focus on DC systems and renewable energy sources, future studies should address the following aspects:

- Identification and evaluation of all relevant boundary conditions (e.g. type of energy source, electricity price, size, legislation, building stock, subsidies, decision-making structures) for the assessment of the status quo as a decision-making tool for optimization strategies (e.g. integration of renewable energy sources, decentralization).

- Research on how and under which boundary conditions is it economically worthwhile to shift from decentralized to centralized cooling supply using DC-networks. The special requirements of cooling supply of universities in terms of heterogeneous building stock with respect to age and usage need special consideration.

- Uniform determination of cooling costs to develop a sound basis for benchmarking various technological options and decision-making processes.

The decarbonization of the cooling supply bears great potential for universities and should be recognized as a chance to develop innovative and efficient supply solutions, which can later be adopted and commercialized for urban quarters and industrial applications.

Acknowledgments

The authors would also like to thank the facility management (FM) of the Campus Nord of the Karlsruhe Institute of Technology (KIT) and in particular Christian Schnurr, Sebastian Sauer and Frank Eißenhardt for providing us with data, assessments and information of the current cooling supply. This work was funded by the Ministry of the Environment, Climate Protection and the Energy Sector Baden-Württemberg in the framework of the research project "GeoSpeicher.bw" (Grant number L75 16014-16019).

Chapter 4

Techno-economic analysis of an Aquifer Thermal Energy Storage in Germany

Reproduced from: Schüppler S, Fleuchaus P and Blum P (2019) Techno-economic and environmental analysis of an Aquifer Thermal Energy Storage (ATES) in Germany. Geothermal Energy 7 (1), 669. doi: 10.1186/s40517-019-0127-6.

Abstract

The objective of the present study is to analyze the economic and environmental performance of ATES for a new building complex of the municipal hospital in Karlsruhe, Germany. The studied ATES has a cooling capacity of 3.0 MW and a heating capacity of 1.8 MW. To meet the heating and cooling demand of the studied building, an overall pumping rate of 963 m3/h is required. A Monte Carlo simulation provides a probability distribution of the capital costs of the ATES with a mean value of €1.3 (± 0.1) million. The underground part of the ATES system requires about 60 % of the capital costs and therefore forms the major cost factor. In addition, the ATES is compared with the presently installed supply technology of the hospital, which consists of compression chillers for cooling and district heating. Despite the 50 % higher capital costs of the ATES system, an average payback time of about 3 years is achieved due to lower demand-related costs. The most efficient supply option is direct cooling by the ATES resulting in an electricity cost reduction of 80 %. Compared to the reference system, the ATES achieves CO_2 savings of about 600 tons per year, hence clearly demonstrating the potential economic and environmental benefits of ATES in Germany.

4.1 Introduction

In regions with moderate climates such as central and northern Europe, Aquifer Thermal Energy Storage (ATES) is a suitable technique to supply buildings with large amounts of heating and cooling. ATES bridges the seasonal mismatch between the ambient temperature and the heating or cooling demand of a building. ATES is an open-loop, bidirectional system, which uses at least one groundwater well in the saturated zone to actively store excess heat in summer and cooling capacity, further named as cold, in winter. The stored thermal energy can be reused when required [47, 50, 217–220]. The principle of a bidirectional ATES system is illustrated in Figure 4-1. In summertime, cold groundwater stored from winter is extracted from the cold well to cool the building. In most cases, the temperature level is sufficient for direct cooling without the application of a heat pump. However, heat pumps can also be utilized for space cooling. The excess heat of the cooling process is reinjected in the warm well and stored in the aquifer [221–223].

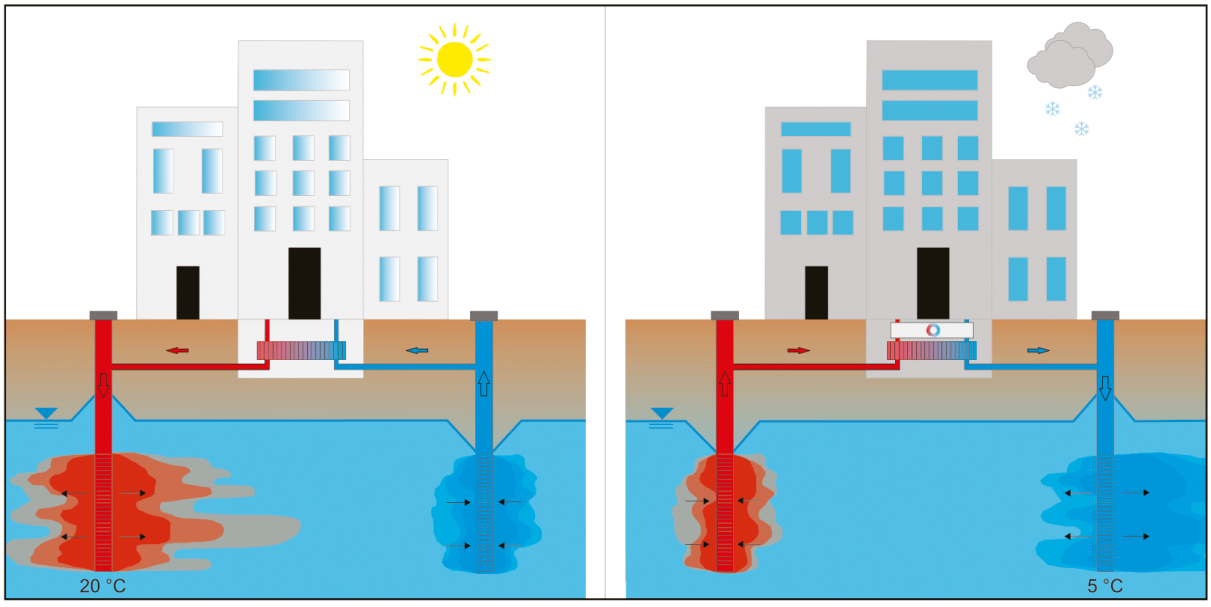

Figure 4-1: Operation mode of a doublet ATES system in summer and wintertime including the current temperature threshold for LT-ATES in Germany.

The reverse process is observed in wintertime by using warm groundwater stored from summer for heating purposes. The temperature level from the aquifer is increased by heat pumps to the required inlet temperature for space heating. The cooled water is reinjected back into the aquifer via the cold well. In an ideal case, a thermal balance is set up in the aquifer after some

seasons [6, 224–227]. In some countries and states, a thermal balance is a legal requirement for the operation of ATES [217, 228]. Most ATES in the Netherlands are shallow and operate with well depths usually ranging between 10 and 150 m [45, 46]. They are classified as low-temperature ATES (LT-ATES) with temperatures < 25 °C.

However, in Germany, the current temperature threshold for these depths is 20 °C for heating and 5 °C for cooling [45, 219]. Worldwide more than 2,800 ATES are installed with more than 90 % operating in the Netherlands alone while currently, only four ATES exist in Germany [45]. ATES is most efficient for buildings with high and constant energy demand over the year, such as offices, airports, universities, shopping malls and in particular hospitals [45, 211, 229–232]. To implement the technology also beyond the Netherlands, the investment in ATES must result in positive economic effects compared to common and in the future other sustainable supply technologies. However, detailed economic studies about ATES are rarely published [45].

In Germany, such techno-economic analyses of the four existing ATES systems are currently not available. Nevertheless, in other countries, such studies were recently published and are summarized in Table 4-1. It shows that several feasibility studies have already discussed the economics of ATES considering the capital costs, capacities and payback times. However, the majority of the studies only briefly summarized the economics of ATES. For instance, payback times and reference systems were rarely discussed together with an exception of the research from Vanhoudt et al. [210] and Ghaebi et al. [26]. Unfortunately, the evaluation of the economic data is in most cases not transparent or already obsolete. In addition, the applied methods are hardly described and not sufficiently discussed for reconstruction. However, a comprehensive techno-economic and environmental evaluation are indispensable to convince governments and decision-makers of the positive impacts of ATES in regions where it is not yet common.

Thus, this study focuses on the techno-economic viability and environmental performance of a representative case. The municipal hospital in the city of Karlsruhe, Germany, was faced with the decision of either using LT-ATES or compression chillers for cooling and district heating for a new building complex. Although the geological and hydrogeological framework of the site shows technical feasibility, the hospital administration finally decided against ATES. One reason for this decision was that the hospital wanted to reinject and store heat above the prescribed limit of 20 °C. However, the local water authorities adhered strictly to this limit.

Table 4-1: Overview of studies discussing the potential economic benefits of ATES.

Refs.	Country	Capital costs [€ kW ^{1}]	Purpose	Wells	Capacity [MW]	Energy supply [MWh]	Pay-back time	Ref. system
Reilly et al. [233]	USA	861[a]	Heating	14	3-50			Electric boiler and oil fired furnace
Zimmer-mann and Drost [234]	USA	89-890[a]	Cooling	2-16	2-20			
Andersson and Sellberg [235]	Sweden		Heating and cooling			1,800 - 10,000	2-10	
Chant and Morofsky [236]	Canada	133-266[b]	Cooling		0.1-10	20-20,000		
van Hove [237]	Nether-lands	1,000[c]	Cooling	6	1.5		6	Mechan-ical cooling
Paksoy et al. [238]	USA	750	Cooling	6	2	2,025		Standard chillers
Vanhoudt et al. [210]	Belgium	580	Heating and cooling	2	1.2	2,207	8.4	Gas boiler and cooling machines
Ghaebi et al. [26]	Iran		Cooling	2		2,417		Gas boiler, chillers; ATES

Exchange rates: [a] EUR/USD: 1.12, [b] EUR/CAD: 1.50, [c] EUR/NLG: 2.20

Hospitals in general have a great demand for efficient and sustainable heating and cooling supply. The average heating demand per patient in German hospitals is 29 MWh. This is equivalent to the thermal energy demand of two modern single-detached family houses [239, 240]. Thus, the current energy supply technology consisting of compression chillers and district heating, further named as reference technology, is compared with the estimated economic performance and energy efficiency of ATES over an observation period of 30 years. The sensitivity of the various costs of the ATES components defining the capital costs is determined with a Monte Carlo simulation considering the uncertainties of the input parameters. Furthermore, a sensitivity analysis provides information about the most relevant parameters for the capital costs. The estimated environmental benefits of the studied ATES during operation are illustrated based on the annual CO_2 savings per year. Finally, the results of the present study are compared with the economic performance of existing ATES systems.

4.2 Material and methods

Site

For the present study, a new building complex of the municipal hospital in Karlsruhe, Germany is considered. The new building with seven floors consists of surgery rooms, intensive care units, normal care and outpatient facilities and is part of the reconstruction measures of the hospital. The completion is scheduled for the year 2020. The load curve for heating and cooling of the building is calculated with RETScreen 4 [241] based on the parameters in Table 4-2 and the climate data of Karlsruhe.

Table 4-2: Parameters defining the heating and cooling supply of the building.

Parameter	Unit	Value
Heated floor space	m^2	35,000
Cooled floor space	m^2	41,000
Heating capacity	kW	1,804
Cooling capacity	kW	3,080
Space heating power demand	W m^{-2}	52
Space cooling power demand	W m^{-2}	75
Heating demand	MWh	3,685
Cooling demand	MWh	4,800

Figure 4-2 shows the annual load curve of the hospital building for space heating and cooling. The loads are assumed as constant over the observation period and correlate with the ambient temperature of the location. Heating and cooling are required from September to June (t_H = 2,043 h) and from May to October (t_C = 1,558 h), respectively. In the present analysis, the ATES system and the reference technology provide the entire heating and cooling demand of the building (Figure 4-3).

Aquifer Thermal Energy Storage (ATES) system

A conceptual design of the ATES system is essential to assess the economic efficiency and environmental benefits [46]. Table 4-3 summarizes the considered dimensioning of the ATES system. The volume of pumped groundwater *V* required for heating and cooling of the building is a key parameter of every ATES system and is calculated as follows:

$$V = \frac{Q}{c_w \cdot \Delta T \cdot \rho} \cdot 3{,}600 \qquad \text{(Eq. 4-1)}$$

Q is the amount of energy, c_w is the volumetric heat capacity of water equal to 4.2 MJ m^{-3} K^{-1}, ΔT is the difference between the extracted and injected temperatures, ρ is the water density equal to 1,000 kg m^{-3}. The larger ΔT the higher the energy output from the aquifer to the building resulting in smaller *V*. Depending on the properties, ATES systems achieve ΔT up to 10 K [210, 242].

However, since the hospital building requires more cooling than heating (Table 4-2) and the groundwater flow velocity is more than 100 m a^{-1} at the location a conservative estimation for ΔT of 4 K is chosen. Eq. 4-1 delivers the extracted groundwater volume to meet the energy demand of the building which amounts to 614,643 and 1,032,999 m^3 a^{-1} for heating and cooling, on average. The appropriate upper aquifer is dominated by unconsolidated rock, mostly consisting of gravel and sand with a thickness of 35 m.

Table 4-3: Design parameters of the considered ATES system.

Parameter	Number	Unit	Lifetime (years)
Cold well	3	-	
Warm well	3	-	
Well depth *H*	35	m	
Well diameter	0.8	m	
Screen length *L*	30	m	
Heat exchanger	1	-	20-30 [36]
Submersible pump	6	m	5-7 [243]
Well distance *D*	106-318	K	
Temperature difference ΔT	4	-	
Heat pump	2	-	20-30 [36, 244]

The production and injection wells form the main part of every ATES system and provide access to the aquifer, i.e. groundwater. After Bloemendal and Hartog [46], the optimal screen length *L* of a well is a function of the groundwater volume *V*, the volumetric heat capacity of water c_w and the aquifer c_a equal to 2.8 MJ m^{-3} K^{-1} and is estimated with Eq. 4-2:

$$L = \sqrt[3]{\frac{2.25 \cdot c_w \cdot V}{c_a \cdot \pi}} \approx 1.02 \cdot \sqrt[3]{V} \qquad \text{(Eq. 4-2)}$$

The required power of the submersible pumps *P* depends on various parameters and can be calculated by:

$$P = \frac{q \cdot \rho \cdot g \cdot h}{3.6 \cdot 10^6} \cdot \eta^{-1}; q = \frac{V}{t_{C/H}} \qquad \text{(Eq. 4-3)}$$

h is the delivery head equal to the well depth, *q* is the pumping rate, *g* is the gravity. Due to several factors such as motor and cable losses, the overall pump efficiency η is defined as 60 % [245]. Based on Eq. 4-2 the optimal screen length *L* for the warm and cold wells is 103 and

87 m in total. Considering the aquifer thickness, a doublet consisting of three warm and three cold fully penetrated wells with a depth *H* of 35 m and a diameter of 0.8 m each is assumed.

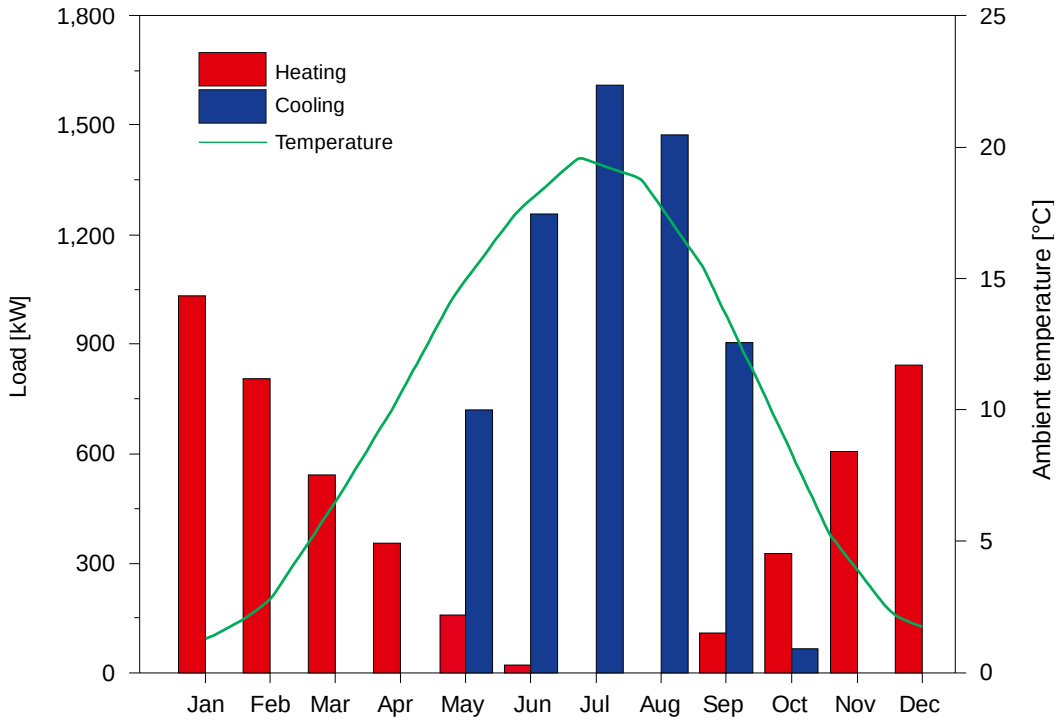

Figure 4-2: Annual heating and cooling loads of the building complex and ambient air temperature in Karlsruhe.

To ensure that the well screens are always in the saturated zone, a screen length *L* of 30 m for each well is chosen. Each well is provided with a submersible pump to pump the groundwater out of the wells to the heat pumps and heat exchangers, respectively [246]. Considering the number of wells, *V* and the heating t_H and cooling t_C periods, the average pumping rate *q* of each submersible pump is 100 $m^3 h^{-1}$ for heating and 221 $m^3 h^{-1}$ for cooling (Eq. 4-3). To prevent thermal interference, a suitable distance between the warm and the cold wells is assumed based on the thermal radius R_{th}.

$$R_{th} = \sqrt{\frac{c_w \cdot V}{c_a \cdot \pi \cdot L}} \qquad \text{(Eq. 4-4)}$$

The thermal radii of cold and warm wells (Eq. 4-4) are 74 and 33 m, respectively. Thus, a minimum well distance *D* of 106 m is required. However, Dutch authorities ensure a distance of three times the thermal radius between the warm and cold wells [46]. Thus, a distance of

318 m is also considered. The expected operational lifetime of ATES is more than 30 years [217, 247, 222]. Figure 4-3 summarizes the energy flows of the ATES system for heating and cooling. Depending on the COP of the heat pump, an average of 2,856 (± 92) MWh or 78 % of the heating demand, is covered by the thermal energy in the subsurface.

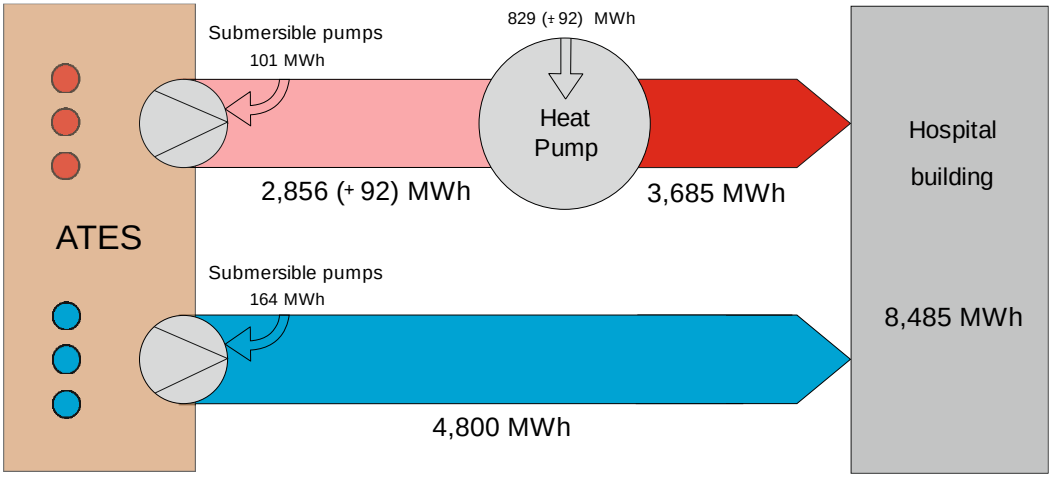

Figure 4-3: Energy flows of the considered ATES system for the heating and cooling supply.

The remaining energy is delivered by the heat pump. Since direct cooling is feasible with the ATES system, the amount of cold delivered from the aquifer is equivalent to the cooling demand of the building. As a consequence, the considered ATES has an energy balance ratio between heating and cooling of 0.25. In some European countries such as the Netherlands, the regulations require ATES systems to maintain the thermal balance between heating and cooling. However, this regulation does not yet exist in Germany. Thus, thermal imbalance can be assumed. Based on Eq. 4-3 t_C and t_H, the submersible pumps have a total electricity demand of 265 MWh for heating and cooling.

Capital costs of ATES system

The parameters used to determine the capital costs of the ATES system C_{ATES} are not site-specific, which means they have a strong variability. Some component costs, such as for the heat exchanger are derived from literature [210, 248]. Others are used from comparable shallow geothermal projects or service catalogues [243, 249, 250]. Thus, a Monte Carlo simulation with 100,000 iterations quantifies the uncertainty of each parameter. The simulation and the sensitivity analysis are both carried out with the software @Risk (version 7.5) [251]. For each parameter, a symmetric triangular distribution bounded by a minimum, mode and maximum

value is used. The most likely value is the mode while towards the minimum and maximum values the probability decreases continuously. In the present simulation, the minimum and maximum values are the best (cheapest) and worst-case (most expensive) scenarios. In addition, a sensitivity analysis determines the components with the strongest influence on the capital costs. A sensitivity analysis delivers insights into the structure of an investment and indicates the impacts of its uncertainties [252]. Table 4-4 summarizes minimum, mode and maximum values for each component of the ATES system used for the Monte Carlo simulation and the sensitivity analysis.

Current costs of ATES system

The current costs of the ATES system CC_{ATES} include the demand-related costs *DC* and the operation-related costs *OC*, derived from the German technical guideline VDI 2067 [36]. The demand-related costs are made up by the costs for the heating *CH* and cooling *CCO* supply (Eqs. 4-5 and 4-6). The operation-related costs comprise the costs for maintenance *M* and replacement *R* of components within the lifetime of the ATES system. The electricity costs *EC* are site-specific costs of the hospital, while the COP_{HP} is a generic value from literature (Table 4-5). The costs for heating are composed of the electricity costs *EC* to drive heat pumps and the submersible pumps. For direct cooling the use of heat pumps is not required, therefore only electricity costs *EC* to power the submersible pumps are considered (Eqs. 4-3 and 4-6). The costs for maintenance are defined as a certain percentage of the C_{ATES}.

$$CC_{ATES} = DC + OC = CH + CCO + M_{ATES} + R_{ATES} \quad \text{(Eq. 4-5)}$$

$$CC_{ATES} = \frac{ED_H}{COP_{HP}} \cdot EC + P \cdot t_H \cdot EC + P \cdot t_C \cdot EC + C_{ATES} \cdot M_{ATES} + R_{ATES} \quad \text{(Eq. 4-6)}$$

The observation period is defined as 30 years, however, some components such as the submersible pumps or the heat pumps have a shorter lifespan and have to be replaced within the observation period. Table 4-5 provides an overview of the parameters defining the current costs CC_{ATES}.

Table 4-4: Minimum, mode and maximum values for the Monte Carlo simulation of the C_{ATES}.

Category	Component	Minimum [€]	Mode [€]	Maximum [€]
Pre-investigation/ Feasiblity	Site inspection[a]	50	1,216	2,382
	Construction schedule[a]	5	846	1,687
	Feasibility study[b]	3,939	22,488	41,037
	Design planning[c]	6,200	47,706	89,212
Preparation	Site equipment[a, d]	1,738	7,319	12,900
	Transport drilling rig[e]	767	4,701	8,636
	Movement drilling rig[a, d]	300	7,950	15,600
	Sampling & core boxes[a, d]	924	9,114	17,304
	Bore log & drilling profile[a, e]	539	803	1,066
	Clear & pressure washing[d]	31,592	36,706	41,820
	Pumping test[a]	26,338	35,319	44,300
Drilling	Well drilling[f]	24,780	90,825	156,780
Well piping & well installation	Filter pipe[a ,d ,e]	35,250	48,735	61,500
	Solid wall pipe[e]	14,160	30,881	47,602
	Centering[d, e]	24	102	180
	Bottom cap[a]	48	480	912
	Well head[a]	1,166	18,313	35,460
	Water chamber[a, e]	40,800	46,305	51,810
	Shaft cover[a, d]	767	2,934	5,100
	Filter gravel/sand[a]	826	21,293	41,760
	Counter filter[a]	28	464	900
	Clay seal[a, d]	2,687	63,077	123,467
	Submersible pumps[d]	15,570	21,585	27,600
	Stand pump[d, g]	25,200	30,823	36,446
	Well connection[a]	1,204	52,982	103,392
Controlling & monitoring	Electronic switchboard[a]	2,213	50,982	99,750
	Water flowmeter[a, f]	893	9,105	17,316
	Pump control system[a, e]	1,779	48,350	94,920
	Site equipment monitoring well[a, e]	2,100	11,550	21,000
	Movenemnt drilling rig monitoring well[a, e]	162	925	1,687
	Drilling monitoring wells[a, e]	2,057	30,729	59,400
	Control line[d]	15,000	20,000	25,000
	Electricity connection[d]	35,000	55,000	75,000
Piping	Horizontal piping[d]	189,815	331,988	474,161
	Pressure washing[d]	7,161	8,638	10,115
Building integration	Heat pump[g]	11,456	41,365	71,274
	Heat exchanger[h, i]	65,600	67,800	70,000

[a] LANUV [250], [b] MacKenzie and Cusworth [253], [c] Chiasson and Culver [254], [d] GHJ [243], [f] Sanderson [255], [g] GWE [249], [h] Seider [248], [i] Vanhoudt et al. [210]

Table 4-5: Input parameters to calculate the current costs of the ATES system.

Parameter	Unit	Minimum	Mode	Maximum
COP heat pump COP_{HP} [256, 257]		4	4.5	5
Electricity costs *EC* [258]c	euro cents kWh^{-1}	16	16.5	17
Maintenance M_{ATES} [47]	%		4	
Replacement R_{ATES}			see Table 4-2	
Heating period t_H	h		2,043	
Cooling period t_C	h		1,558	

Reference technology

In Karlsruhe, a widespread district heating network (180 km) exists fed with over 770 GWh of heat. This network is mostly supplied by industrial waste heat of a large mineral oil refinery (MiRo) and by combined heat and power generation (CHP) of a steam power plant and is being expanded further [259]. The mineral oil refinery itself currently supplies over 30,000 homes in Karlsruhe. The hospital is already connected to the district heating network of Karlsruhe including substations. Thus, only costs for maintenance and pipe construction from the heating centre to the building collected from different district heating providers are considered in Table 4-6.

The maintenance costs depend on the capital costs defined as the costs for pipe constructions. The distance between the heating centre and the building is 100 m. The demand-related cost for district heating DC_{DH} depend on the consumption of the end-user and are calculated with Eq. 4-7 based on the parameters of Table 4-6.

$$DC_{DH} = CP \cdot (ED_H \cdot \eta_{DH}) + PP + BP \quad \text{(Eq. 4-7)}$$

CP, *PP* and *BP* are derived from the municipal utility of Karlsruhe and for comparison of three surrounding cities in Baden-Württemberg. The municipal hospital uses magnetic bearing compression chillers for cooling. These specific types of chillers are frequently used in hospitals and data centres and are therefore representative of a standard cooling supply technology [260].

Table 4-6: Parameters defining the capital and current costs of the district heating supply.

Category	Parameter	Unit	Minimum	Mode	Maximum
Capital costs C_{DH}	Excavation work	€ m^{-1}	101.15 [261]	113.05	124.95[262]
	Piping	€ m^{-1}	232.05 [262]	431.40	630.70[263]
	Contingency	%		10 [264]	

Category	Parameter	Unit	Karlsruhe[265]	Ulm[266]	Pforzheim[267]	Emmendingen[268]
Current costs	Commodity price *CP*	euro cents kWh^{-1}	5.87	5.90	8.96	8.94
	Power Price *PP*	€ kW^{-1}	35.16	50.54	18.72	23.80
	Basic Price *BP*	€	191.00	558.00	-	257.04
	Efficiency η_{DH}[269]	%			98	
	Maintenance [270]	%			1	

Table 4-7: Input parameters defining the capital costs C_{CCH} and current costs C_{CCH} of the compression chillers.

Parameter	Unit	Minimum	Mode	Maximum
Capital costs $C_{CCH\ [271–273]}$	€ kW^{-1}	125	163	200
Feasibility [253]	%		2.3	
Development [274]	%		3	
Engineering [254]	%		5	
Contingency	%		10	
COP compression chiller $COP_{CCH\ [272, 275]}$		5	6	7
Maintenance M_{CCH} [276]	%		4	
Electricity costs *EC* [258]	euro cents kWh^{-1}	16	16.5	17
Lifespan [36]	a		15	

Given the required cooling capacity of 3,080 kW, the estimated capital costs C_{CCH} of the compression chillers range between 125 and 200 € kW^{-1} [271–273]. The costs for the feasibility

study, development and engineering are defined as a certain percentage of the capital costs Table 4-7. The current costs of the compression chillers CC_{CCH} depend on the energy demand of the system and are composed of the COP_{CCH}, the electricity costs EC and the cost for maintenance M_{CCH} and replacement R_{CCH} (Eq. 4-8 and Table 4-7). The recommended depreciation period of a compression chiller is 15 years resulting in a replacement investment within the observation period of 30 years [36].

$$CC_{CCH} = \frac{ED_C}{COP_{CCH}} \cdot EC + C_{CCH} \cdot M_{CCH} + R_{CCH} \quad \text{(Eq. 4-8)}$$

Economic efficiency

The costs for electricity and district heating are both subject to an annual price increase based on the general trend of the recent years in Germany. For electricity costs, a factor of 2.7 % is considered and for district heating, an annual price increase of 0.5 % is chosen. [277]. For comparison, all current costs are discounted with an interest factor to the beginning of the observation period. The interest factor q^T is calculated with Eq. 4-9.

$$\frac{1}{q^T} = \frac{1}{(1+i)^T} \quad \text{(Eq. 4-9)}$$

$$NPV = -C_{ATES} + \sum_{t=1}^{T} R_t \cdot q^{-1} \quad \text{(Eq. 4-10)}$$

T is the payment date with $T \geq 0$. $T = 0$ being the beginning of the investment of both technologies. The discount rate, defined as i, is set at 5 %. The net present value NPV of the investment is defined as the present value of the net payments of an investment at the time $t = 0$. The NPV is calculated from the sum of the present value of all revenues and the present value of all expenses within the observation period [270]. In the present study, the revenues are the total costs of the reference technology, while the expenses are the total costs of the ATES system Figure 4-4. The NPV is calculated using Eq. 4-10 with C_{ATES} being the capital costs of the ATES. R_t is the return at the time t, which results from the difference between the current costs of the ATES system and the reference technology. The investment in an ATES

system is beneficial towards the investment in the reference technology if the *NPV* of the ATES system is positive.

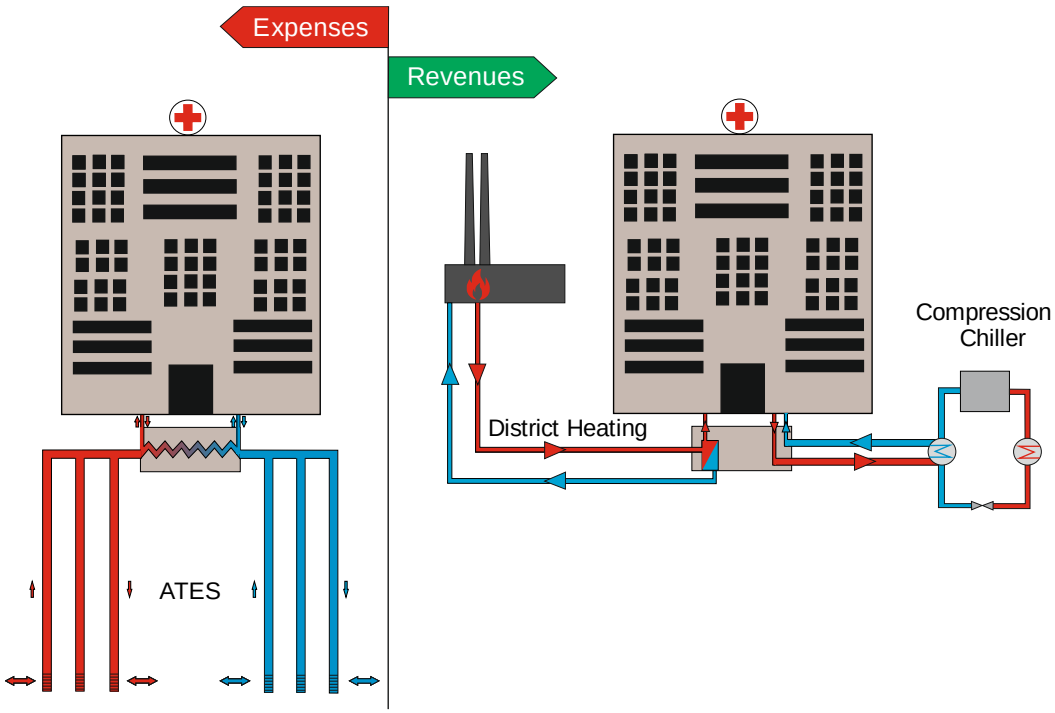

Figure 4-4: ATES system and the compared reference technologies of the municipal hospital of Karlsruhe.

Environmental analysis

The environmental analyses of the ATES system and the reference technology are based on their annual CO_2 emissions *CE* resulting from operation. The particular CO_2 emissions are calculated as follows:

$$CE_{ATES} = E_{ATES} \cdot EF_{el} \quad \text{(Eq. 4-11)}$$

$$CE_{ref} = E_{CCH} \cdot EF_{el} + ED_{DH} \cdot EF_{DH} \quad \text{(Eq. 4-12)}$$

Here E is the annual electricity consumption of the particular technologies and ED_{DH} is the district heating demand based on E_{DH} and η_{DH}. EF_{el} and EF_{DH} are the emissions factors for electricity and district heating, summarized in Table 4-8.

Table 4-8: CO_2-emission factors for district heating and electricity supply.

CO_2 emission factor	Unit	Minimum	Mode	Maximum
Electricity [278, 259]	t MWh^{-1}	0.357	0.417	0.476
District heating [259, 279]	t MWh^{-1}	0.068	0.10	0.24

4.3 Results and discussion

The result of the Monte Carlo simulation for the capital costs of the ATES system after 100,000 iterations is presented in Figure 4-5, showing a normal distribution with a mean value of €1.285 (± 0.08) million.

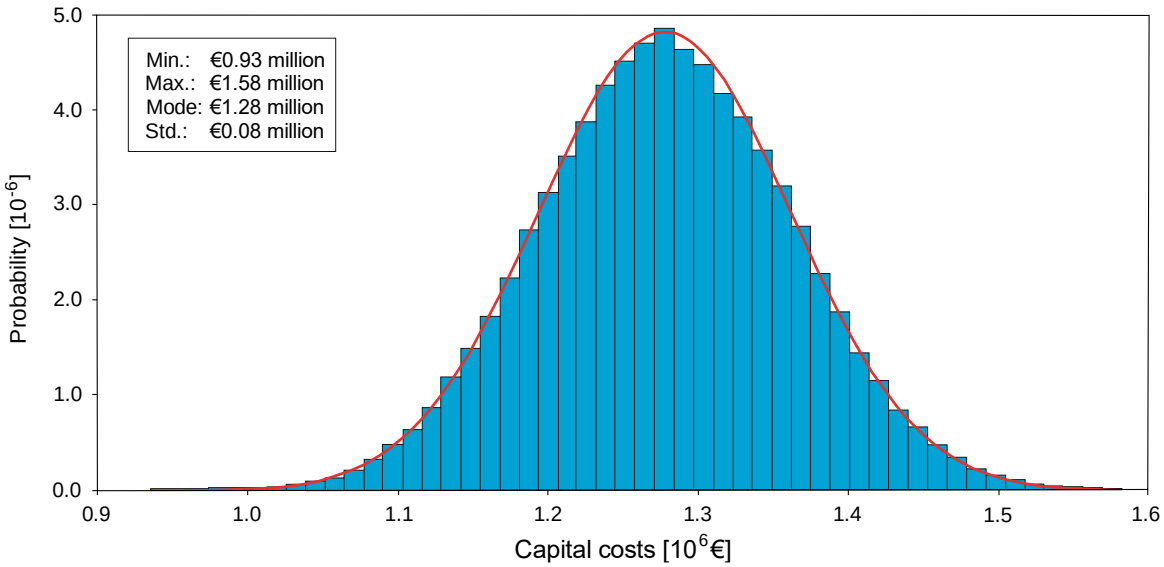

Figure 4-5: Probability distribution of the capital costs of the studied ATES system.

The major cost factor of about 60% is associated with the underground part consisting of six wells, pipes and groundwater measuring points. The part of the ATES system above the ground includes the building integration (heat pumps and heat exchanger) and contributes to 23 % of the capital costs. The remaining 15 % of the capital costs belong to the pre-investigations and the construction site installation. The capital costs are dominated by well piping and well installation (Figure 4-6). The pricing level is dependent on the service provider and the quality of the installed components. Higher costs for well piping and installation could increase the capital costs by more than 10 %.

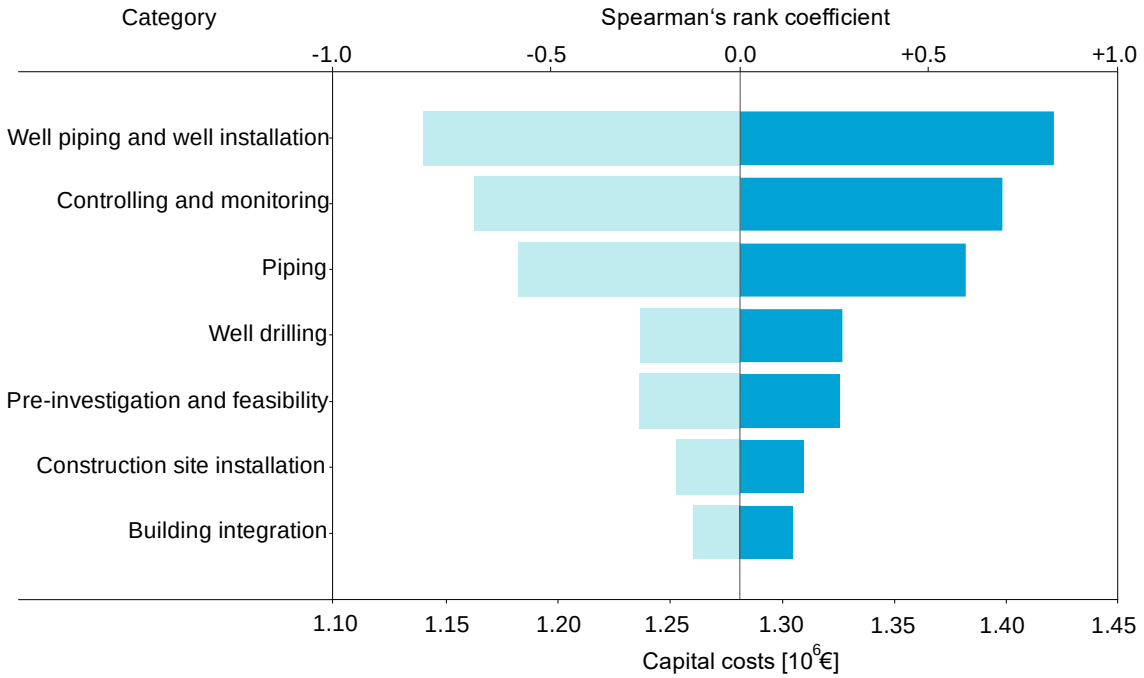

Figure 4-6: Spearman's rank coefficients representing the degree of correlation between the input parameters of the different categories to the variance of the capital costs. The relative importance of the single categories of the ATES system on the capital costs is also illustrated.

Thus, the planner of an ATES system should carefully choose the components for the implementation of the wells according to actual requirements. Controlling and monitoring are also significant factors when taking into account the capital costs. Accurate monitoring is crucial to assure an efficient, long-term operation of an ATES system [222]. The building integration, including heat pumps and heat exchanger, is less sensitive to the capital costs. However, the performance of the heat pump is particularly significant to the efficiency of the ATES system and therefore to the current costs as discussed in the subsequent chapter.

Comparison

The ATES system and the reference system differ in terms of their cost structures as illustrated in Figure 4-7. The ATES system is the more capital-cost-intensive technology with one-quarter of the total costs made up by the capital. For both systems, the largest portion of the total costs is attributed to the heating supply of the building. The difference is that the heat pumps and submersible pumps of the ATES system operate with electricity and the reference system uses district heating with coal and crude oil as primary energy source. The electricity consumption of the heat pump, defined by the COP, is the most significant parameter regarding the cost-effectiveness of the ATES system. Figure 4-7 clearly shows a substantial difference between

the electricity costs for cooling. The operation of the submersible pumps of the ATES system represents only 5 % of the total costs, while the electricity costs for the compression chillers of approximately 30 % are the second largest for the reference system.

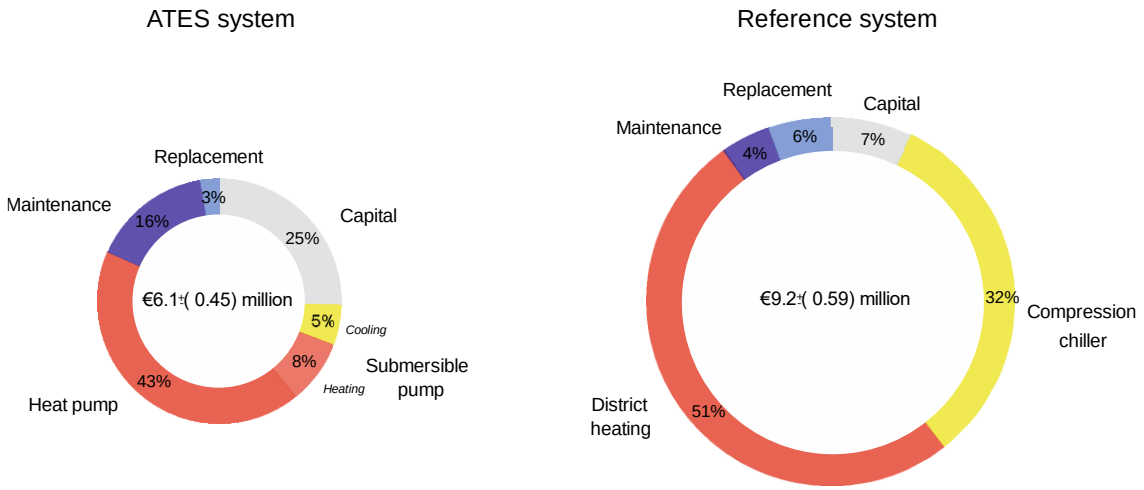

Figure 4-7: Comparison of the relative structure of the total costs of the ATES system and the reference system after 30 years of operation.

The maintenance of the ATES system requires more effort and strongly depends on the number of wells and the hydrochemical conditions of the aquifer [10]. Figure 4-8a-c compares the capital and current costs of the ATES system and the reference technology of the hospital over an observation period of 30 years. The comparison is carried out for the ATES operating as a hybrid system as well as for cooling and heating purposes only. The beginning of the investment is the year zero. The estimated capital costs of the reference technology are €667,000 (± 119,000) which is about 50 % lower than the capital costs of the ATES system. The expected additional specific capital costs for the ATES system amount to 192 (± 12) € kW^{-1}. This is consistent with the range given by Chant and Morofsky [236] for higher specific capital costs of ATES systems, which is between 130 and 265 € kW^{-1}, compared to common supply technologies. The implementation of ATES potentially leads to mean energy savings of 3,500 MWh or 76 % compared to the reference technology. An average COP of 28.5 for the subsurface installation of the ATES is calculated. Despite higher capital costs, the expected *NPV* of the hybrid ATES is €3.1 (± 1.0) million after 30 years. Thus, the investment in the ATES system is rather positively evaluated in comparison to the reference technology. The estimated saved amount of energy corresponds to the heating demand of 240 modern single-family houses or 120 hospital beds.

Table 4-9: Summary of the estimated average capital and current costs and energy consumption of ATES system and reference technology.

Parameter	**Unit**	**ATES system**		**Reference technology**	
		ATES heating	ATES cooling	DH	Compression chillers
Capital costs	k€	1,259		60	607
Electricity consumption	MWh	930	164	-	823
DH consumption	MWh			3,758	
Electricity costs	k€	153	27		136
DH costs	k€			332	
Maintenance	k€	50		0.6	24
Replacements	k€	8.5			33.0

Due to the lower energy consumption, a potential average payback time of 2.7 years is achieved. The main reason for the positive economics of the ATES system is direct cooling in summertime, which is the cheapest supply option. Compared to the compression chillers the expected annual demand-related costs are reduced by €109,000 and 80 %, respectively (Figure 4-8c and Table 4-9). Thus, the ATES system is most suitable for buildings with a large cooling demand such as hospitals or data centres. The estimated average seasonal performance factor (SPF) of the ATES system for heating is four and mainly influenced by the efficiency of the heat pumps. Since the hospital already has access to the district heating network of Karlsruhe, the economic burden of the capital costs and maintenance in relation to district heating is relatively low.

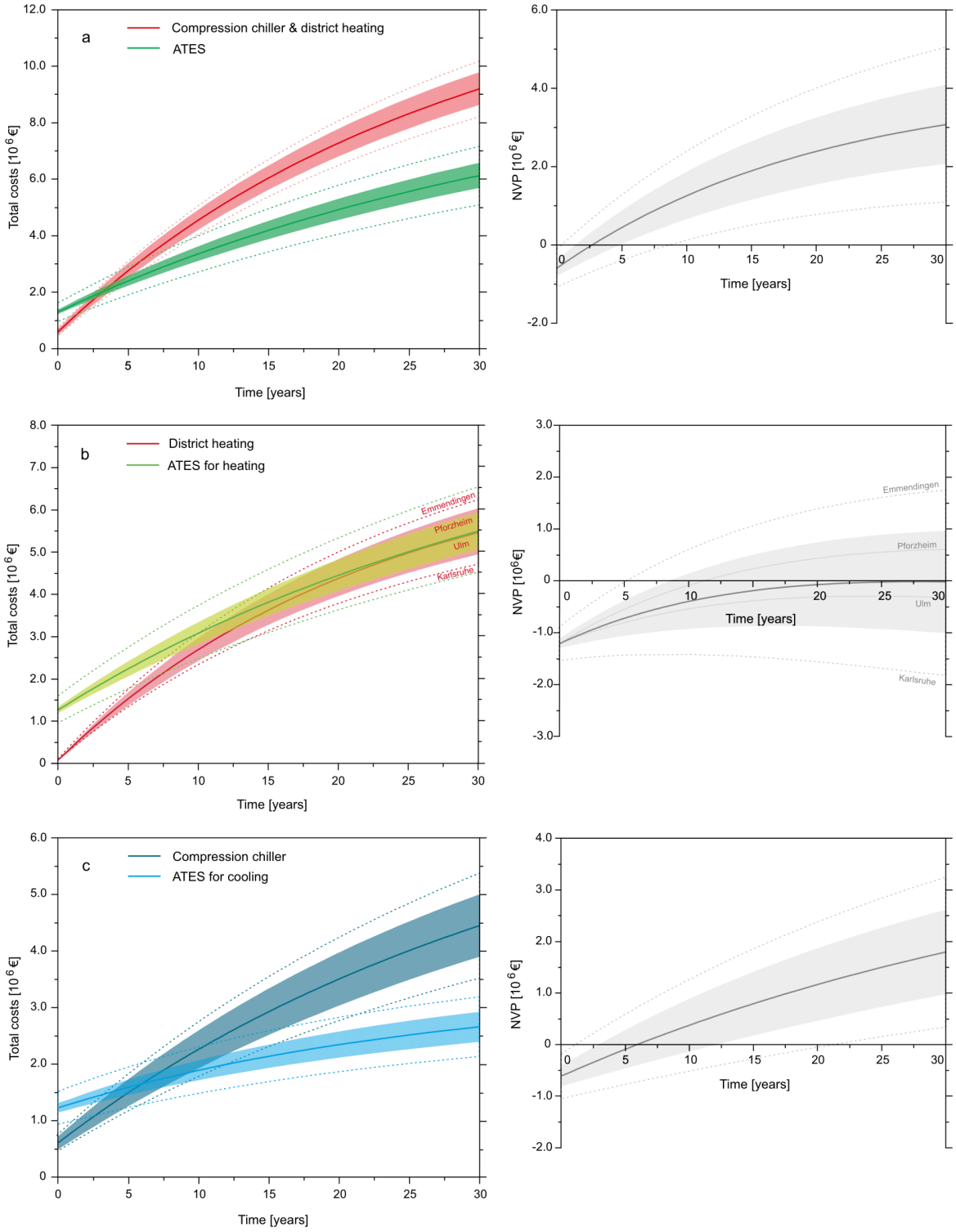

Figure 4-8: a) Economic analysis of the ATES operating as a hybrid system and the reference technologies over the observation period of 30 years divided into total costs and the *NPV* of the ATES system; b) Total costs of the ATES system only for heating supply of the building compared with district heating; c) Specific comparison of the total costs for the direct cooling supply by the ATES system and the compression chillers.

In contrast, the ATES system has extra costs for maintenance and replacement (Figure 4-7 and Table 4-9). The expected demand for district heating is over four times higher than the electricity demand of the ATES system for heating. This leads to potential mean energy cost savings of €179,000 per year. However, the economic benefit of ATES for heating is not always given due to the estimated low capital costs for district heating in the present case (Figure 4-8b). Thus, direct cooling provides most of the economic benefit of the ATES compared to the reference technology.

The input parameters of Table 4-6 and Figure 4-8b show a large variation of the demand-related costs for district heating. Depending on region and provider, the district heating costs range between €285,000 and €379,000 for the same heating demand of 3,685 MWh only in the state of Baden-Württemberg. Since the district heating network of Karlsruhe is partially supplied by industrial waste heat of the MiRO (57 %), the city has a significant site-specific advantage. Consequently, the price for district heating is up to 25 % less than in other regions, deeming the ATES system for heating uneconomical in Karlsruhe. However, the situation is the opposite in the city of Emmendingen where the district heating network is supplied by power plants operating with natural gas and wood chips [280]. For this reason, the costs for district heating per year are almost €100,000 higher than in Karlsruhe for the same heating demand of the hospital. Thus, the ATES system for heating shows a payback time of 5 years in Emmendingen. It is important to note that the district heating costs can vary greatly even within small distances. Hence, it is essential to conduct a detailed cost analysis of the reference technology particularly for locations where district heating is used.

Another aspect is the future planning reliability with regard to the demand-related costs of the heating supply. The price for district heating can change rapidly within a short period of time. For example, in the city of Ulm, Germany, the commodity price for district heating varied by 27 % in 1 year alone. Consequently, the economic planning of the future heat supply via district heating is more challenging than for systems driven by electricity. In general, ATES systems and heat supply via district heating do not automatically exclude each other. The city of Neubrandenburg, Germany integrated an ATES system in a district heating network. Here the waste heat of a power plant is stored in summertime and reinjected into the district heating network in wintertime to supply residential areas [281]. This special usage is only possible for high-temperature ATES (HT-ATES) systems. Greater well depths ensure higher storage loading temperatures (e.g. 90 °C), which can supply district heating networks in Germany, typically operating with temperatures above 20 °C [282].

Comparison with realized ATES systems

The estimated specific capital costs of the considered ATES system in the present study are 416 (± 27) € kW^{-1} (Figure 4-9). The present value is consistent with the specific capital costs of various Dutch ATES systems ranging between 1,600 € kW^{-1} for small and 200 € kW^{-1} for large systems [283]. Since the present ATES can be classified as a medium-sized system after Fleuchaus et al. [45], the results of previous investigations, showing a decrease of the specific capital costs with increasing size can be confirmed [238, 283].

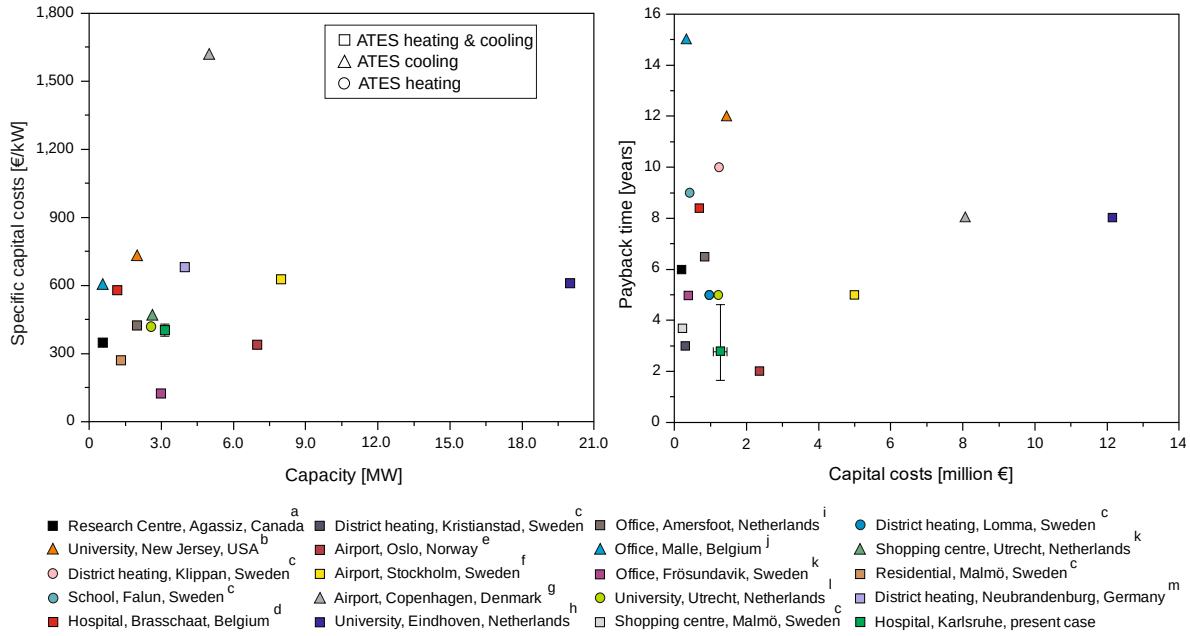

Figure 4-9: Specific capital costs, capacity and payback times of different ATES systems in operation. [a] Bridger and Allen [226], [b] Paksoy et al. [238], [c] Andersson and Sellberg [235], [d] Vanhoudt et al. [210], [e] Eggen and Vangsnes [230], [f] Wigstrand [211], [g] Baxter et al. [284], [h] Worthington [285], [I] Dincer and Rosen [221], [j] Hoes et al. [286], [k] Bakema et al. [246], [l] Sanner [282].

Thus, it can be stated that the Monte Carlo simulation is an appropriate method to estimate the capital costs of ATES systems. However, most of the specific capital costs of the 14 ATES systems (0.43–20 MW) in Figure 4-9 are higher. In addition, Figure 4-9 does not show the relation between decreasing specific capital costs and increasing capacity, which is due to several reasons. Some ATES were built together with scientific partners during research projects with less focus on economics (Agassiz, New Jersey, Utrecht, Eindhoven). Others are integrated into district heating networks (Neubrandenburg), resulting in deeper wells. The high sensitivity of the well construction to the capital costs (Figure 4-6) is therefore also derivable

from Figure 4-9. For instance, the ATES for heating and cooling of the Copenhagen airport has specific capital costs of 1,600 € kW^{-1}, which could result from the rather large depths of 110 m of 10 installed wells [284, 202].

The expected average payback time of 2.7 years of the present study is less than the estimated average payback time of 7 years of the 16 ATES illustrated in Figure 4-9. However, it is important to mention that the payback times in the literature are often discussed without mentioning the reference technology. Some of the ATES in Figure 4-9 with payback times higher than 8 years are among the very first systems implemented during the 1980s and early 1990s (Utrecht, Klippan, Falun) or are related to research projects (Agassiz, New Jersey). Lack of experience and focus on scientific issues could lead to a less efficient operation, resulting in higher payback times. Figure 4-8 demonstrates that the hybrid ATES of the present study has shorter payback times than the ATES only for heating and cooling. Figure 4-9 confirms this result and shows that hybrid ATES systems potentially have much lower payback times with an average of 5.6 years compared to the two Swedish ATES for heating or the ATES systems used exclusively for cooling. In addition, the maximum payback time of all of the hybrid ATES systems in Figure 4-9 is 8.4 years (Brasschaat, Belgium), which strongly corresponds with the estimated maximum payback time of 8.7 years of the present study. The ATES for heating and cooling of the Klina hospital in Brasschaat, Belgium, has a capacity of 1.2 MW and is a rare example of an ATES which is comprehensively described in the literature [287, 286, 210]. Thus, this ATES is compared in more detail with the ATES of the present study (Table 4-10).

The specific capital costs of the ATES in Belgium are 580 € kW^{-1} and 28 % higher than the estimated specific capital costs in the present study. This is almost equivalent to the reverse ratio of the number of wells with two in Braasschat and six in the present study. This again confirms the large sensitivity of the well construction to the capital costs. In total, the ATES of the Klina hospital saves 85 % of energy compared to gas boilers and cooling machines. This is 9 % more than the ATES in the present study, mostly resulting from the lower estimated SPF of the reference cooling machines in Belgium. Assuming that the compression chillers of the present study have the same COP, the percentage share of saved energy (88 %) by the ATES is almost equal to the Belgium ATES. This shows that the economic comparison in the present study between the ATES for cooling and the compression chillers is a rather conservative approach.

Table 4-10: Comparison of the most important parameters defining the ATES system of the Klina hospital in Belgium [210] and the ATES system of the present study.

	Parameter	Unit	ATES present study	ATES Klina hospital
General	Capital costs	k€	1,258 (± 80)	695
	Capacity	MW	3.0	1.2
	Number of wells		6	2
	Well depths	m	35	65
	Temperature difference	K	4	~ 10
	Electricity costs	ct kWh^{-1}	16.5 (± 0.5)	11.0
Heating	Demand	MWh	3,685	1,335
	Efficiency	-	3.6 - 4.4 (COP)	5.9 (SPF)
	Costs reference technology	ct kWh^{-1}	8.83 (± 1.26)	Gas boiler (3.50)
	Energy savings	%	75.0	85.6
Cooling	Demand	MWh	4,800	1,335
	Efficiency	-	29 (COP)	26 (SPF)
	Efficiency reference technology	-	5.0 – 7.0 (COP)	Cooling machines (SPF 3.5)
	Energy savings	%	80	87

Thus, ATES for cooling can potentially save more energy compared to compression chillers resulting in an even better economic viability. However, the present study shows that even though the efficiency of compression chillers will improve in the future, ATES for cooling is still more economical. Despite larger relative savings of energy, the payback time of the ATES in Belgium is higher than the average payback time in the present study. This mainly results from the low heating costs of the reference gas boiler system, despite an efficiency of only 85 % and the relatively high capital costs for this specific ATES system as shown in Figure 4-9. Transferred to the heating demand of the hospital in the present study, the demand-related costs of gas boilers under Belgian conditions are €130,000 (46 %) lower compared to the district heating in Karlsruhe. Considering the current gas price in Karlsruhe of 5.2 euro cents kWh^{-1} [288], gas-driven heat pumps for ATES systems can also be considered from an economic perspective, however, not from a perspective of sustainability.

ATES systems in practice

The design of an ATES system can deviate strongly from the approach of the present study depending on the local conditions. In contrast to the present study, the large imbalance between the extracted and reinjected heating and cooling energy can be a major issue in practice. The much larger cooling demand of the building (Table 4-1) can result in a successive temperature increase of the aquifer after some periods. This could lead to conflicts with water authorities or neighbouring installations as well as to a significant loss of efficiency, mainly in terms of direct cooling. If the aquifer temperature becomes insufficient for direct cooling, additional cooling machines must be activated which greatly increases the electricity consumption and demand-related costs of the system. To compensate for the larger amount of heat energy in the injection well as a result of the higher cooling demand, additional installations such as cooling towers, recooling plants, heat pumps or air handling units are used [26, 210, 238, 289].

Another approach to achieve thermal balancing is night ventilation of a building. This reduces the cooling demand on the ATES which results in a decreased quantity of heat injection [290]. However, most of these measures are related to additional expenses, which are not considered in the present study. In contrast to the present study, ambient temperatures and heating and cooling demands can vary within a short period of time. To comprehensively understand the impact of energy demand variations or hydrogeological changes in the subsurface on the economic performances of ATES, more simulations tools should be used in the future. Since ATES is a rather slow-acting system, additional supply technologies also for peak loads are needed. Thus, buildings often partially use ATES in combination with compression and/or absorption chillers for cooling and boilers and/or CHP systems for heating [291, 292].

Experience from other countries shows that adjustments from the authorities allow the number of LT-ATES installations to grow [45]. In the Netherlands, a hospital similar to that in the present case is less restricted by authorities and would perhaps have decided otherwise. Future ATES projects can only be successfully implemented in Germany if the responsible housebuilder, technical building planners, building technicians, as well as public and local water authorities closely cooperate in the early stages of the planning process. Furthermore, an extensive and permanent system to monitor the subsurface installation and the building connection is an important factor for ATES systems ensuring the long-term and sustainable operation of the systems as assumed in the present study.

Environmental analysis

Figure 4-10 illustrates the CO_2 emissions of the different supply technologies estimated with Eq. 4-11 and Eq. 4-12. The replacement of the reference technology with the ATES systems for heating and cooling results in an expected average CO_2 emission savings of 262 t year^{-1} (36 %). Considering the observation time of 30 years, 7,854 t CO_2 could potentially be saved. The defined CO_2 savings of the present study are within the range of CO_2 savings of ATES systems in the Netherlands, varying between 150 and 1,500 t year^{-1} [45]. However, much higher amounts of CO_2 savings are feasible. The ATES system for the heating and cooling of the University of Technology in Eindhoven with a capacity of 20 MW achieves CO_2 emissions savings of 13,000 t year^{-1} [283, 285].

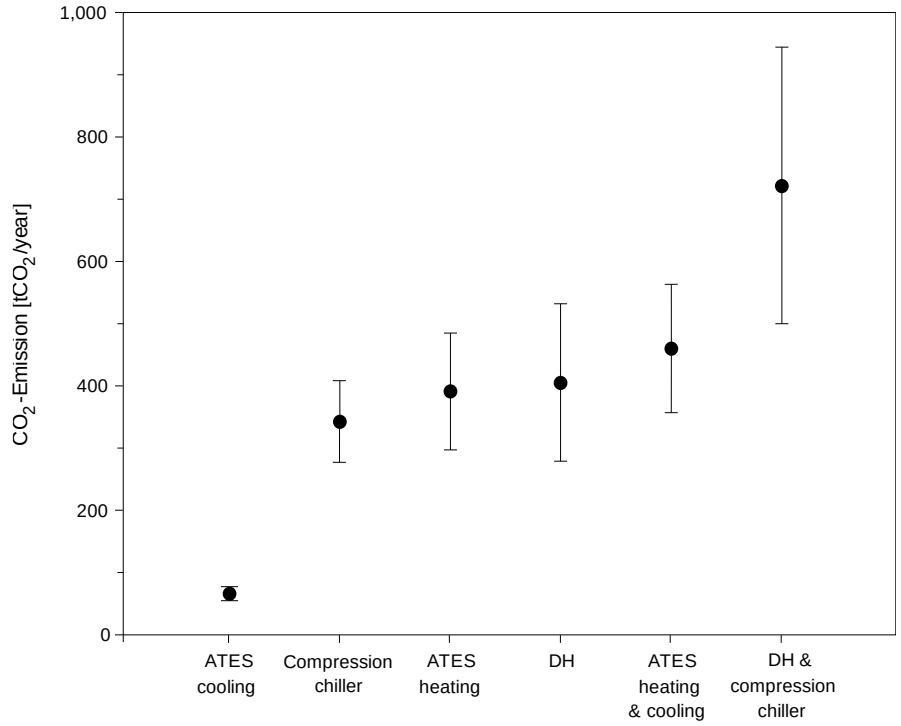

Figure 4-10: Annual CO_2 emissions of the compared technologies for the heating and cooling supply of the hospital building.

The relative CO_2 savings for direct cooling compared to the compression chillers are equivalent to the energy savings. Both systems are driven by electricity and therefore have the same emission factor. Per m^3 of pumped groundwater for direct cooling, approximately 0.27 kg of CO_2 is saved. District heating has a low emission factor at the studied site and can therefore compete with renewable energies. Thus, the relative amount of saved energy does not always

correlate with the percentage of CO_2 savings. However, it is important to consider that the environmental evaluation excludes the CO_2 emissions resulting from the heat sources of the district heating. A life cycle assessment (LCA) would provide a more detailed and comprehensive analysis of the potential environmental benefits of the ATES system. Depending on the replaced system and the emission factor, most of the ATES systems discussed in the literature save around 60 % of CO_2 emissions during operation [238, 292]. Based on the studied literature, ATES systems, which save less than 60 % of CO_2 emissions, are compared with reference technologies associated with a lower emission factor than the emission factor of electricity.

Considering the environmental damage caused by CO_2 emissions, even more costs can be saved by the implementation of ATES. According to the Federal Environmental Agency, 1,000 kg of emitted CO_2 cause environmental damages of €180 [293]. In the context of our results, the replacement of the reference technology with the ATES potentially reduces the environmental damages by €1.4 million after 30 years of operation. Converted to the supplied energy in the present study, the ATES causes expected environmental damages of 0.007 euro cents kWh^{-1}, which is half the amount produced by wind energy (0.014 euro cents kWh^{-1}) and only a small fraction of the environmental damages of lignite-based electricity of 20.81 euro cents kWh^{-1} [293].

4.4 Conclusion

Decision-makers and stakeholders should be aware of the composition of the capital costs with the main expenses of 60 % related to the underground section of the ATES system. The expected payback time of the present study (2.7 years) and other ATES systems (less than 10 years) should raise the awareness of the potential economic benefits of ATES despite higher capital costs. The most efficient usage of ATES is for both the heating and cooling supply of a building. Thus, we recommend ATES operating as hybrid systems for heating and cooling particularly in countries where ATES is not yet common. However, since the economic competitiveness of ATES regarding sustainable technologies has not yet been examined in detail, further comprehensive analyses are needed. In the long-term, the number of installed ATES will only increase, if there are economic benefits, higher reliability and wide social acceptance compared to competing renewable technologies. In addition, further studies should be performed to fully understand the benefit of ATES towards open geothermal systems such as groundwater heat pump (GWHP) systems without active storage, which are already

frequently used in Germany. For this reason, important parameters such as ΔT as well as the different flow temperatures of the heat pumps between ATES and GWHP systems need to be studied in more detail. Additionally, monitoring and evaluation of ATES systems already in operation need to be improved and intensified with focus on injection and extraction temperatures, performance of the submersible pumps, volume flows, efficiencies of the heat pumps as well as efforts for maintenance. Thus, site-specific parameters instead of generic values could lead to higher reliabilities and better transparencies of techno-economic analyses of ATES systems. Finally, as many large buildings such as hospitals are likely to require more cooling than heating supply, the effects of larger cooling demands of buildings on the economics of ATES and associated preventing measures should be investigated.

Acknowledgments

The authors would like to thank Roland Stindl, environmental representative of the municipal hospital of Karlsruhe, for providing us with helpful information about the hospital. The helpful comments of the two reviewers are also gratefully acknowledged.

Chapter 5

Uncertainty analysis of wireless temperature measurement in borehole heat exchangers

Reproduced from: Schüppler S, Zorn R, Steger H and Blum P (2021) Uncertainty analysis of wireless temperature measurement (WTM) in borehole heat exchangers. Geothermics 90. doi: 10.1016/j.geothermics.2020.102019.

Abstract

The reliability of temperature measurements in open and closed geothermal systems is closely related to their design, quality control and performance evaluation. Thus, wireless and miniaturized probes providing highly resolved temperature profiles in borehole heat exchangers (BHEs) experience a growing interest in research. To ensure quality assurance and reliability of these emerging technologies, errors and uncertainties relating to wireless temperature measurements (WTMs) must be determined. Thus, we provide a laboratory analysis of random, systematic and dynamic measurement errors, which lead to the measurement uncertainties of WTMs. For the first time, we subsequently transfer the calculated uncertainties to temperature profiles of the undisturbed ground measured at a BHE site in Karlsruhe, Germany. The resulting precision of 0.011 K and accuracy of -0.11 K ensure a high reliability of the WTMs. The largest uncertainty is obtained within the first five meters of descent and results from the thermal time constant of 4 s. The fast and convenient measurement procedure results in substantial advantages over Distributed Temperature Sensing (DTS) measurements using fiber optics, whose recorded temperature profiles at the site serve as qualitative comparison. We additionally provide recommendations for technical implementations of future measurement probes. Our work will contribute to an improved understanding and further development of WTMs.

Graphical abstract

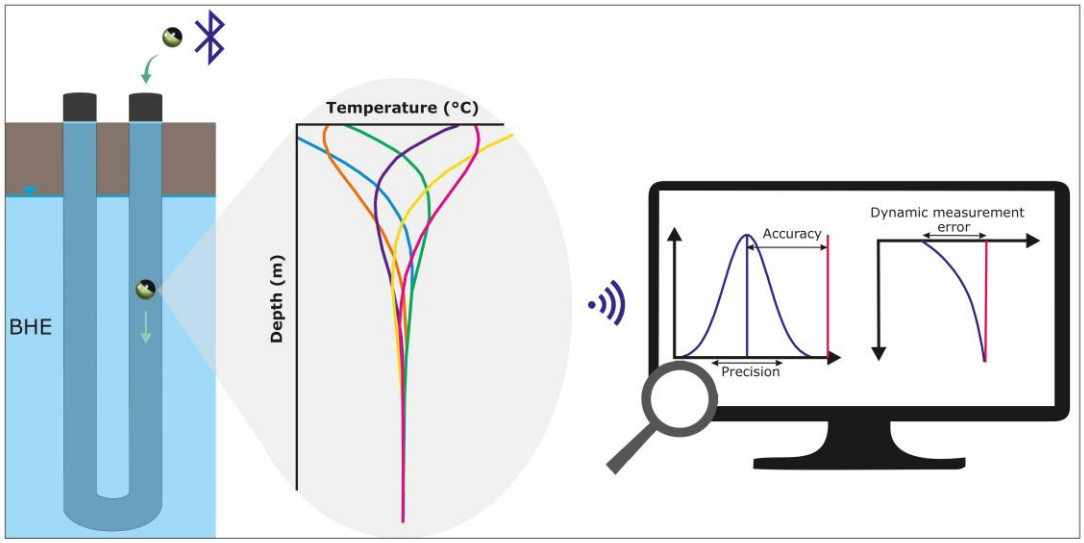

5.1 Introduction

Vertical borehole heat exchangers (BHEs) are the most common technology to extract thermal energy from the shallow underground. The standard BHE is a closed-loop U-pipe system, where a circulating heat carrier fluid transports the thermal energy from the underground to the heat pump of a building [10, 294, 52, 295, 296]. The design of a BHE mainly follows standardized procedures using commercial software [297–299], design tools [300, 301], and national guidelines [32, 302]. These different approaches all require the undisturbed ground temperature (UGT) as a design parameter. The UGT results from the thermal properties of the subsurface as well as the geothermal and surface heat flow and is defined as the ground temperature before the BHE operation [303, 304]. Although the UGT directly influences the sizing and performance of a BHE, it is probably the most overlooked parameter in the planning and design of BHEs [40, 300, 305–308]. Various analytical approaches exist for estimating the UGT as a function of time and depth [309–313]. The quality of these models strongly depends on the reliability of the collected climate and geological data [314]. However, temperature measurements at the proposed site with appropriate measurement technologies are not common.

The UGT is also an important parameter for the evaluation of thermal response tests (TRTs), which are essential for the design of large-scale BHE fields [315–317, 304]. The measurement of the UGT is performed before the start of a TRT and directly affects its accuracy [318]. Claesson and Eskilson [319] propose to measure the average UGT while circulating the heat-carrier fluid of the BHE without extraction or injection of heat. However, the pumping process significantly heats up the system resulting in an increased measured UGT [318]. Thus, measurements of vertical temperature profiles, also referred to as T-logs [320], along the entire length of a borehole evolved as an increasing research focus in recent years. Meanwhile, the measurement of undisturbed and disturbed T-logs in BHEs is mostly carried out over the course of distributed and enhanced thermal response tests (DTRT/ETRT) [41]. This is based on distributed temperature sensing (DTS) using fiber optic and hybrid cables [321–326]. Alternative devices to fiber optic cables are wired data loggers, which are either manually [318] or automatically [327, 328] lowered into a BHE. Raymond et al. [329] for instance, manually lowered a wired data logger with a measurement frequency of 1 Hz into two BHEs to measure undisturbed T-logs at the site of Saint-Lazara, Canada. The measured T-logs allowed conclusions on the geothermal gradient and seasonal temperature variations at the site.

However, the small diameter of a BHE pipe generally limits the selection of suitable measurement technologies for T-logs.

Moreover, the measurement of T-logs, particularly when carried out with fiber optics, are time-consuming, cost-intensive, and require cumbersome handling, while wired data loggers unintentionally displace the fluid in the BHE [329]. In addition, strongly twisted or inclined BHEs can produce a discrepancy between the cable length of a wired logger and the actual depth of the BHE [330]. For this reason, different concepts of miniaturized wireless temperature probes were recently developed. Pioneers in the field of wireless temperature measurements (WTM) were Rohner et al. [331], who developed a cylindrical probe, later called NIMO-T, with an adjustable weight depending on the actual requirements [332]. This device records pressure and temperature at pre-selected time intervals during the descent. Bayer et al. [320] used the NIMO-T for measurements in the urban environment of Zurich, showing a relation between the perturbation of the T-logs and the lifetime of buildings and asphalted streets. Martos et al. [333, 334] introduced a spherical sensor system, containing a Pt100-sensor embedded in a polyoxymethylene (POM) shell, for T-log measurements over the course of a TRT. This probe has a density very close to the thermal fluid of a BHE and is therefore only suitable for measurements during a pumping process. Knowledge about flow rate and BHE diameter enables the calculation of the probe's velocity indicating its position in the BHE. Due to the small density difference between BHE fluid and probe, this particular device is less suitable for measurements of the UGT. Aranzabal et al. [335] further developed this sensor system and compared it with various measurement technologies including wired data loggers, fiber optics, and GEOsniff®. The latter is a spherical sensor system, which is commercially available on the market and the further development of NIMO-T [336].

Questions regarding errors and measurement uncertainties, which relate to WTMs have not yet been addressed and discussed. However, these investigations are essential for the suitability and further development of this type of probe as well as for the reliability of the recorded data. Thus, we analyze this by using the GS as a representative device for WTMs. In the following, we first describe the principle of WTMs and related basic equations. Then, we provide a quantitative analysis of statistic, random, and dynamic measurement errors by investigating their major causes under various boundary conditions. Based on this, we discuss the expanded measurement uncertainty U and evaluate its impact on the wirelessly measured UGT in BHEs. We compare them with T-logs measured with common stationary measurement technologies

including fiber optics and punctual Pt100-sensors. This allows valuable conclusions on potential optimization needs and appropriate application fields of WTMs.

5.2 Material and methods

5.2.1 Wireless temperature measurement (WTM)

In our study, we perform WTMs using the GEOsniff® (GS). Figure 5-1 shows a summary of the WTM procedure carried out with the GS. The latter has a spherical shape with a diameter of 20 mm and includes sensors for temperature and pressure. The shell protects the sensor system and is composed of two half-spheres consisting of anodized aluminum and polyoxymethylene (POM).

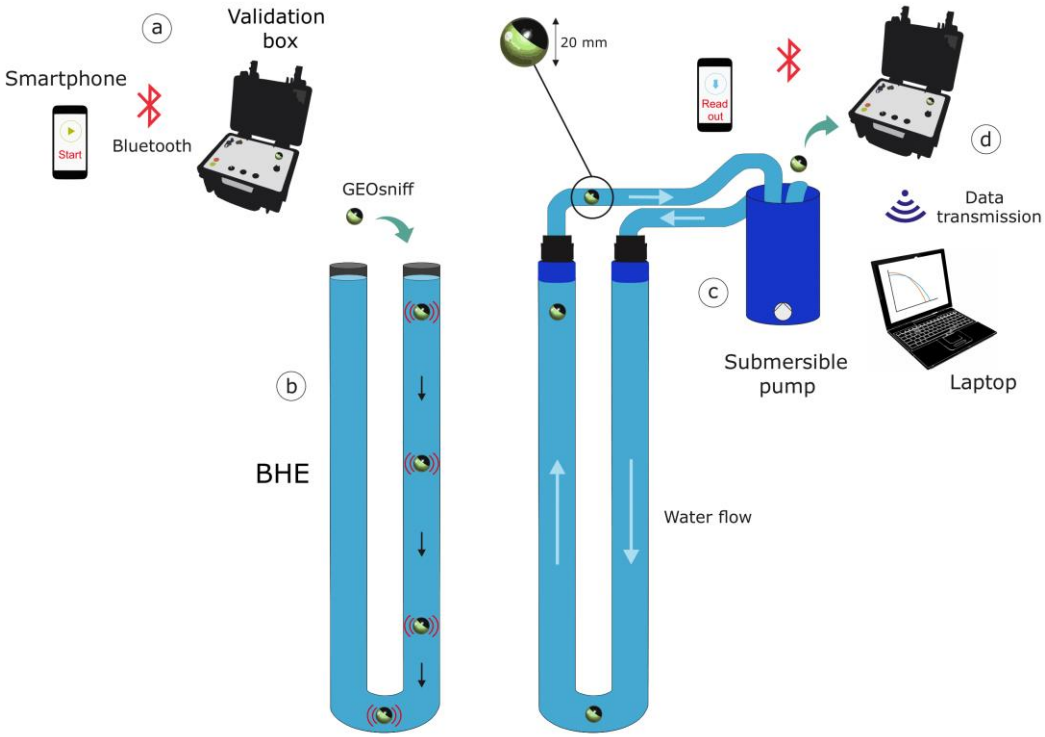

Figure 5-1: Schematic procedure of WTM by means of the GS including the most important components and steps (a-d).

The analogue sensor signals are converted into digital formats. A Pt1000-sensor [337] for temperature recording is directly integrated on the circuit board behind the outer aluminum part of the GS. Pressure and temperature resistance of the probe is 60 bar and between -25 °C to

70 °C, respectively. The usage of a smartphone is a prerequisite to control the measuring procedure via Bluetooth. The GS contains a radio-frequency identification (RFID) antenna to inductively charge the integrated capacitor via validation box (Figure 5-1a). The latter is additionally used to read out the data memory after the measurement (Figure 5-1d). The capacitor stores up to 0.602 J enabling approximately 3,200 single measurements with a selectable measurement frequency ranging between 1/30 and 8 Hz. After charging and selection of the frequency, the GS is manually inserted into one shank of the U-pipe BHE, where it sinks along the course of the BHE (Figure 5-1b). Once the GS reaches the bottom of the U-pipe BHE, a connected pumping circuit flushes the GS back to the surface (Figure 5-1c). The material parameter and technical data of the GS are summarized in Table 5-1.

Table 5-1: Material parameters and technical specifications of the GS measurement probe.

Parameter	**Unit**	**Value**
Surface GEOsniff A_{sh}	m^2	1.26×10^{-3}
Surface temperature sensor A_s	m^2	2.13×10^{-6}
Specific heat capacity aluminum c_{sh}	J kg^{-1} K^{-1}	900
Specific heat capacity sensor c_s	J kg^{-1} K^{-1}	130
Shell thickness d_{sh}	m	2.0×10^{-3}
Sensor thickness d_s	m	1.2×10^{-4}
Stored energy E	J	0.602
Shell mass m_{sh}	kg	3.0×10^{-3}
Sensor mass m_s	kg	1.70×10^{-5}
Volume shell V_{sh}	m^3	2.70×10^{-6}
Volume sensor V_s	m^3	2.73×10^{-9}
Thermal conductivity aluminum λ_{sh}	W m^{-1} K^{-1}	237
Thermal conductivity sensor λ_s	W m^{-1} K^{-1}	72
Density aluminum ρ_{sh}	kg m^{-3}	2,700

The GS and its temperature sensor with an initial temperature $T_s(0)$, equal to the ambient temperature, are immersed into the fluid at constant temperature T_f, causing a heat flow $\dot{Q}$ through the thermal resistance R_{th} [338]:

$$\dot{Q} = \frac{T_f - T_s(0)}{R_{th}} \quad \text{(Eq. 5-1)}$$

Thus, the temperature of the sensor changes as follows:

$$\frac{dT}{dt} = \frac{\Delta T(t)}{R_{th}C} = \frac{T_f - T(t)}{R_{th}cm} \quad \text{(Eq. 5-2)}$$

Here, thermal exchange $\Delta T(t)$ results from the difference between the time-dependent temperature of the sensor $T(t)_s$ and T_f while R_{th} and heat capacity C, defined by mass m and specific heat capacity c of the device, remain constant. However, considering that the temperature sensor is embedded in a protective shell, thermal coupling with the fluid initially takes place by convection through the convective heat transfer resistance $R\alpha$ of the shell of the GS [339, 340]:

$$R_\alpha = \frac{1}{\alpha A_{sh}} \quad \text{(Eq. 5-3)}$$

where A_{sh} is the effective surface area which here is equal to the surface of the sphere, and α is the heat transfer coefficient between the fluid and shell.

The dynamic performance of the temperature sensor can be described with a RC-system as summarized in Figure 5-2. The conductive inner thermal resistances relate to the temperature sensor $R_{\lambda s}$ and the surrounding shell $R_{\lambda sh}$ of the GS. The same applies to the heat capacity C. Applying Ohm's law for series connection, the entire R_{th} of the measurement sphere results from the addition of the individual resistances:

$$R_{th} = R_\alpha + R_{\lambda sh} + R_{\lambda s} = \frac{1}{\alpha A_{sh}} + \frac{d_{sh}}{\lambda_{sh} A_{sh}} + \frac{d_s}{\lambda_s A_s} \quad \text{(Eq. 5-4)}$$

where λ_{sh}, λ_s, d_{sh} and d_s are the respective thermal conductivity λ and thickness d of shell sh and temperature sensor s. When using the GS, other contributions to R_{th}, for instance, that of the thermal grease, can be neglected as a result of its insignificant d and large λ. However, we are aware that for other measurement technologies additional R_{th} must be considered.

5.2.2 Temperature calibration

Temperature calibration of the GS is carried out using a standard JULABO refrigerated/heating circulator F32. This device is used with several additional installations in order to automatically calibrate the GS (Figure 5-2). A specially written software using LabVIEW enables the control of the calibration unit and the regulation of the calibration parameters. After the inductive charging process, which follows prior to each temperature step, a motor driven chain carries the GS into the calibration liquid (ThermalG) of the circulator. The calibration range is set between – 10 and +35 °C with temperature steps of 5 K. Each GS successively passes through each temperature step with a dwell time of 300 s and 50 single measurement values in the same position of the calibration bath.

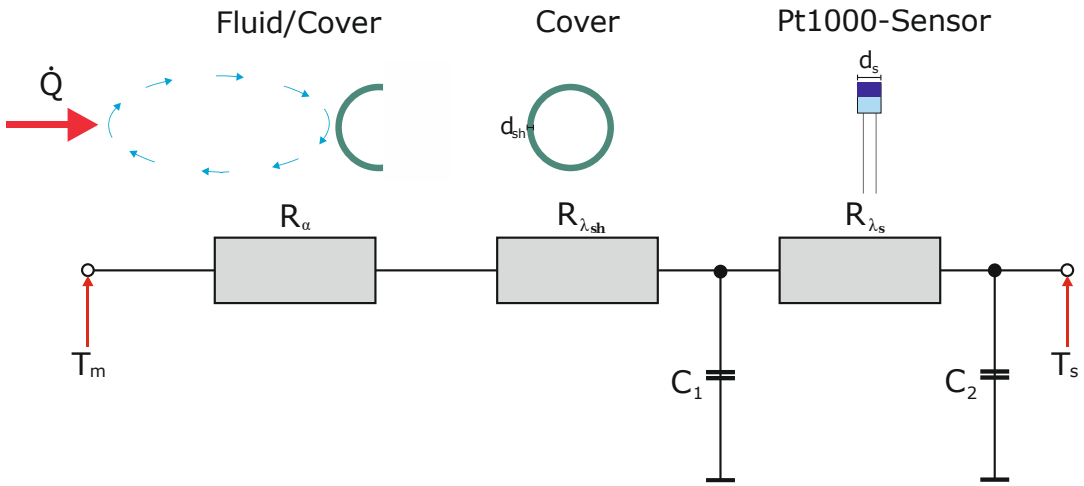

Figure 5-2: Equivalent network describing the static measurement performance of the GS. The illustrated $R_{th}s$ are connected in series and are therefore analogous to the electrical resistance and Ohm's law.

Simultaneously, the reference temperature measured with a calibrated Fluke thermometer consisting of a Pt100-sensor is recorded every second. Please note that according to the certificate of calibration, the measurement uncertainty u_1 of the reference thermometer amounts to 0.009 K in the selected calibration range while the inhomogeneity u_2 is 0.006 K. After each temperature step, the recorded data of the GS are inductively read out and stored. The calibration process considers the average values for each temperature step recorded with GS and Fluke thermometer. A fifth-degree polynom serves as calibration curve, whose six coefficients are stored and retrievable for every measurement. The GS writes the collected

calibration data directly to memory. The calibration unit enables the temperature calibration of up to 14 GSs at the same time.

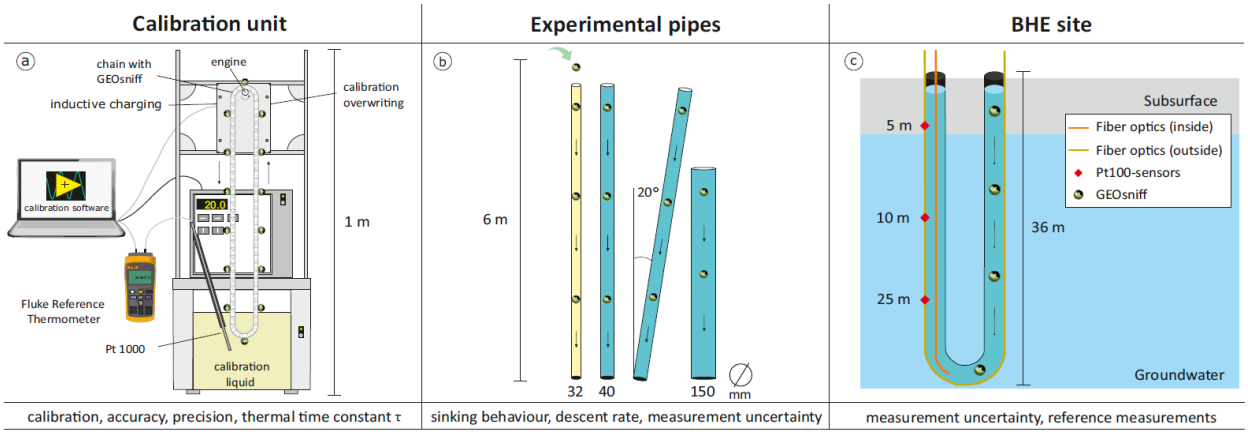

Figure 5-3: Overview of the applied methods to analyze measurement behavior, measurement errors and *U* of the GS. In the box below are the results and objectives achieved by each experimental setup.

5.2.3 Measurement error

In the following, we describe the terminologies measurement error and measurement uncertainty in detail in order to emphasize their different definitions related to WTMs.

- Accuracy is the deviation between the respective mean temperature values of GS and reference measurement technology. The closer the mean temperature value of the GS is to the reference, the higher its accuracy. Note that this temperature deviation is a correctable and systematic error. Thus, it is assumed that after the correction, the expected value of error approaches zero [341].

- The precision u_3 of the GS is the dispersion of the single measured temperature values around their mean value. Thus, it provides a measure of the uncertainty of the mean resulting from random effects [342]. Random errors follow the Gaussian distribution given by the standard deviation [343]. Accuracy and precision of the GS are both manually determined with the calibration unit (Figure 5-3a) after the calibration procedure. This is done based on 50 individual measurements for each selected temperature, which are similar to the aforementioned calibration range.

- The standard measurement uncertainty u is expressed by the standard deviation and is equal to the positive square root of the estimated variances u^2 [344]. The combined

standard uncertainty u_c is the positive square root of the sum of the estimated variances [341]:

$$u_c = \sqrt{u_1^2 + u_2^2 \dots u_n^2} \quad \text{(Eq. 5-5)}$$

Here, u_c of the WTMs consists of precision u_3 and the measurement uncertainty u_4 resulting from the dynamic measurement error of the GS, as well as measurement uncertainty u_1 and inhomogeneity u_2 of the reference thermometer [345]. The dynamic measurement error is described in more detail in the subsequent chapter.

- *U* provides a measure of the uncertainty of WTMs, defining an expected interval about the measurement results [344]. This is obtained by multiplying u_c with a coverage factor *k*, which is set at two. By applying the Gaussian distribution, the interval has a level of confidence of approximately 95 % [344].

The insertion of the GS in the fluid filled BHE relates to an unintended thermal input, which causes a thermal deviation in the fluid of the BHE. If the initial temperature of the GS T_{GS} differs from the temperature of the BHE fluid T_f, a mixing temperature *Tmix* between GS and BHE fluid occurs after thermal equilibrium. T_{mix} is determined by considering that the sum of heat quantities received by fluid and GS is vanishing:

$$m_f c_f (T_{mix} - T_f) + m_{GS} c_{GS} (T_{mix} - T_{GS}) = 0 \quad \text{(Eq. 5-6)}$$

where m_f, c_f and m_{GS}, c_{GS} are the respective mass and specific heat capacity of GS and BHE fluid. As it is more convenient, we consider to choose the mass of the fluid given by the filling volume of the BHE and the density of the fluid for a certain time interval of descent of the GS. The relation of Eq. 5-6 enables the determination of *Tmix*, also known as the Richmann's mixing rule equation [346], as follows:

$$T_{mix} = \frac{c_f m_f T_f + c_{GS} m_{GS} T_{GS}}{c_f m_f + c_{GS} m_{GS}} \quad \text{(Eq. 5-7)}$$

However, before the GS is inserted the initial temperature of the BHE fluid is unknown. Thus, we approximately consider the average fluid temperature of the chosen time interval of descent and use the first recorded value of T_{GS} as we expect that sensor and shell of the GS have still

the same temperature at this stage. This relation determines the relative measurement error *X* resulting from the thermal input of the GS:

$$X = \frac{T_{mix} - T_f}{T_{GS} - T_f} \quad \text{(Eq. 5-8)}$$

The conversion of stored electric energy *E* into thermal energy over *t* after Joule's law causes another potential measurement error. The absolute temperature change is covered as follows:

$$X = \frac{E}{\alpha A_{sh} t} \quad \text{(Eq. 5-9)}$$

Potential measurement errors due to the residual heat of the capacitor arising from the charging process in accordance with Joule heating are not considered. However, we anticipate that the available time from charging to insertion of the GS in the BHE is sufficient to cool the probe, especially because the charging current can be considered as low. This is assured by reviewing the first measurement values of the GS before the insertion in the BHE.

5.2.4 Dynamic properties of WTMs

Dynamic measurement error

The usage of wireless temperature probes in BHEs implies dynamic temperature measurements caused by varying temperatures during the descent of the probe. Due to a certain delay, resulting from the time the sensor requires to reach thermal equilibrium with T_f, a dynamic measurement error $\Delta T_{dyn}(t)$, arises, defined as [347]:

$$\Delta T_{dyn}(t) = T_s(t) - T_f \quad \text{(Eq. 5-10)}$$

The thermal equilibration process of the temperature sensor after the insertion of the GS in the fluid, causing a step-like response, is defined as the transfer function *h(t)* [348]:

$$h(t) = \frac{T_s(t) - T_s(0)}{T_f - T_s(0)} \quad \text{(Eq. 5-11)}$$

$T_s(t)$ equalizes with T_f over time, until $h(t)$ amounts to 1. Figure 5-4 shows an example of $h(t)$ for the cooling procedure of the GS. The velocity of thermal equilibration, also named as response speed of a sensor [349] is characterized by the thermal time constant τ. The latter is defined as the time the temperature change of the sensor reaches 63.2 % of the target temperature, which is equal to the time the transfer function $h(t)$ reaches the value 0.632 as defined in Eq. 5-11 The smaller the τ, the more closely the sensor follows the temperature change of the measured medium [350]. After five times τ, the temperature sensor of the GS reaches 99.3 % of the target temperature (Figure 5-4). Based on Figure 5-2, τ mainly depends on C and R_{th} of the shell and temperature sensor of the GS probe. Bernhard [339] delivers an appropriate equation for the calculation of τ of the GS probe:

$$\tau = R_{th}C_s + R_{\lambda sh}(C_s + C_{sh}) + \frac{C_s + C_{sh}}{\alpha A_{sh}} \qquad \text{(Eq. 5-12)}$$

By the substitution of the occurring R and C with the relation of Eq. 5-4 , Eq. 5-12 becomes:

$$\tau = \frac{d_s}{\lambda_s A_s} c_s m_s + \frac{d_{sh}}{\lambda_{sh} A_{sh}} (c_s m_s + c_{sh} m_{sh}) + \frac{c_s m_s + c_{sh} m_{sh}}{\alpha A_{sh}} \qquad \text{(Eq. 5-13)}$$

Considering the descent of the GS in the BHE fluid, α is approximately determined as follows:

$$\alpha = 2100\sqrt{v} + 580 \qquad \text{(Eq. 5-14)}$$

where v is equal to the descent velocity of the GS in the BHE fluid. In the calibration liquid v corresponds to the flow velocity of the moving fluid with an estimated value of 0.4 m s^{-1}. Given the specific design of the GS, τ of the shell is of particular interest [339]:

$$\tau = c_{sh} m_{sh} R_{sh} = c_{sh} \rho_{sh} V_{sh} \left(\frac{d_{sh}}{\lambda_{sh} A_{sh}} + \frac{1}{\alpha A_{sh}} \right) \qquad \text{(Eq. 5-15)}$$

By replacing the shell parameters with those of the temperature sensor (Table 5-1), the same equation can be used to obtain τ only of the integrated temperature sensor. The relation between $h(t)$ and τ is defined as follows [339]:

$$h(t) = 1 - e^{\frac{-t}{\tau}} \qquad \text{(Eq. 5-16)}$$

Substituting *h(t)* with the relation of Eq. 5-11 enables the calculation of $T_s(t)$:

$$T_s(t) = T_f - T_s(0)\left(1 - e^{\frac{-t}{\tau}}\right) + T_s(0) \qquad \text{(Eq. 5-17)}$$

However, T_f over the entire length of the BHE is unknown. Thus, we introduce the parameters $T_{s(1)}$ and $T_{s(2)}$, which represent temperature values of two consecutive measurement points of the GS. The difference between $T_{s(2)}$ and $T_{s(1)}$ shows the temperature change during the travelled distance and passed time between two measurement points. Considering Eq. 5-13 and its relation to Eq. 5-10 enables the interpolation of the measured temperature value to its nominal value. Here, the nominal value is equal to the target temperature, which is the asymptote of *h(t)* (Figure 5-4). However, since the GS is exposed to varying temperatures during the descent in the fluid, the nominal value corresponds to the maximum deviation of an insufficient measurement time, here equal to $\Delta T_{dyn}(t)$:

$$\Delta T_{dyn}(t) = \frac{T_{s(2)} - T_{s(1)}}{(1 - e^{\frac{t}{\tau}})} \qquad \text{(Eq. 5-18)}$$

Here, the measured value $T_{s(2)}$ and the sum of $\Delta T_{dyn}(t)$ and $T_{s(2)}$ form the upper and lower limits *a* and *b* of an interval *I* in which the value is located with equal probability, which is also referred to as uniform probability distribution. Thus, we assume that the expected value is the midpoint of *I* after JCGM [341] and calculate the resulting standard uncertainty u_4 by applying Eq. 5-19 derived from and modified after Eurachem [342] and Taylor et al. [344]:

$$u_4 = \frac{(a-b)}{2}\frac{1}{\sqrt{3}} = \frac{\Delta T_{dyn}(t)}{2}\frac{1}{\sqrt{3}} \qquad \text{(Eq. 5-19)}$$

We additionally perform an experimental determination of τ. This is manually done with the similar device and the temperature steps as used for the calibration of the GS (Figure 5-3a). Here, the dwell time is 500 s and the measurement frequency of the GS is set at 1 Hz.

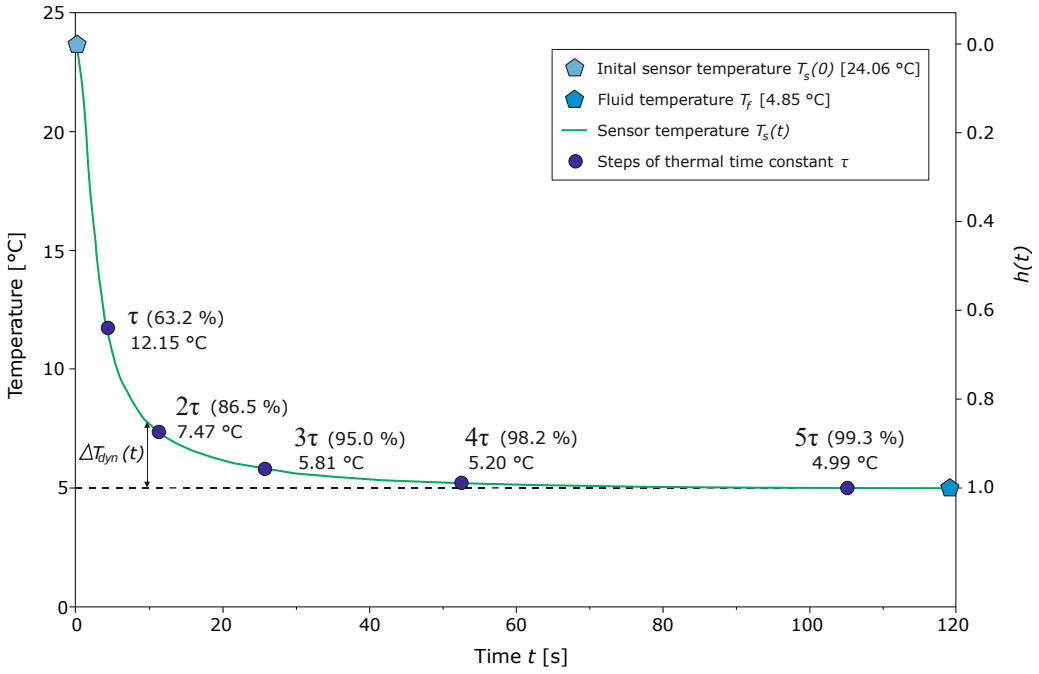

Figure 5-4: Transfer function *h(t)* during the immersion of the GS in the fluid of the calibration unit.

Descent experiments

Figure 5-4 and Eq. 5-18 emphasize the time dependence of $\Delta T_{dyn}(t)$. Thus, we perform various descent tests under different laboratory conditions to determine the effects of descent behavior and rate of the GS on $\Delta T_{dyn}(t)$ and U (Figure 5-3b). For this purpose, we use two single pipes with a length of six meters each and outer diameters of 32 mm and 40 mm, which are the most commonly used diameters of U-pipe BHEs in practical applications [351, 352]. The pipes are filled with water diluted with different shares of antifreeze to observe the effects of varying density ρ and dynamic viscosity η on the descent velocity. The antifreeze is a commonly used concentrate (Vollmer N) consisting of monoethylene glycol and corrosion inhibitors with ρ of 1.11 g cm^{-3} and η of 21 Ns m^{-2}. The chosen amount of antifreeze ranges between 5 and 25 vol%, the latter being the maximum permissible share of glycol in Germany [353–355]. In addition, we use a 150 mm transparent pipe to compare the free descent of the GS without touching the inner pipe walls. Installed U-pipe BHEs sectionwise have inclination angles causing a deviation from its vertical axis. Thus, we additionally perform descent tests with pipes of varying inclination angels from 5 to 20°.

5.2.5 Site

The undisturbed T-log measurements in the field are carried out in a water-filled U-pipe BHE with a diameter of 32 mm. The site is located in Karlsruhe, Germany. The BHE, which is installed without backfilling in unconsolidated sediments, mostly consisting of sand and gravel, has a depth D of 35.6 m and a filling volume V_{BHE} of 1.9×10^{-2} m^3. The average groundwater depth is 6 m below the surface. The BHE is not yet connected to a building and is therefore accessible for various test measurements. Since we aim to analyze U of WTMs based on measurements of the UGT, care is taken to ensure thermal equilibrium of the BHE fluid with the surrounding ground, as pointed out by Gehlin and Nordell [318]. However, anthropogenic heat fluxes have already caused an increase in the groundwater temperatures in Karlsruhe [356, 357].

To qualitatively compare the WTMs, we additionally record T-logs with the Distributed Temperature Sensing (DTS) method using two fiber optic cables. One cable is installed along the outer wall of the U-pipe, whereas the other is manually inserted into the BHE (Figure 5-3c). Both cables are connected to an Agilent Technologies DTS unit (N4385A) following the proven Raman-Optical Time-Domain Reflectometry (ROTDR) technique [358]. The single-end DTS measurements are performed with a sampling interval of 30 s and a spatial resolution of 1.0 m. Please note that both T-logs recorded with fiber optics represent the average value of ten single measurements over a period of 20 min each. Even though we are aware of the importance of fiber optic calibration, this comprehensive procedure exceeds the scope of the present work, which focuses on WTMs.

Since the calibration procedure of fiber optics is extensive and still being further improved, the whole process is comprehensively discussed in previous studies [359–361]. Hence, our DTS-measurements only serve as qualitative comparison since this measurement technology is mainly used for monitoring of BHEs. However, to compensate for this, Pt100-sensors measured with an ALMEMO 2590 are installed in three selected depths (5 m, 10 m, 25 m) on the outside of one BHE shank and serve as punctual reference values. The measurement frequency of the WTMs is set at 1 Hz. The entire WTM procedure (Figure 5-1) requires approximately ten minutes at the site. Since the deviation of the T-logs measured with GS and fiber optics to the punctual reference values are systematic errors, we correct these T-logs based on the values recorded with the Pt100-sensors. The insertion of the GS causes a small rise of

the water level inside the BHE, provided the BHE is not filled to the top. Thus, we correct the recorded *D* using Eq. 5-20, modified after Raymond et al. [329]:

$$D^* = D - \frac{V_{sh}}{2\pi r^2{}_{BHE}} \quad \text{(Eq. 5-20)}$$

where *r* is the inner diameter of the BHE and *D** the corrected depth. V_{sh} displaces the corresponding amount of water inside the BHE. When using multiple probes in immediate succession, without flushing the probes back to the surface, the correction is particularly relevant. Before taking the first measurement, we analyze potential site-specific measurement errors, which result from the insertion of the GS in the BHE to reveal necessary corrections of the measurements in advance. The measurement error resulting from the influence of temperature and pressure at the site on the conversion of the hydrostatic pressure to the actual BHE depth is -1.06 mm. This is equal to 0.003 % and therefore negligible. Assuming that *c* for water is 4.18 kJ kg^{-1} K^{-1} at 20 °C, *X* from the thermal input of the GS amounts to 0.04 % for a descent time of 30 s which is equal to the descent to a depth of 3.9 m at the site following Eq. 5-8 and Eq. 5-9 and the parameters of Table 5-1. Also negligible is the maximum absolute temperature change ΔT in case of a conversion of electric *E* into thermal energy, which is 0.23 K conservatively assuming that the conversion takes only one second. Hence, corrections of the WTM at this site are not required. However, a decrease in *c* or *m* of the BHE fluid, for instance by adding antifreeze, can cause a larger error. The same applies to probes with a larger energy storage. Thus, we recommend considering these potential measurement errors case specific.

5.3 Results and discussion

5.3.1 Calibration procedure

The automated calibration yields several benefits compared to conventional calibration procedures, which are predominantly manually performed. The position of each GS and therefore, the orientation of the temperature sensor in the calibration bath, as well as the distance to the reference thermometer, remains stable over the entire dwell time. Thus, discrepancies between each calibration procedure can be avoided. The average accuracy of the used GSs amounts to -0.11 K for the given temperature range. The coefficient of determination R^2 for each calibration is between 0.999 and 1. The calibration of the GS improved the accuracy

by an average of 0.08 K, which is equal to 42 %. The average and lowest value of precision u_3 are 0.011 and 0.038 K, respectively. Thus, considering the lowest precision u_3, inhomogeneity u_2 and uncertainty of the reference thermometer u_1 the combined standard uncertainty u_{c1} amounts to 0.039 K. This means the expanded measurement uncertainty U accounts for 0.077 K.

5.3.2 Thermal time constant

Figure 5-5 illustrates each τ of the GS measurement device for different target temperatures. The values of τ are plotted depending on the relative share of the target temperature the GS has reached, which are derived from Figure 5-4.

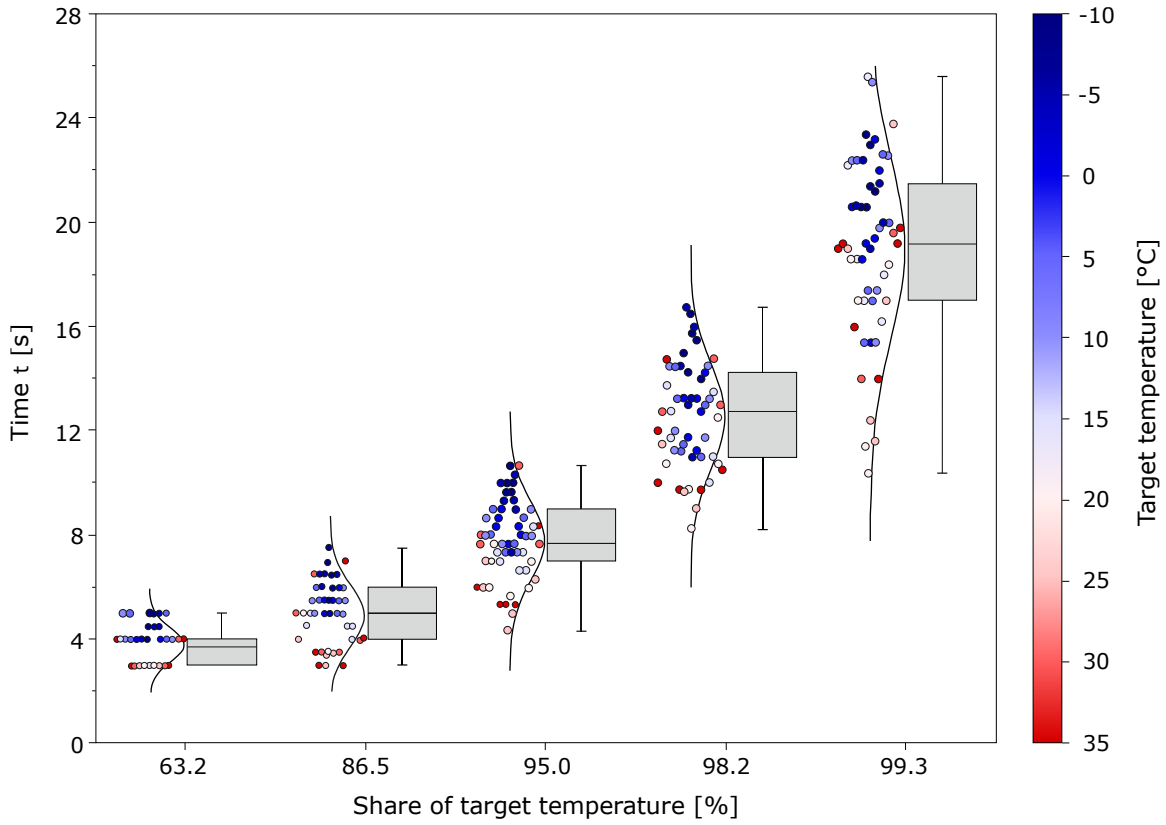

Figure 5-5: Required time (left vertical axis) of the temperature sensor of the GS to reach a prescribed share of the target temperature (horizontal axis) as a function of the target temperature. Each point represents one single GS measurement performed in the calibration unit. Blue colors indicate a target temperature colder than the initial temperature of the GS, while red colors indicate a warmer target temperature. The boxplots describe the distribution of the associated scatter plot.

The smaller the τ, the faster the thermal equalization between GS and the fluid temperature of the calibration unit. The plot predominately shows smaller τ for warmer target temperatures above 15 °C, while more time is required to reach thermal equilibrium with colder target temperatures (-10 – 5 °C).

As a result of the relatively high c_{sh}, the aluminum shell of the GS stores the initial temperatures equal to the ambient air temperature before the insertion of the GS in the fluid over a certain time period. Hence, warmer target temperatures (> 15 °C) are reached faster by an average of approximately 23 % than colder target temperatures (≤ 10 °C). However, the absolute difference between target and initial temperatures seems to have no influence on τ and the measurement dynamics of the GS. According to Eq. 5-13 , the thermal time constant τ of the GS amounts to 3.2 s. This is slightly smaller than the average value of the measured τ (Figure 5-5). This discrepancy can be attributed to some uncertainties of the chosen parametric values of the Pt1000 sensor, which are difficult to access and determine as a result of its miniaturization. However, according to Eq. 5-15 , τ of the Pt1000-sensor alone is 0.6 s, which corresponds in terms of magnitude to the response time of 0.12 s provided by the manufactures of the sensor [337].

In addition, the assumed value of the flow velocity v in the calibration unit, which defines the heat transfer coefficient α, is considered as heterogeneous and deviates during the calibration procedure. Since τ of the GS mostly depends on the protecting shell and α, we focus on the latter and the material properties of the shell. Thus, Figure 5-6 provides a sensitivity analysis of these parameters based on Eq. 5-15 , which also emphasizes the focus for future probes. It can be seen that τ can be improved by an increase of the heat transfer coefficient α and the surface A of the probe. The latter is generally limited by the small diameter of the BHE pipe, while a high α in the field is ensured by constantly high flow conditions mostly influenced by the descent velocity of the GS in the fluid of the BHE. In contrast, an increase of mass m and specific heat capacity c of the shell causes higher τ, while τ is less sensitive to changes of thermal conductivity λ and thickness d. However, λ of aluminum is already comparatively large (Table 5-1) and therefore R_{th} of the shell, which is 8.0×10^{-3} K W^{-1}, relatively small. On the other hand, the convective heat transfer between shell and fluid is more dominant with R_{th} 50 times larger compared to the shell alone. Hence, improvements of τ can be achieved by thermal decoupling of temperature sensor and shell by exposing the sensor with a free punch in the shell. This would lead to an optimized incident flow at the temperature sensor and smaller τ. Aranzabal [327] implemented this measure for the Geoball, which resulted in τ of 0.5 s.

However, this measure can cause higher susceptibility to sensor drifting or reduce the robustness and long-term stability of the sensor.

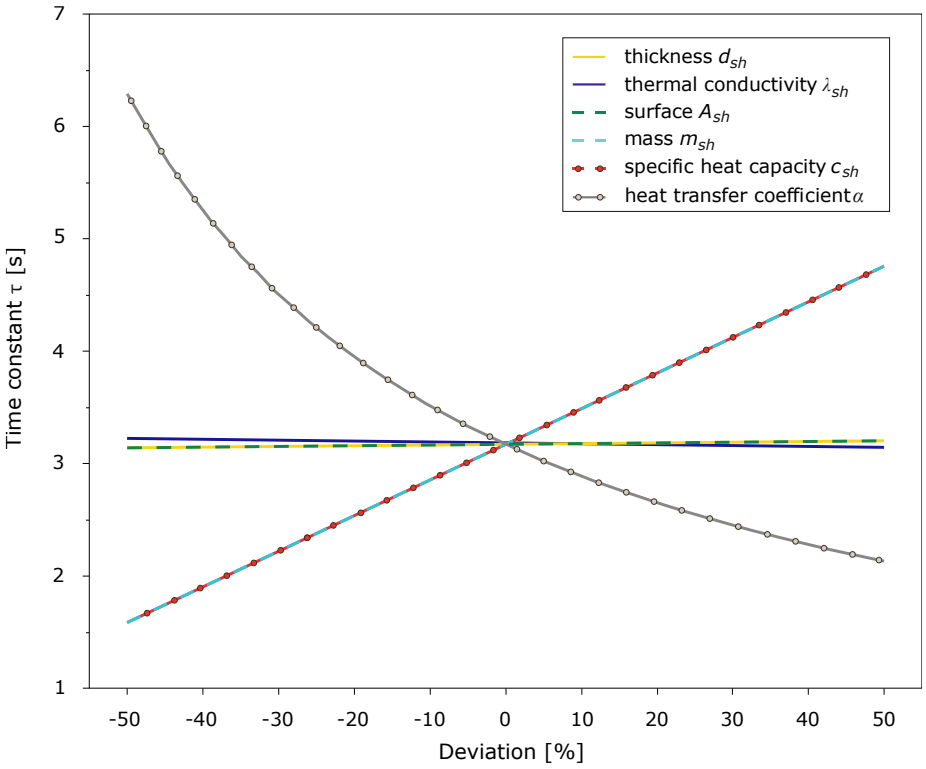

Figure 5-6: Sensitivity analysis of the thermal time constant τ based on Eq. 5-16 with respect to relative changes of the material properties of the shell of the GS.

5.3.3 Sinking behaviour

Experimental descent tests in transparent pipes with a large diameter of 150 mm and without disturbance of the inner pipe walls show tumbling movements of the GS during descent. Thus, the centroid of the GS does not correspond to the center of mass. Since the cover of the GS is a symmetrical and homogeneous object, the spatial arrangement of sensors and other components in the inner part mainly influences the center of mass of the GS.

In BHEs the steady descent of the GS is disturbed by touching the inner walls of the pipe. Thus, the impact of the GS on the inner pipe is considered as oblique and eccentric, since the descent direction is not parallel to the impact normal, which in turn does not pass the center of mass. The descent behaviour of the GS and its contact with the inner pipe walls can have a negative effect on τ as a result of the irregular flow conditions, which lead to varying v. The descent rate of the GS in the 32 mm outer diameter pipe is generally lower compared to the 40 mm outer

diameter pipe resulting from more frequent contact with the inner pipe walls along with friction losses as a consequence of the smaller space for the undisturbed descent. It can be assumed that the descent velocity of the GS reduces with increasing pipe angle as a result of the increasingly frequent contacts with the inner pipe wall. This expected sinking behavior is revealed by the descent tests in the 40 mm outer diameter pipe (Figure 5-7a).

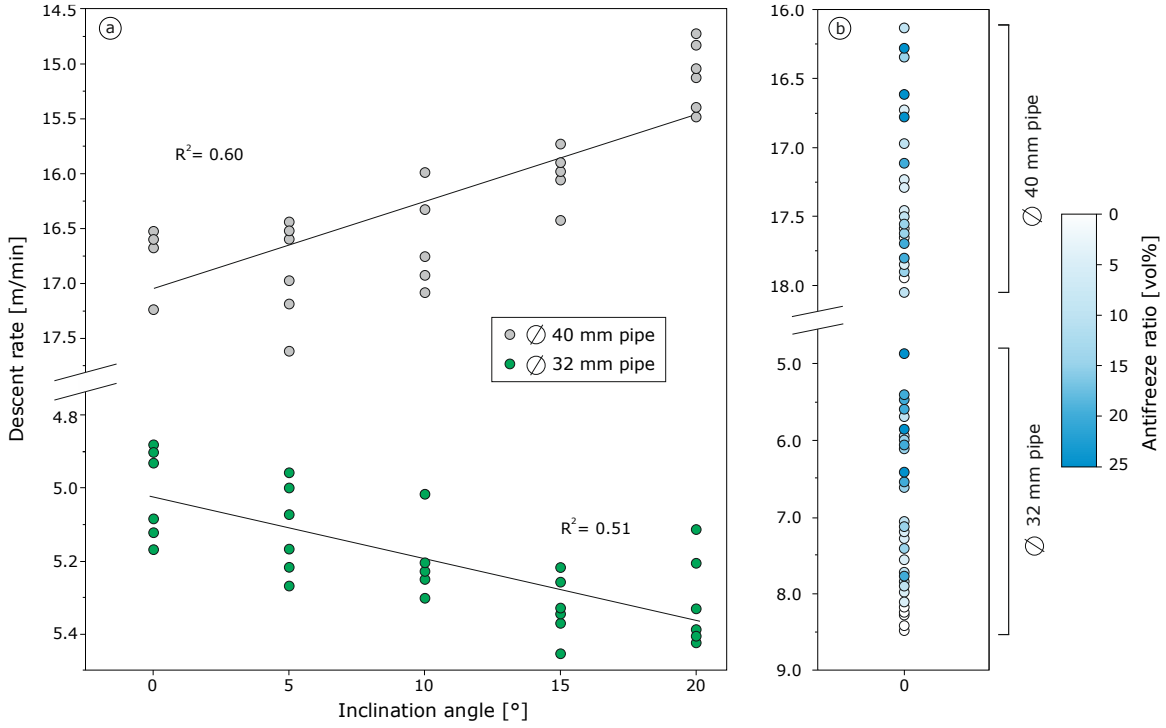

Figure 5-7: Relationship between the descent rate of the GS in two different pipes and its inclination angle (a) and effects of increasing amount of antifreeze in the fluid on the descent rate (b).

However, the opposite is observed in the 32 mm outer pipe. Since the descent velocity is higher in the 40 mm outer diameter pipe, the rotation around the center of mass and the rebound effects are stronger with increasing pipe angle, in turn resulting in a deceleration. It is expected that above a certain pipe angle, which is not reached in the present experiments, the same deceleration effects as in the 40 mm outer diameter pipe can also be observed in the 32 mm outer diameter pipe. Since the descent tests in the present work were carried out to determine the effects of different descent velocities of the GS on the uncertainty of the measured T-logs, further experimental descent tests as well as numerical solution processes are required to comprehensively understand the sinking behavior of the spherical probes.

As can be seen in Figure 5-7b, the descent rate of the GS is also sensitive to ρ and η of the fluid, here realized by increasing the amounts of antifreeze, which leads to a rise of ρ and η of the fluid. This increases the drag force of the fluid, which causes a reduction of the descent rate. For example, the quantity of 25 vol% of antifreeze, for instance, decreases the descent rate of the GS of up to 40 %. However, the large dispersion of the descent rates of Figure 5-7b shows that there is no linear correlation between the amount of antifreeze and the descent rate. Other factors, such as the quality of mixing between antifreeze and water, as well as the slightly different tare weight of each GS (± 0.05 g), influences its descent rate. Even though the temperature dependence of ρ and η of a fluid is well known, the temperature distribution of the fluid during the descent of the GS only has minor effects on the descent rate. Thus, the geothermal gradient of a site has only minor effects on the descent rates of wireless probes and its related expanded measurement uncertainty *U*.

5.3.4 Expanded measurement uncertainty

Laboratory investigations

Figure 5-8 shows T-logs and their associated U performed in the frame of the experimental descent tests. Here, we determine *U* based on Eq. 5-18, Eq. 5-19 and Chapter 5.3.2. The calculation of $\Delta T_{dyn}(t)$ follows with the average value of τ for 99.3 % of the target temperature, which amounts to 19 s (Figure 5-5). The different descent rate, as illustrated in Figure 5-7, affects the measurement dynamic of the GS and therefore its related *U*. The faster the descent of the GS, the larger the difference between actual fluid temperature and measured temperature. Thus, *U* of the T-log measured in the vertical 40 mm pipe (Figure 5-8a) is larger and reaches to greater depths compared to the T-log of the vertical 32 mm pipe (Figure 5-8b). Similarly, faster descent rates in the 32 mm pipe, here caused by an inclination angle of 20°, yield larger *U* compared to the vertical pipe (Figure 5-8c). In addition, *U* of the T-logs in the 40 mm diameter pipe is also more sensitive to possible temperature changes of the fluid during the descent, which can be observed at a depth between four to six meters (Figure 5-8a). Consequently, slow descent rates are preferred, which yield more time for the same distance to compensate for the slow measurement dynamic of the GS. In this context, the common addition of antifreeze has a positive effect on the descent rate and therefore on *U* (Figure 5-8d). Generally, slower descent rates can be achieved by using different materials or different

geometries of wireless probes. For instance, a larger sphere diameter of the GS for the same d_{sh} leads to a decrease in ρ_{sh} causing slower descent rates.

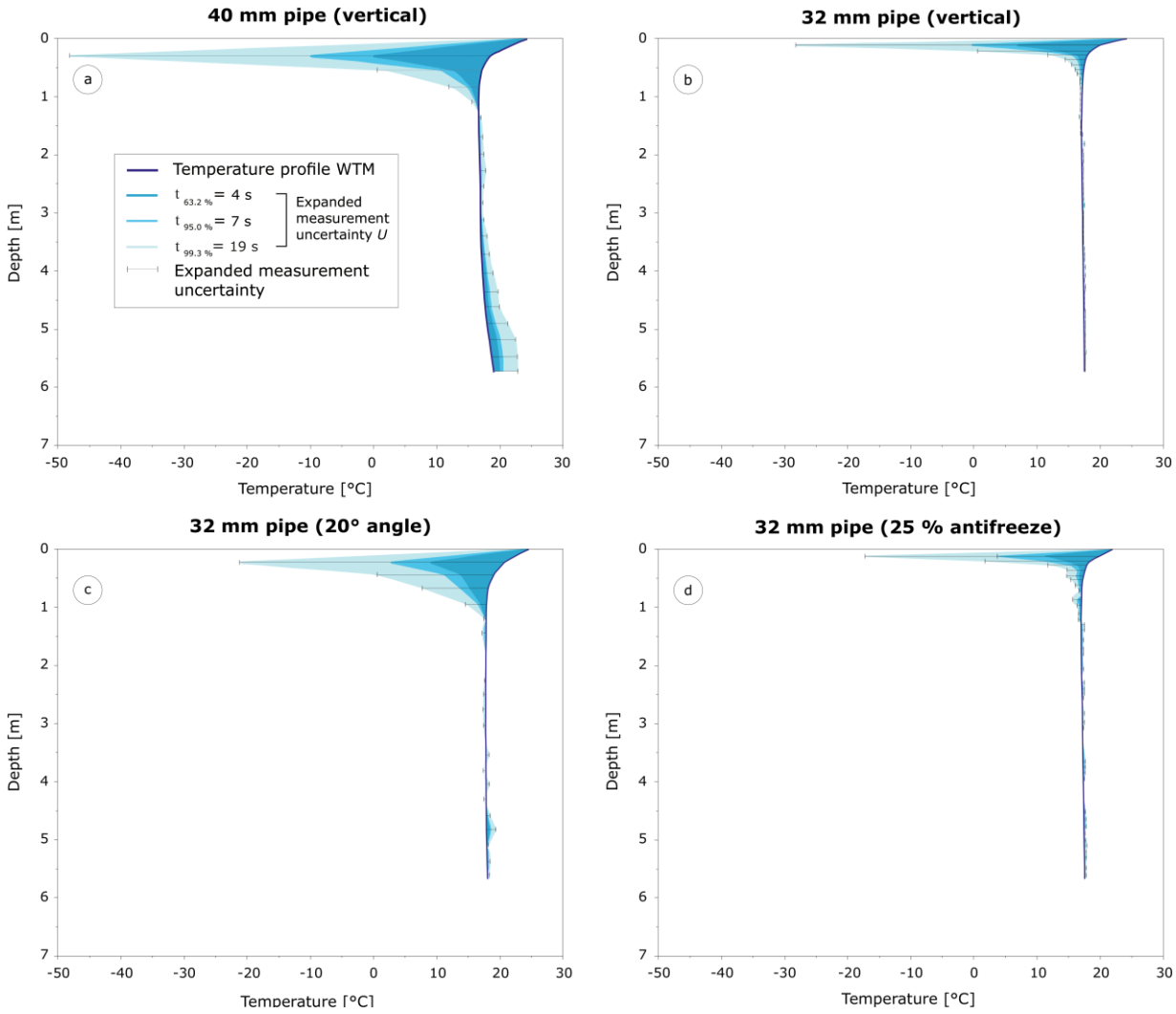

Figure 5-8: T-logs and related expanded measurement uncertainty *U* for four different conditions measured with the GS during the experimental descent tests in the laboratory. Each error bar corresponds to one measurement value of the GS. The three different *U*, illustrated with different blue colors, correspond to h = 0.632 (t = 4 s), h = 0.950 (t = 7 s), h = 0.993 (t = 19 s) as illustrated in Figure 5-5.

The descent rate of wireless probes with ρ close to the BHE fluid, such as the Geoball [335], depends on the chosen pumping rate (e.g. 27 m^3 min^{-1}) [334], which is approximately five times faster than the descent rate of the GS in a 32 mm BHE. In this example, the descent rate is countered by a faster measurement dynamic with response times of 1.5 s to reach 90 % of the target temperature [334]. The shell of the NIMO-T probe also consists of aluminum [331] and τ is almost the same as for the GS. However, adjustable weight allows lower descent rates of

the NIMO-T of up to 2.80 m/min and therefore a smaller U for the first meters of descent is expected. Hence, future dynamic measurement devices both wired and wireless should consider the connection between descent rate and τ. The device materials defining τ and the descent rate, therefore, should be set carefully via experimental investigations in the laboratory.

Site measurements

Figure 5-9 shows T-logs measured with GS and fiber optics and punctual Pt100-sensors measurements in the aforementioned U-pipe BHE. The measurements represent the UGT at the studied site. Due to urbanization and date of measurement (May 2019), the measurements show inverse T-logs with a reversed geothermal gradient. The influence of the ground surface temperature appears to be relatively high and ranges to a depth of approximately 30 m. The three T-logs recorded with the GS are corrected with Eq. 5-20 and strongly correspond to each other, showing an average deviation of 0.025 K. To ensure thermal rebalance between the BHE fluid and the subsurface, the WTMs are performed in a one-hour interval. The average descent rate of the GS is 6.7 m min^{-1}, which enables the generation of 316 measurement data points from the top to the bottom of the BHE. However, the analysis of the descent rate as a function of depth allows no conclusion on potential inclination or other deviations of quality of the U-pipe BHE.

The WTMs show a high accuracy with an average value of -0.038 (± 0.06) K compared to the Pt100-sensors, while the deviation of the fiber optics inside and outside, also referred to as offset, is -0.93 and -0.16 K. Thus, we recommend performing DTS measurements in BHEs in combination with accurate reference measurements or after a comprehensive dynamic calibration procedure using various water baths with changing temperatures [359]. However, since the present study focuses on WTMs using the GS, the calibration of the installed fiber optics is not further considered here. In addition, longer measuring and sampling time of the DTS measurements lead to a higher accuracy. Based on its high accuracy, the GS is also suitable for corrections of systematic errors of T-logs recorded with fiber optics.

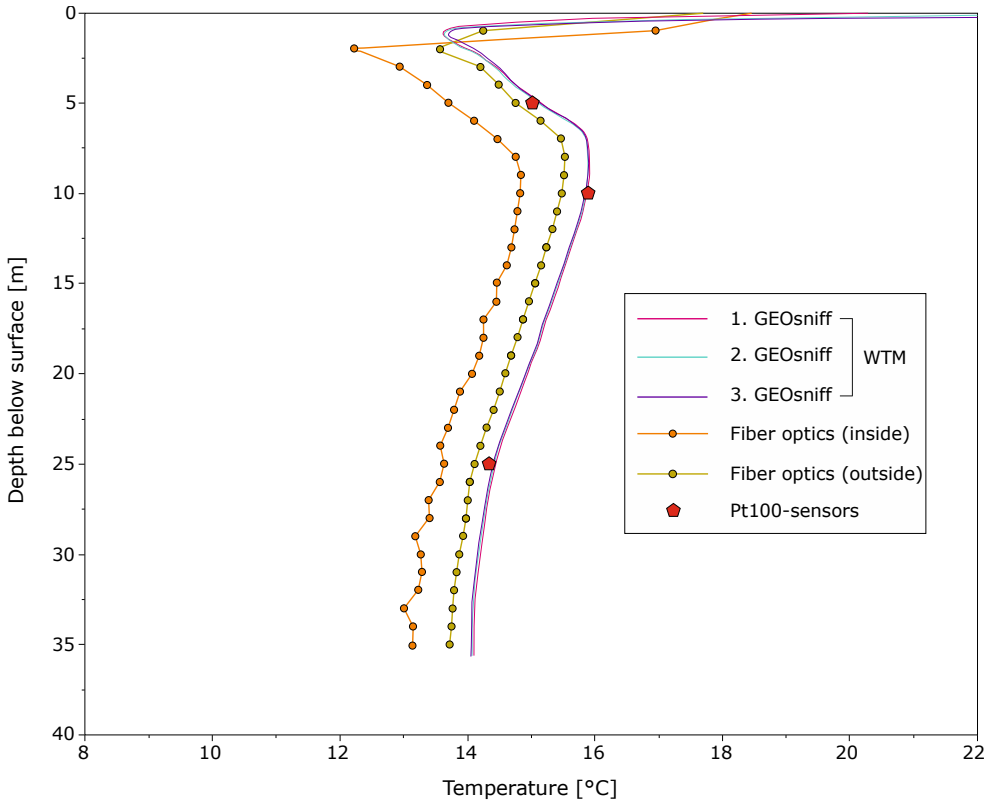

Figure 5-9: Measured T-logs of the undisturbed ground temperature (UGT) in a U-pipe BHE using comparative measurement technologies.

Aranzabal et al. [335] determined an average deviation of 0.075 K between GS and Pt100–sensors, which is comparable with the values of the present study. However, various reasons can affect the accuracy of the measurement with Pt100-sensors. This includes potential sensor drifts, accuracy of the calibration procedure, positioning of the sensor with respect to the BHE pipe and heterogeneity of the subsurface. Given the relatively short length of the BHE, corrections as a result of the attenuation of the fiber optics are not required in this case. The larger discrepancy between GS and fiber optics within the very first meters below surface indicates a certain sensitivity of the DTS measurements on site specific operating conditions. Thus, in order to improve fiber optic measurements, it is important to examine the effects of the surface conditions (e.g. temperatures and solar radiation) and the vadose zone on the required components of the DTS measurements.

Figure 5-10 illustrates the related U of the T-logs of the UGT of Figure 5-9. Table 5-3 additionally summarizes the related errors and uncertainties for various depths. After approximately five meters of descent, the GS approaches thermal equilibrium with the fluid temperature of the BHE and $\Delta T_{dyn}(t)$ approaching zero.

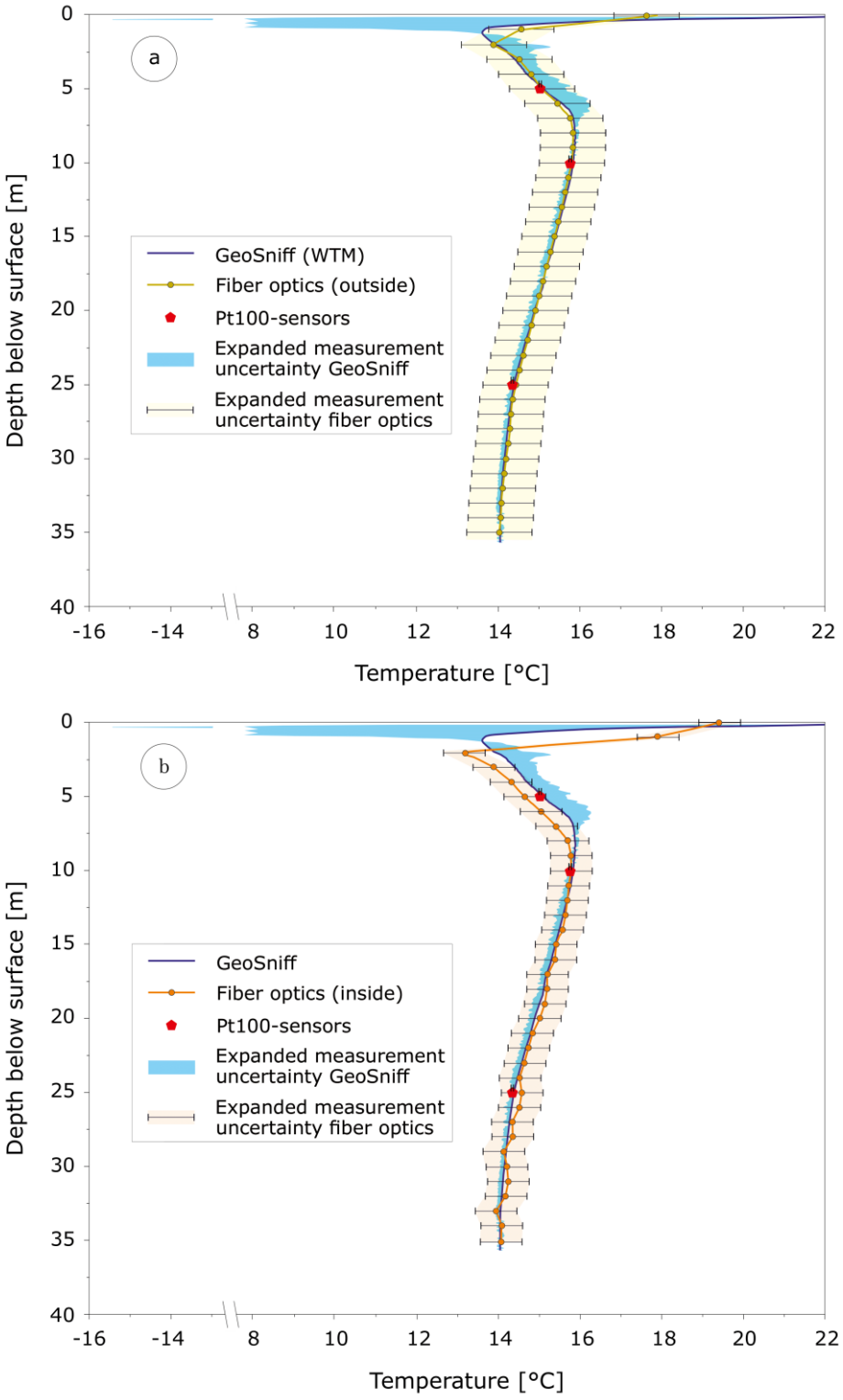

Figure 5-10: T-logs of Figure 5-9 provided with their related expanded measurement uncertainty *U*. The T-logs measured with fiber optics and GEOsniff are corrected based on the temperature values measured with Pt100-sensors.

Since the subsequent temperature only slightly changes and the T-log is rather smooth, *U* of the GS measurement is almost negligibly small and mostly consists of the occurring random error. In addition, *U* does not change with further depths. Thus, the GS probe provides reliable T-logs of the UGT and is a suitable device for low enthalpy geothermal systems such as shallow U-pipe BHEs.

In comparison, the DTS measurements show a greater *U* of 0.51 K for the fiber optics inside and 0.80 K for the fiber optics outside of the BHE pipe. Please note that *U* of the DTS measurements is derived from the precision of the fiber optics. However, we are aware that further investigations are essential to detect all errors related to DTS measurements. The influence, for instance, of subsurface heterogeneity, stacking of errors over depths, and interpolations between measurement points of the fiber optics on the DTS measurements should be investigated. Considering *U* of 0.031 K, the Pt100-sensors proved to be suitable for reliable reference measurements.

In addition to the technical aspects and their reliability of the measured T-logs, other factors such as capital costs, required measurement time, calibration procedure and handling influence the usage decision of each measurement technology. Thus, in Table 5-3 we compare and assess WTM with DTS measurements using fiber optic cables. The main advantages of the WTM using the GS is the fast and easy measurement procedure, the good mobility with respect to field measurements and the relatively simple calibration. In comparison to the GS, the DTS measurements show a broad range of application and are the preferred technology for long-term monitoring and thermal response tests. Nevertheless, for initial T-log measurements in shallow BHEs, the GS is the more practical and suitable device.

Table 5-2: Depths, related temperatures and associated errors and uncertainties of the temperature profile illustrated in Figure 5-10 recorded by means of WTM.

Depth [m]	**Measured temperature T_s [°C]**	**Dynamic measurement error $\Delta T_{dyn}(t)$** (Eq. 5-18)	**Standard measurement uncertainty u_4** (Eq. 5-19)	**Precision u_1**	**Combined measurement uncertainty u_{c1}**	**Combined measurement uncertainty u_{c2}** (including u_1,u_2, u_3,u_4)	**Expanded measurement uncertainty** U $(k=2)$
5	15.1457	0.9445	0.2730	0.0375	0.0387	0.2757	0.5514
10	15.8551	-0.0310	-0.0090	0.0375	0.0387	0.0398	0.0795
15	15.4139	-0.2166	-0.0626	0.0375	0.0387	0.0736	0.1472
20	14.9186	-0.1543	-0.0446	0.0375	0.0387	0.0590	0.1181
25	14.4117	-0.0616	-0.0178	0.0375	0.0387	0.0426	0.0852
30	14.1662	-0.1230	-0.0356	0.0375	0.0387	0.0525	0.1051
35	14.0726	0.0307	0.0089	0.0375	0.0387	0.0397	0.0795

While currently most of the design tools and software for ground source heat pump systems only require the estimated average UGT of a site, the integration of reliably measured T-logs would further improve the significance of these tools. According to Radioti et al. [308], the error in the UGT estimation should not exceed ±1.5 °C to limit the related error of the extracted power of the BHE and the coefficient of performance (COP) of the heat pump to less than 5 %. They recommend temperature monitoring by lowering temperature sensors into the pipe to provide accurate estimation of the geothermal gradient particularly for short BHEs (~ 40 m).

In their case study, Kurevija et al. [362] conclude that the consideration of the ground temperature in the simulation software can reduce the required pipe length up to 7 %, especially for regions with high geothermal gradients. By applying the line source model, the reliability of UGT directly influences the borehole resistance derived from a TRT. Urban [363] states that the error in the borehole resistance may be up to 35 % if the UGT is measured with a precision as high as 1 K.

Table 5-3: Summarizing overview and assessment of the applied technologies for the measurement of T-logs in BHEs.

	Wireless temperature measurement	**Distributed temperature sensing**
Requirements	• GEOsniff • Smartphone/Tablet • Validation box (Figure 5-1)	• Fiber optic cables/ hybrid cables • Splice box and splice unit • DTS unit • Power source • Laptop and associated software
Application possibilities	• Shallow (≤ 300 m) U-pipe BHEs • T-log measurements of the undisturbed and thermally disturbed (ETRT/DTRT/TRT) ground • Single measurement and long-term monitoring	• Open and closed, high and low temperature geothermal systems • ETRTs/DTRTs • Specifically used for long term monitoring [364] • Various fields of applications, far beyond geothermal systems [365]
Calibration	• Simple (Chapter 5.2.2)	• Complex and time consuming [360][360][73] • Calibration strongly affected by operation conditions (e.g. ambient temperature) [359]
Investment Cost	Moderate (~ 10,000 €)	High (> 50,000 €) [366, 367]
Measurement time	< 20 min	>1h
Handling	Easy	Moderate, some experience is required
Mobility	Good	Poor
Durability	Good	Good [368]

Hence, for the practical implementation, design parameters of a BHE including measured UGT, effective thermal conductivity and borehole resistance should all be considered with uncertainties and applied with sensitivity analyses in the respective design tools. In addition to the uncertainties of the recorded UGT resulting from the measurement technology, further uncertainties arise from seasonal temperature variations of the surface. Thus, we recommend long term temperature monitoring of the UGT over the period of one year in combination with climate data of the surface to obtain naturally induced effects on the average UGT, in particular for shallow BHE applications. Furthermore, comprehensive and reliable data sets of measured

T-logs are the basis of training artificial neural networks, which optimizes flexibility, planning reliability and energy efficiency of geothermal systems [369, 370]. Moreover, reliable temperature measurements are also important for the assessment of the operational performance of geothermal systems. This especially applies to shallow and low enthalpy geothermal systems, which are characterized by small differences between injection and abstraction temperatures. For example, Fleuchaus et al. [51] showed average temperature differences of 5.2 K of 73 monitored ATES systems. Assuming a related *U* similar to the DTS measurements of the present study, the expected performance of the systems may be significantly lower.

5.4 Conclusion

The measurement of reliable T-logs is indispensable for the design and monitoring of geothermal systems. T-log measurements of the undisturbed ground temperature and during TRTs are particularly important for large-scale BHE fields. Thus, we analyzed the errors and uncertainties of WTM in BHEs by means of the GS measurement sphere to provide insights into the significance and reliability of this emerging measurement technology. The applied methods, which are based on experimental laboratory and field tests, as well as analytical approaches, point out the sources of errors and potential optimization needs. The analyzed accuracy of -0.11 K and precision of 0.011 K indicate high suitability of WTMs, which constitute an adequate alternative to commonly used measurement technologies such as Pt100-sensors and fiber optics. The largest potential for improvement for future probes is the reduction of the dynamic measurement error. Here, this error is particularly dominant within the first five meters of descent and depends on the thermal time constant τ, which is 4 s on average, and the descent velocities which amount to 5.0 m min^{-1} (32 mm diameter BHE pipe) and 15.0 m min^{-1} (40 mm diameter BHE pipe), respectively. Thus, the development of futures probes should focus on the smallest possible descent velocity and lower thermal time constants τ, which is accessible with a steady descent or smaller specific heat capacity and mass of the protecting shell of the probe. While this study mostly focuses on the principles of WTMs, quantitative laboratory test, and measurements of the UGT, future research on WTM should strive to extend this work by considering the following investigations:

- The design of the GS enables the usage of the probe during DTRTs and ETRTs using heating cables and related power supply as recommended by Wilke et al. [41]. The

analysis of $\Delta T_{dyn}(t)$ and U of WTMs, which are expected to differ from the UGT measurements, should be considered in this context and directly affect the reliability of the evaluated thermal properties of the subsurface such as the borehole resistance.

- Even though we focused on temperature measurements, we are aware that different issues require the uncertainty analysis of the pressure and related depths measurement of wireless sensors. Thus, laboratory investigation and analytical methods are required to determine errors and uncertainties of wireless pressure measurements and their effects on site measurements.

We expect that our study and applied methods help to deepen the knowledge and understanding of WTMs, and that we contribute to the quality assurance and further improvement of wireless probes.

Acknowledgments

We acknowledge funding support from the Ministry of the Environment, Climate Protection and the Energy Sector Baden-Wurttemberg for the project GeoSpeicher.bw (grant number L75 16014-16019) in the context of BWPLUS and the funding support from the Federal Ministry of Economics and Energy for the project "Qualitätssicherung bei Erdwärmesonden II" (grant number 03ET1386C). The authors would also like to thank two anonymous reviewers for their valuable input.

Chapter 6

Synthesis

6.1 Conclusion

Holistic techno-economic feasibility (TEF) studies of low-temperature geothermal heating and cooling systems are required to provide a sound basis for the subsequent project planning phase and to contribute to the overall project success. Furthermore, TEF studies facilitate the demonstration of potential benefits and opportunities of SGE towards customers, energy planners and decision-makers who are often not familiar with the considered technologies. The individual studies presented in Chapter 2 to 5 aim not only to address site specific issues but also to create an awareness of developing holistic TEF analyses. Thus, associated opportunities and current shortcomings of TEF studies, particularly for the promotion of large-scale SGE systems, are emphasized. The major findings addressing each of the individual stages of the TEF are briefly summarized hereinafter:

The first two studies analyze the cooling supply of the Campus North of the KIT investigating capacities, demands and related supply costs of 23 buildings. A novel method is presented (Chapter 2) enabling the straightforward detection of air-cooled chillers and the estimation of installed cooling capacities by utilizing its correlation with the number of installed fan units. The practical applicability was demonstrated for 36 chillers with capacities ranging from 350 to 1,200 kW, with an average overestimation of 36 %. Even though this method still requires optimization with respect to the accuracy of the estimated values as well as the time-efficient and area-wide applicability, it is a powerful tool to easily identify and quantify cooling demands as a first step. Based on this, potential usage of SGE systems can be derived and the approaches of a TEF analysis can be initiated. Furthermore, the approach addresses the huge lack of knowledge regarding market figures of chillers and cooling requirements of industrial, commercial or public areas in general. On this basis, the approach of Chapter 3 reveals that cooling supply costs of 47 chillers at the Campus North range between 5.4 and 11.4 euro cents kWh^{-1}. The comparison of the mean values of the simulated cooling costs with actual data of two reference buildings shows a maximum deviation of 5 % indicating

a high validity of the approach. Cumulative annual demand-related costs of €2.5 million to power the chillers which provide 70 GWh of cooling energy are determined. There was a large knowledge gap regarding cooling requirements and related supply costs at the site, impeding the development of sustainable cooling solutions. Considering the findings of Chapter 2 and 3, a holistic and centralized cooling supply concept can be developed that focuses on campus buildings with high demands or large cooling supply costs to foster a climate-neutral and efficient campus operation. The approach in Chapter 3 demonstrates how other facilities can easily determine their supply costs without requiring major efforts. In practice, however, this is often not addressed resulting in the use of overpriced and inefficient systems. Consequently, benchmarking of cooling supply costs with other sites and technologies is usually not possible, which leads to a standstill in technological progress impeding the decarbonization of the thermal energy sector.

The third study addresses the stage of the economic analysis by comparing LT-ATES with conventional technologies, which include compression chillers and district heating. This analysis is performed for a specific building of the municipal hospital to address the lack of awareness of ATES technology in general and its economic potential, as pointed out by Fleuchaus et al. [45], towards the hospital administration. Since this building is still under construction, demand and loads are estimated based on the ambient air temperatures and expected heating (1.8 MW) and cooling (3.0 MW) capacity. To meet the demand, the basic concept of the considered LT-ATES implies six groundwater wells with a depth of 35 m each resulting in average initial capital costs of €1.28 (± 0.08) million. The high efficiency of direct cooling using ATES (COP of 29) enables potential electricity cost reduction of 80 % compared to the chillers, which significantly contributes to possible payback times of 3 years. The economic analysis was carried out shortly after the hospital administration decided to use chillers and district heating instead of ATES to supply the new facility. However, the revealed economic benefits are rekindling interest in implementing ATES or groundwater cooling solutions at the site to either recool the chiller plant or to partially feed the cooling network to relieve the chiller operation. This emphasizes the importance of a timely demonstration and communication of potential economic benefits of SGE systems towards decision-makers.

The fourth study focuses on the exploration stage dealing with the measurement of vertical temperature profiles (T-logs) in BHEs using wireless probes. In contrast to the studies in Chapter 2 to 4, this study is based on actual measurement in the laboratory and at the study site, which allows for the detection of errors and uncertainties associated with the applied

technology. Hence, the reliability of the recorded data is higher compared to the previously performed simulations. Access to the BHE field of the HsKA enables the measurement of T-logs of the undisturbed ground and the first-time visualization of its expanded measurement uncertainties based on the findings from the laboratory investigations. The expanded measurement uncertainty of the recorded T-logs decreases from 0.55 at 5 m depth to 0.08 at 10 m depth, mainly influenced by the descent velocity of the wireless probe and the thermal time constant τ determined as 4 s. The average ground temperature at the site is 15 °C and is strongly influenced by the heat sources of the urban area [371, 372]. This impedes the initial plans of the university to utilize the BHE for direct cooling of the laboratories and requests for additional cooling technologies which are currently in development [125]. Technological advancement of existing devices for temperature measurements in SGE systems, which is representatively demonstrated for wireless measurement technology in Chapter 5, yields highly resolved T-logs even allowing the assignment of expanded measurement uncertainties for each of the recorded data points. This enables not only a detailed review of the measured data but also the selection of suitable measurement technology depending on the actual requirements at the site. Thus, research and development (R&D) activities facilitate a sound exploration phase and ensure the robustness of the determined values of the subsurface properties.

In contrast to the exploration phase, the determination of heating and cooling requirements of buildings, as demonstrated from Chapter 2 to 4, is subject to considerable uncertainties. This is a major shortcoming not only of the presented thesis but also for TEF studies of SGE in general. The Campus North and the municipal hospital data sets currently impede more reliable approaches. While new constructions, as described in Chapter 4, only allow the estimation of demands and loads, existing systems bear the chance to conduct comprehensive measuring campaigns including thermal energy metering [373]. At the Campus North, the latter is, however, only carried out on two reference buildings, which reduces the reliability of the determined cooling demands and loads. Hence, lack of heating and cooling requirement data, together with low priorities in developing approaches to tackle this issue is a major bottleneck in implementing SGE systems.

In order to finally derive the scope of comprehensive TEF analysis of SGE, insights into past and present TEF studies of best practice examples of SGE systems are crucial for optimization measures. Therefore, Table 6-1 provides a checklist of actual approaches of TEF analysis of large-scale SGE projects that were finally implemented and contrasts these with the approaches at the study sites considered in this thesis. The latter are derived from the findings of this thesis

and the additional investigations and studies carried out as part of the Geospeicher.bw research project [374].

While the Campus North of the KIT and the municipal hospital lack a common goal and vision, typically expressed in a master plan, the latter is an integral part of all considered best practice examples and was elaborated prior to the TEF analysis. At the ETH Zürich, for instance, the master plan “Science City” was developed in 2005 focusing on a new energy concept to halve carbon emissions by 2020 [375]. One year later, the first studies on the energy demand of the campus facilities started and a basic concept of the BTES field under consideration was developed to feed the anergy network. The goal of Ball State University (BSU) was to implement a demonstration site to stimulate broader application of GSHP technology. To achieve this, early consultation with policymakers, the university board, consultants, geothermal experts and potential funders were undertaken, finally resulting in the largest GSHP system in the US. The latter consists of 3,600 boreholes and 10 miles of distribution pipes associated with initial capital costs of USD83 million [376]. Furthermore, the implementation of large-scale SGE projects at research facilities is also associated with the development of research infrastructure where multiple projects and studies can be realized accordingly. At BSU, several faculties used the exploration stage as an opportunity to perform various measurement campaigns that go beyond the procedure of commercial projects, as exemplified in Chapter 5. Table 6-1 shows that at all considered sites, special attention was paid to measure the heating and cooling requirements of existing facilities by considering future demand trends. On this basis, the economic analysis includes the considered technology variants and all related cost factors resulting in possible savings and amortizations. In contrast, there are discrepancies in the scope of investigations during the exploration stage. While the geological conditions at TU Eindhoven or Utrecht University were already well examined before, less effort was required to additionally determine subsurface properties.

Table 6-1: Applied investigations of holistic TEF analyses of large best practice SGE projects, summarized after consultation with participating experts Lowe [80], Andersson [377], Godschalk [378] Haussler-Pause [379] and Kolb [373], are compared with the considered projects and the study sites of this thesis.

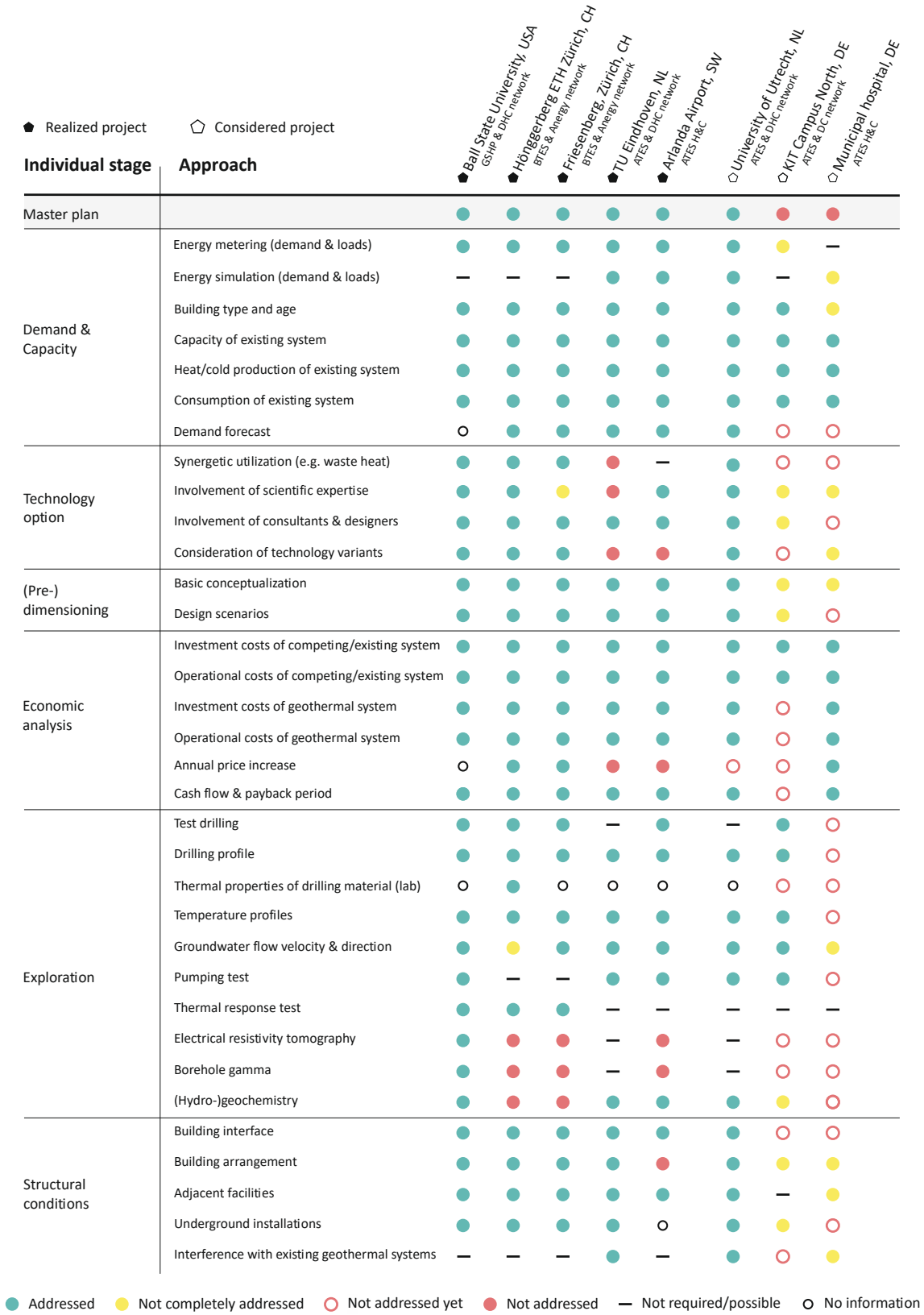

As concluding remarks of Chapter 2 – 5 by considering the approaches of the best practice examples presented in Table 6-1, the following proposed aspects and procedures are derived which are considered as key to the development of holistic TEF analyses of large-scale SGE systems:

- Development of a global master plan that defines and compiles common goals, visions and actions through consultation with all customers, decision-makers and relevant stakeholders.
- Comprehensive determination of heating and cooling requirements of relevant buildings considering the development of future demands. For existing buildings, this is fulfilled by thermal energy metering on the currently installed supply technology over a representative period to determine capacities, demands and loads. For new constructions, the required data can be derived from empirical values of similar projects in the past.
- Investigation and comparison of potential technology options by considering site-specific characteristics. The pre-dimensioning of the variants includes the evaluation of synergetic usage with existing supply technologies (e.g. waste heat) and the required supply security of the facilities.
- Economical analysis of all considered technology options estimating initial investment costs as well as demand-related and operation-related costs. Possible economic savings and payback times indicate the most economical variant. Furthermore, the sensitivity of future energy prices and the development of the energy market situation should be evaluated.
- The initial steps of the exploration stage are typically based on desktop work to identify which on-site investigation is required. This stage is more comprehensive when conducted as part of a research project, while the approach is simpler for purely commercial projects. The test drilling should be implemented in accordance with the considered overall design of the entire SGE system to later use the borehole or well for operation.
- When implementing DHC networks fed by SGE, assessments regarding structural conditions are particularly important to minimize the expenses of the horizontal distribution while still ensuring the reliability of supply. Early considerations of the

existing building interface are required to develop solutions for a proper integration of retrofit SGE installations.

- To complete the overall feasibility analysis, previous findings on heating and cooling demands, technology variants, exploration and structural conditions are considered in a heat transport simulation. For large-scale systems, numerical simulations are required to investigate thermal and hydraulic effects on the subsurface and elaborate well or borehole arrangements.

6.2 Perspective

Based on the findings of chapter 2-5, further research efforts are required to improve techno-economic feasibility analyses of SGE and to extend the applied approaches and methods of this thesis. The identified needs for optimization and research approaches are addressed for each of the individual stages of the TEF analysis:

- **Capacity and requirements:** Chapter 2 introduces the basic approach to determine the spatial distribution and quantity of installed cooling capacities using aerial images. The general suitability of this method is demonstrated at the Campus North of the KIT. While little is known about the cooling requirements of cities, this approach can address this knowledge gap if further applied on a larger scale. A first manual implementation for the city of Freiburg, Germany, yields promising results showing a total proportional cooling capacity of detected chillers of 118 MW [380]. Currently, further efforts in training convolutional neural networks (CNN) are made to automatically detect chillers and estimate the related cooling capacities within a reasonable amount of time. This is associated with a significant increase in efficiency of the whole process and enables the development of entire cooling capacity maps. These maps indicate areas with large cooling demands, which can subsequently be utilized for city-planners. To improve the accuracy of the estimated capacities, further data of technical specifications from chiller manufacturers currently available on the market are essential. While first analyses yield an overestimation compared to actual installed capacities, comprehensive data sets and gaining application experience should lead to a reliability increase of the determined values. So far, the technical potential of LT-SGE systems is associated with the heat demand in the study area [124, 381, 16, 382]. In order to tap the large potential of LT-SGE systems for cooling, the determined cooling capacities can be linked to thermal groundwater models or analytical

approaches, which is particularly promising for regions with large cooling demand densities such as cities in warm climate zones or industrial areas.

- **Technology option and (pre-)dimensioning:** In order to exploit the full capabilities of LT-SGE systems, forward planning and smart usage concepts are required to ensure sustainable and efficient operation and to increase the overall acceptance of LT-SGE usage. Early pre-dimensioning should therefore examine synergetic SGE usage between buildings with heating or cooling dominated loads. This is particularly required for new installations utilized for large-scale cooling supply in urban and industrial settings, where anthropogenic heat sources and already existing SGE systems result in overall increasing groundwater temperatures, defined as subsurface urban heat islands (SUHI) [8, 356, 371]. Expected subsurface heat plumes due to groundwater cooling systems should therefore be quantified in the early TEF analysis and integrated into heat utilization concepts. An important prerequisite for this is available (thermal-) groundwater models, which should be an integral part of the subsurface management of large cities. In the absence of heat consumers, regeneration measures such as recooling plants or cooling towers should be considered [383], to achieve a thermal rebalancing of the subsurface. This reduces potential impacts on biology and ecology and conflicts with water authorities can be avoided. Furthermore, heating of the aquifer is prevented and energy planners are forced to find either heating and cooling consumers equally or consider recooling installations already at an early stage of the TEF analysis. Due to its basic operating principle, ATES can be considered the most suitable SGE technology option to achieve balanced and sustainable usage. Fleuchaus et al. [51] reveal only a small thermal imbalance of 2.3 % on average for 73 Dutch ATES system analyzed, which is additionally induced by the Dutch regulative framework claiming a balanced operation of ATES within a three years period [228].

- **Economic analysis:** Chapter 4 analyzes the economic viability of LT-ATES compared to conventional heating and cooling technologies and additionally marks the operation-related CO_2 emissions. However, given the ambitious EU-wide targets to reduce carbon emissions, decision-makers are forced to reflect more thoroughly upon potential CO_2 savings along with technology investments. The related expenses to save carbon emissions can be specified with CO_2 abatement costs (ACs) commonly defined as euros (or the respective currency) per metric ton of CO_2 emissions avoided [384]. Negative ACs indicate that the considered technology option not only saves carbon emissions but also has economic advantages over the reference system. While ACs are mostly addressed for large-scale

power plants or renewable electricity producing technologies [385, 386], there is less focus on renewable heating and cooling technologies in general and on SGE systems in particular. Thus, comprehensive approaches to determine ACs for SGE systems are required considering all arising lifetime costs and carbon emissions. Since SGE systems not only compete with chillers or conventional heating systems, reference scenarios including absorption chillers, air-source heat pumps, bioenergy, or solar thermal energy should be considered.

- **Exploration:** Chapter 5 provides a comprehensive analysis of measurement uncertainties associated with wireless probes used to record vertical temperature profiles of the undisturbed ground. As these devices can also be utilized for temperature measurement in the context of advanced thermal response tests (TRTs) [372, 387], the examined uncertainties should be further applied to evaluation procedures of TRTs considering subsurface parameters such as thermal conductivity and borehole resistance. While Witte [388] comprehensively analyzes all sources of error of TRTs and their impacts on the reliability of the determined subsurface parameters, Schelenz et al. [28] demonstrate a reduction of uncertainties in the determination of the required borehole length as a result of proper site-specific parametrization in the field. To further emphasize the close relationship between on-site exploration and economic viability of BHEs, both approaches can be merged and further developed. Thus, the implementation of modified design tools for BHEs that specifically consider depth resolved design parameters and related uncertainties is proposed. This allows for the first time to quantify the impact of measurement uncertainties on borehole lengths directly related to installation costs. Furthermore, sensitivity analyses are suggested to quantify the influence of all required design parameters on the installation costs. This approach should include not only measured and evaluated subsurface parameters but also recorded heating and cooling requirements of a selected building and should therefore be comprehensively carried out for a specific case.

Since feasibility studies strive to evoke the eventual realization of the analyzed initiatives, research and development (R&D) should aim to timely realize large-scale demonstration projects to promote the types of LT-SGE technologies that are not considered state of the art in the respective country. This not only enables the demonstration of operational robustness but also allows holistic insights into technical characteristics of the system that can only be revealed through actual implementation and operation. Applied to the current situation in Germany and considering the major findings of this thesis, a demonstration project is proposed

consisting of LT-ATES for heating and cooling supply of a commercial or industrial building or to feed a combined low-enthalpy DH and DC network. For the latter, the challenge is to combine the comprehensive planning procedure of the LT-SGE system, as shown in Figure 1-1, with the development processes (Figure 3-1) of thermal networks. The number of low-enthalpy thermal networks is expected to increase in the coming years, with reduced competition from less suitable current market-leading heating and cooling technologies. Hence, large-scale LT-SGE applications should strive to take full advantage of this emerging potential to become an indispensable key technology in future heating and cooling supply concepts of cities.

Acknowledgments

The help and support that I received from many people paved the way for this thesis. I particularly would like to thank…

…my supervisor Prof. Dr. Philipp Blum for providing me with the opportunity to do the PhD. I particularly appreciate that you directly included me in your research group from the first day that led to a sense of trust and spirit that I needed to write this thesis. I furthermore would like to thank you for inspiring and motivating discussions, for showing me how to develop concepts and ideas for publications, for introducing me to "KISS", for trusting in my abilities, and for your open mind towards new topics and ideas also beyond geothermal issues. I really enjoy(ed) working with you and it was a pleasure to work under your supervision and guidance;

…Dr. Roman Zorn for his scientific advice, for sharing his deep knowledge of shallow geothermal applications, and his passion and enthusiasm for scientific issues. I highly appreciate that you gave me the required freedom besides project work fostering my PhD progress, the immersion in new topics and the development of my own ideas;

…Prof. Dr. Peter Bayer for taking the responsibility of being co-examiner, and for interesting exchanges during his visits in Karlsruhe and at the EGU;

…Dr. Paul Fleuchaus for the nice atmosphere in the office, for fruitful brainstorming sessions implementing paper ideas, his great support during my PhD and particularly for the off-campus activities during the time we spent together in Karlsruhe;

…Dr. Hagen Steger for his countless support and advice particularly regarding laboratory issues which contributed to the realization of study 4;

…Kyle Busch for language editing of Chapter one and six and even more for a great time the past three years in Karlsruhe;

…Matthias Kolb for taking his time to provide me with profound practical insights on how to plan and develop new generations of thermal energy networks in Switzerland;

…Bas Godschalk, Olof Andersson, Reto Haussler-Pause and for providing valuable insights into the investigations of feasibility analysis of large-scale best practice shallow geothermal energy projects;

…the facility management of the Campus North and in particular Frank Eißenhardt who patiently answered all of my extensive questions about cooling supply at the campus;

…the engineering geology and hydrogeology working groups for enjoyable activities during times when get-togethers were normality and for the great atmosphere during lunch and coffee breaks;

…my EIFER colleagues and in particular the “Laborhelden” for providing an enjoyable, instructive working atmosphere;

...the colleagues and partners in the GeoSpeicher.bw project;

...the Ministry of the Environment, Climate Protection and the Energy Sector Baden-Württemberg for funding the project “GeoSpeicher.bw“ (grant number L75 16014-16019) in the context of BWPLUS;

…finally and especially Monika, Robert, Miriam, Marille, Christa who made me the person I am today.

Declaration of Authorship

Study 1

Citation: Schüppler S, Fleuchaus P, Zorn R, Salomon R and Blum P (2021) Quantifying installed cooling capacities using aerial images. Journal of Photogrammetry, Remote Sensing and Geoinformation Science (PFG). News item. doi: 10.1007/s41064-021-00137-0.

Declaration of authorship: Simon Schüppler (SiS), Philipp Blum (PB) and Paul Fleuchaus (PF) developed the idea and methodology. Robert Salomon performed the survey. SiS evaluated the results in consultation with PB and PF and wrote the manuscript. The final manuscript was reviewed by PB and PF.

Study 2

Citation: Schüppler S, Fleuchaus P, Duchesne A and Blum P: Cooling supply costs of a university campus. Energy [submitted manuscript].

Declaration of authorship: Simon Schüppler (SiS), Philipp Blum (PB) and Paul Fleuchaus (PF) designed the study. Antoine Duchesne collected the data and implemented an initial simulation in consultation with SiS and PF. SiS subsequently adjusted the simulation. SiS evaluated the results in consultation with PB and PF and wrote the manuscript. The final manuscript was reviewed by PB and PF.

Study 3

Citation: Schüppler S, Fleuchaus P and Blum P (2019) Techno-economic and environmental analysis of an Aquifer Thermal Energy Storage (ATES) in Germany. Geothermal Energy 7 (1), 669. doi: 10.1186/s40517-019-0127-6.

Declaration of authorship: Simon Schüppler (SiS), Philipp Blum (PB) and Paul Fleuchaus (PF) designed the study. SiS performed and evaluated the simulation in consultation with PB and PF. SiS wrote the manuscript and accompanied it through the review process. The final manuscript was reviewed by all authors.

Study 4

Citation: Schüppler S, Zorn R, Steger H and Blum, P (2021) Uncertainty analysis of wireless temperature measurement (WTM) in borehole heat exchangers. Geothermics 90. doi: 10.1016/j.geothermics.2020.102019.

Declaration of authorship: Simon Schüppler (SiS) conducted the laboratory experiments and field measurements in consultation with Roman Zorn (RZ) and with the support of Hagen Steger (HS). SiS evaluated the results in consultation with RZ. SiS and PB designed the study. SiS wrote the manuscript and accompanied it through the review process. The final manuscript was reviewed by all authors.

References

[1] European Commission (2019) The European Green Deal. COM(2019) 650, 24 pp.

[2] IRENA and European Commission (2018) Renewable Energy Prospects for the European Union: Preview for policy makers, 120 pp.

[3] IEA (2020) European Union 2020. Energy Policy Review. https://www.iea.org/reports/european-union-2020 (last accessed: 02 Mar 2021).

[4] IEA (2019) Renewables. Market analysis and forecast from 2019 to 2024. https://www.iea.org/reports/renewables-2019/heat (last accessed: 03 Mar 2021).

[5] Dennis K (2015) Environmentally Beneficial Electrification: Electricity as the End-Use Option. The Electricity Journal 28, 100–112. doi: 10.1016/j.tej.2015.09.019.

[6] Bayer P, Saner D, Bolay S, Rybach L and Blum P (2012) Greenhouse gas emission savings of ground source heat pump systems in Europe: A review. Renewable and Sustainable Energy Reviews 16, 1256–1267. doi: 10.1016/j.rser.2011.09.027.

[7] Fridleifsson IB, Bertani R, Huenges E, Lund JW, Ragnarsson A and Rybach L (2008) The possible role and contribution of geothermal energy to the mitigation of climate change. In: Hohnmeyer O and Trittin T (eds). IPCC Scoping Meeting on Renewable Energy Sources, Proceedings, Luebeck, Germany, 20-25 January 2008. Proceedings, 59–80.

[8] Blum P, Menberg K, Koch F, Benz SA, Tissen C, Hemmerle H and Bayer P (2021) Is thermal use of groundwater a pollution? Journal of Contaminant Hydrology 239, 1–12. doi: 10.1016/j.jconhyd.2021.103791.

[9] Freeden W and Heine C (2018) Geothermie - Ein kurzer Abriss. In: Bauer M, Feeeden W, Jacobi H and Neu T (eds). Handbuch Oberflächennahe Geothermie. Springer Spektrum, 1–22. doi: 10.1007/978-3-662-50307-2_1.

[10] Hähnlein S, Bayer P, Ferguson G and Blum P (2013) Sustainability and policy for the thermal use of shallow geothermal energy. Energy Policy 59, 914–925. doi: 10.1016/j.enpol.2013.04.040.

[11] Sarbu I and Sebarchievici C (2014) General review of ground-source heat pump systems for heating and cooling of buildings. Energy and Buildings 70, 441–454. doi: 10.1016/j.enbuild.2013.11.068.

[12] Self SJ, Reddy BV and Rosen MA (2013) Geothermal heat pump systems: Status review and comparison with other heating options. Applied Energy 101, 341–348. doi: 10.1016/j.apenergy.2012.01.048.

[13] Arghand T, Javed S, Trüschel A and Dalenbäck J-O (2021) A comparative study on borehole heat exchanger size for direct ground coupled cooling systems using active chilled beams and TABS. Energy and Buildings 240. doi: 10.1016/j.enbuild.2021.110874.

[14] Goetzl G, Dilger G, Grimm R, Hofmann K, Holecek J, Cernak R, Janza M, Kozdroj W, Klonowski M, Hajto M, Gabriel P and Gregorin S (2020) Strategies for Fostering the Use of Shallow Geothermal Energy for Heating and Cooling in Central Europe - Results from the Interreg Central Europe Project GeoPLASMA-CE. Proceedings World Geothermal Congress 2020. Reykjavik, Iceland, April 26 – May 2, 2020, 17 pp.

[15] Murphy D and Westphal K (2011) Project Negatherm for Ground Source Heat Pumps. Improving the Geothermal Borehole Drilling Environment in California. Final Project Report, 336 pp.

[16] Tissen C, Menberg K, Bayer P and Blum P (2019) Meeting the demand: geothermal heat supply rates for an urban quarter in Germany. GeothermEnergy 7, 213. doi: 10.1186/s40517-019-0125-8.

[17] Desideri U, Sorbi N, Arcioni L and Leonardi D (2011) Feasibility study and numerical simulation of a ground source heat pump plant, applied to a residential building. Applied Thermal Engineering 31, 3500–3511. doi: 10.1016/j.applthermaleng.2011.07.003.

[18] Focaccia S, Tinti F, Monti F, Amidei S and Bruno R (2016) Shallow geothermal energy for industrial applications: A case study. Sustainable Energy Technologies and Assessments 16, 93–105. doi: 10.1016/j.seta.2016.05.003.

[19] Emmi G, Zarrella A, Carli M de, Moretto S, Galgaro A, Cultrera M, Di Tuccio M and Bernardi A (2017) Ground source heat pump systems in historical buildings: two Italian case studies. Energy Procedia 133, 183–194. doi: 10.1016/j.egypro.2017.09.383.

[20] Liu Z, Li Y, Xu W, Yin H, Gao J, Jin G, Lun L and Jin G (2019) Performance and feasibility study of hybrid ground source heat pump system assisted with cooling tower for one office building based on one Shanghai case. Energy 173, 28–37. doi: 10.1016/j.energy.2019.02.061.

[21] Schiel K, Baume O, Caruso G and Leopold U (2016) GIS-based modelling of shallow geothermal energy potential for CO2 emission mitigation in urban areas. Renewable Energy 86, 1023–1036. doi: 10.1016/j.renene.2015.09.017.

[22] Blum P, Campillo G and Kölbel T (2011) Techno-economic and spatial analysis of vertical ground source heat pump systems in Germany. Energy 36, 3002–3011. doi: 10.1016/j.energy.2011.02.044.

[23] Casasso A and Sethi R (2014) Efficiency of closed loop geothermal heat pumps: A sensitivity analysis. Renewable Energy 62, 737–746. doi: 10.1016/j.renene.2013.08.019.

[24] Luo J, Zhang Y and Rohn J (2020) Analysis of thermal performance and drilling costs of borehole heat exchanger (BHE) in a river deposited area. Renewable Energy 151, 392–402. doi: 10.1016/j.renene.2019.11.019.

[25] Kim S, Jang Y, Shin Y and Kim G-H (2014) Economic Feasibility Analysis of the Application of Geothermal Energy Facilities to Public Building Structures. Sustainability 6, 1667–1685. doi: 10.3390/su6041667.

[26] Ghaebi H, Bahadori MN and Saidi MH (2017) Economic and Environmental Evaluations of Different Operation Alternatives of an Aquifer Thermal Energy Storage in Tehran, Iran. Scientia Iranica 24, 610–623. doi: 10.24200/sci.2017.4046.

[27] Lu Q, Narsilio GA, Aditya GR and Johnston IW (2017) Economic analysis of vertical ground source heat pump systems in Melbourne. Energy 125, 107–117. doi: 10.1016/j.energy.2017.02.082.

[28] Schelenz S, Vienken T, Shao H, Firmbach L and Dietrich P (2017) On the importance of a coordinated site characterization for the sustainable intensive thermal use of the shallow subsurface in urban areas: a case study. EnvironEarthSci 76, 1256. doi: 10.1007/s12665-016-6331-9.

[29] AHO (2011) Planungsleistungen im Bereich der Oberflächennahen Geothermie. Leitungsbild und Honorierung. Ausschuss der Verbände und Kammern der Ingenieure und Architekten für die Honorarordnung e.V., 24 pp.

[30] Bücherl K and Walker-Hertkorn S (2018) Anforderungen an ein Geothermieprojekt aus der Sicht eines Bauherren. In: Bauer M, Freeden W, Jacobi H and Neu T (eds). Handbuch Oberflächennahe Geothermie. Springer Spektrum, 353–370. doi: 10.1007/978-3-662-50307-2_10.

[31] ECES Annex 27 (2020) Quality Management in Design, Construction and Operation of Borehole Systems. Final Report. IEA Technology Collaboration Programme on Energy Conservation through Energy Storage, 272 pp.

[32] VDI 4640 (2010) Thermische Nutzung des Untergrunds. Grundlagen, Genehmigungen, Umweltaspekte. Verein Deutscher Ingenieure e.V., Düsseldorf.

[33] Lindberg KB, Bakker SJ and Sartori I (2019) Modelling electric and heat load profiles of non-residential buildings for use in long-term aggregate load forecasts. Utilities Policy 58, 63–88. doi: 10.1016/j.jup.2019.03.004.

[34] WKOtool (2021) WKO-bodemenergietool (WKOtool): Ontdek de mogelijkheden van bodemenergie. https://wkotool.nl/ (last accessed: 16 Mar 2021).

[35] Smart Geotherm (2021) Geothermische Screeningstool. https://tool.smartgeotherm.be/geo/alg (last accessed: 16 Mar 2021).

[36] VDI 2067 (2012) Wirtschaftlichkeit gebäudetechnischer Anlagen. Grundlagen und Kostenberechnung. Verein Deutscher Ingenieure e.V., Düsseldorf.

[37] Sartori D, Catalano G, Genco M, Pancotti C, Sirtori E, Vignetti S and Del Bo C (2014) Guide to cost-benefit analysis of investment projects. Economic appraisal tool for cohesion policy 2014 - 2020. Luxembourg: Publ. Office of the Europ. Union Dec. 2014, 358 pp.

[38] Witte JLH, van Gelder G and Spitler DJ (2002) In Situ Measurement of Ground Thermal Conductivity. ASHRAE Transactions 108, 263–272.

[39] Luo J, Rohn J, Xiang W, Bertermann D and Blum P (2016) A review of ground investigations for ground source heat pump (GSHP) systems. Energy and Buildings 117, 160–175. doi: 10.1016/j.enbuild.2016.02.038.

[40] Spitler JD and Gehlin S (2015) Thermal response testing for ground source heat pump systems—An historical review. Renewable and Sustainable Energy Reviews 50, 1125–1137. doi: 10.1016/j.rser.2015.05.061.

[41] Wilke S, Menberg K, Steger H and Blum P (2019) Advanced thermal response tests: A review. Renewable and Sustainable Energy Reviews, 109575. doi: 10.1016/j.rser.2019.109575.

[42] Li X, Li C, Parriaux A, Wu W, Li H, Sun L and Liu C (2016) Multiple resources and their sustainable development in Urban Underground Space. Tunnelling and Underground Space Technology 55, 59–66. doi: 10.1016/j.tust.2016.02.003.

[43] Stauffer F, Bayer P, Blum P, Giraldo NM and Kinzelbach W (2014) Thermal Use of Shallow Groundwater. CRC Press, 290 pp.

[44] Behrens W and Hawranek PM (1991) Manual for the preparation of Industrial Feasibility Studies. Newly revised and expanded edition. United Nations Industrial Develpment Organization, 404 pp.

[45] Fleuchaus P, Godschalk B, Stober I and Blum P (2018) Worldwide application of Aquifer Thermal Energy Storage - A review. Renewable and Sustainable Energy Reviews 94, 861–876. doi: 10.1016/j.rser.2018.06.057.

[46] Bloemendal M and Hartog N (2018) Analysis of the impact of storage conditions on the thermal recovery efficiency of low-temperature ATES systems. Geothermics 71, 306–319. doi: 10.1016/j.geothermics.2017.10.009.

[47] Sommer W, Valstar J, Leusbrock I, Grotenhuis T and Rijnaarts H (2015) Optimization and spatial pattern of large-scale aquifer thermal energy storage. Applied Energy 137, 322–337. doi: 10.1016/j.apenergy.2014.10.019.

[48] Bloemendal M, Jaxa-Rozen M and Olsthoorn T (2018) Methods for planning of ATES systems. Applied Energy 216, 534–557. doi: 10.1016/j.apenergy.2018.02.068.

[49] Fleuchaus P, Schüppler S, Stemmle R, Menberg K and Blum P (2021) Aquiferspeicher in Deutschland. Grundwasser 84. doi: 10.1007/s00767-021-00478-y.

[50] Nordell B, Snijders A and Stiles L (2015) The use of aquifers as thermal energy storage (TES) systems. In: Cabeza LF (ed). Advances in Thermal Energy Storage Systems. Methods and Applications. Elsevier, 87–115. doi: 10.1533/9781782420965.1.87.

[51] Fleuchaus P, Schüppler S, Godschalk B, Bakema G and Blum P (2020) Performance analysis of Aquifer Thermal Energy Storage (ATES). Renewable Energy 146, 1536–1548. doi: 10.1016/j.renene.2019.07.030.

[52] Florides G and Kalogirou S (2007) Ground heat exchangers—A review of systems, models and applications. Renewable Energy 32, 2461–2478. doi: 10.1016/j.renene.2006.12.014.

[53] Rivera JA, Blum P and Bayer P (2015) Ground energy balance for borehole heat exchangers: Vertical fluxes, groundwater and storage. Renewable Energy 83, 1341–1351. doi: 10.1016/j.renene.2015.05.051.

[54] Choi W and Ooka R (2016) Effect of natural convection on thermal response test conducted in saturated porous formation: Comparison of gravel-backfilled and cement-grouted borehole heat exchangers. Renewable Energy 96, 891–903. doi: 10.1016/j.renene.2016.05.040.

[55] Günther D, Walper J, Langner R, Helmling S, Miara M, Fischer D, Zimmermann D, Wolf T and Hausmann-Wille B (2020) Wärmepumpen in Bestandsgebäuden: Ergebnisse aus dem Forschungsprojekt "WPsmart im Bestand". Abschlussbericht. Fraunhofer Institut für Solar Energiesysteme ISE, 258 pp.

[56] Eugster WJ and Rybach L (2000) Sustainable production from borehole heat exchanger systems. Proceedings World Geothermal Congress, Kyushu - Tohoku, Japan, May 28 - June 10., 6 pp.

[57] Naicker SS and Rees SJ (2018) Performance analysis of a large geothermal heating and cooling system. Renewable Energy 122, 429–442. doi: 10.1016/j.renene.2018.01.099.

[58] Kim S-K, Bae G-O, Lee K-K and Song Y (2010) Field-scale evaluation of the design of borehole heat exchangers for the use of shallow geothermal energy. Energy 35, 491–500. doi: 10.1016/j.energy.2009.10.003.

[59] Arghand T (2021) Direct Ground Cooling Systems for Office Buildings. Dissertation, Chalmers University of Technology, Goethenburg, Sweden, 101 pp.

[60] Weber J, Born H and Moeck I (2019) Geothermal Energy Use, Country Update for Germany 2016 - 2018. European Geothermal Congress 2019, Den Haag, The Netherlands, 11-14 June 2019., 16 pp.

[61] IEA (2020) Cooling. https://www.iea.org/reports/cooling (last accessed: 12.03.21).

[62] IEA (2018) Air conditioning use emerges as one of the key drivers of global electricity-demand growth. https://www.iea.org/news/air-conditioning-use-emerges-as-one-of-the-key-drivers-of-global-electricity-demand-growth (last accessed: 12 Mar 2021).

[63] Ikem IA, Ubi PA, Ibeh MI, Ofem SE and Assam AT (2018) Review of refrigerants for steam compression refrigeration machines. International Journal of Engineering and Technology 10, 1172–1180. doi: 10.21817/ijet/2018/v10i4/181004056.

[64] Subiantoro A, Ooi KT and Junaidi AZ (2013) Performance and suitability comparisons of some R22 possible substitute refrigerants. In: City University London (ed). 8th International Conference on Compressors and their Systems. Woodhead Publishing, 67–76.

[65] Blesl M and Kessler A (2013) Energieeffizient in der Industrie. Berlin Heidelberg: Springer Vieweg, 369. doi: 10.1007/978-3-642-36514-0.

[66] Braungardt S, Bürger V, Zieger J and Kenkmann T (2018) Contribution of Renewable Cooling to the Renewable Energy Target of the EU. On behalf of Netherlands Enterprise Agency (RVO.nl). Öko-Institut e.V., 57 pp.

[67] Grand View Research (2020) Chillers. Market analysis, 65 pp.

[68] Refrigeration Industry (2019) The HVAC&R Market in the EMEA Region in 2018. https://refindustry.com/articles/mart-research/the-hvac-r-market-in-the-emea-region-in-2018/ (last accessed: 12 Mar 2021).

[69] Dincer I and Abu-Rayash A (2020) Energy Sustainability. Amsterdam: Elsevier 1st edition, 266 pp.

[70] Olama AA (2017) District cooling Theory and Practice. CRC Press, 109 pp.

[71] Werner S (2004) District Heating and Cooling. In: Cleveland JC (ed). Encyclopedia of Energy. Elsevier, 841–848. doi: 10.1016/B0-12-176480-X/00214-X.

[72] Tredinnick S and Phetteplace G (2016) District cooling, current status and future trends. In: Wiltshire R (ed). Advanced District Heating and Cooling (DHC) Systems. Woodhead Publishing, 167–188.

[73] Werner S (2017) International review of district heating and cooling. Energy 137, 617–631. doi: 10.1016/j.energy.2017.04.045.

[74] Felsmann C, Tvärne A, Frohm H and Rubenhag A (2014) Rescue - Renewable Smart Cooling for Urban Europe. EU District Cooling Market and Trends. RESCUE, 64 pp.

[75] US DOE (2019) Energy Efficiency and Energy Security Benefits of District Heating. Report to Congress. United States Deparment of Energy, 56 pp.

[76] Baker L (2021) District cooling system University of North Carolina. Personal communication. University of North Carolina (UNC)

[77] Buffa S, Cozzini M, D'Antoni M, Baratieri M and Fedrizzi R (2019) 5th generation district heating and cooling systems: A review of existing cases in Europe. Renewable and Sustainable Energy Reviews 104, 504–522. doi: 10.1016/j.rser.2018.12.059.

[78] Godschalk B (2021) District cooling systems of universities. Personal communication. IF Technology.

[79] Verhoeven - de Weert (2021) ATES at TU Eindhoven. Personal communication.

[80] Lowe J (2021) District cooling at Ball State University. Personal communication. Ball State University (BSU).

[81] Stau S (2021) Kältenetz KIT Campus Süd. Personal communication. Karlsruhe Institute of Technology (KIT)

[82] Mehta RH (2011) Yale University District Cooling Systems Capacity & Operations Improvements. WM Group Engineers, 12 pp.

[83] Hall M Cooling the Desert. Salt Rivers Stories. https://saltriverstories.org/items/show/357. (last accessed: 09 Apr 2021).

[84] Mischissin S, Howe G and Schuett J (2016) Fifty years of district cooling and beyond. International District Energy Association, 12 pp.

[85] Shabbar A (2012) University of Toronto. One hundred years of district energy. International District Energy Association, 17 pp.

[86] 8760 Engineering (2012) Integrated Energy Master Plan. Indiana University - Bloomington, 207 pp.

[87] P2S Engineering I (2016) California State University San Bernardino. MEP Utilities Master Plan, 96 pp.

[88] Heizkraftwerk Pfaffenwald Universität Stuttgart Heizkraftwerk. Technik. Technische Daten unserer Energieerzegungsanlagen. https://www.hkw.uni-stuttgart.de/technik/ (last accessed: 09 Apr 2021).

[89] Hentze H (2021) Kältenetz Universität Stuttgart. Personal communication. Universität Stuttgart.

[90] Panossian VN (2019) Thermal and AC Power Systems Dispatch Optimization Incorporating Storage and unit Commitment. Dissertation, Washington State University, Pullman, 162 pp.

[91] Müller D, van Treeck, Christoph, Braun DH, Wenner and Dietmar (2017) EnEff: Campus RoadMap RWTH Aachen. Schlussbericht, 161 pp.

[92] Powell KM, Cole WJ, Ekarika UF and Edgar TF (2013) Optimal chiller loading in a district cooling system with thermal energy storage. Energy 50, 445–453. doi: 10.1016/j.energy.2012.10.058.

[93] Stagner CJ Stanford Energy System Innovations. General information. Stanford Energy System Innovations, 19 pp.

[94] Stagner CJ (2016) Stanford University's "fourthgeneration" district energy system. Combined heat and cooling provides a path to sustainability. International District Energy Association, 6 pp.

[95] Stagner CJ (2021) District cooling system at Stanford University. Personal communication. Stanford University.

[96] Coffin G (2017) University of Missouri District Energy System. Award Application for International District Energy Association System of the Year Award, 14 pp.

[97] Castro DD (2016) Development of a Model and Optimal Control Strategy for the Cal Poly Central Plant and Thermal Energy Storage System. Master Thesis, California Polytechnic State University, 145 pp.

[98] Doucette D (2021) Cooling supply at UNBC. Personal communication. UNBC.

[99] Oltmanns J, Sauerwein D, Dammel F, Stephan P and Kuhn C (2020) Potential for waste heat utilization of hot-water-cooled data centers: A case study. EnergySciEng 8, 1793–1810. doi: 10.1002/ese3.633.

[100] Hilckmann D (2021) District cooling system Radboud University. Personal communication. Radboud University.

[101] Buiting T (2021) District cooling system Radboud University. Personal communication. Radboud University.

[102] Perez-Mora N, Lazzeroni P, Repetto M, Canals V and Martinez-Moll V (2016) Optimal Solar District Cooling Harvesting Scenarios. In: Martínez V and González J (eds).

Proceedings of EuroSun2016. Freiburg, Germany: International Solar Energy Society, 1–11. doi: 10.18086/eurosun.2016.05.07.

[103] Knight J (2021) Bucknell University District Cooling. Personal communication. Bucknell University.

[104] Uribarri-Gomez B, Fedrizzi R, Cozzini M and D'Antoni M (2018) Fifth generation, low temperature, high exergy district heating and cooling networks. Flexynets Project, 42 pp.

[105] ETH Zürich (2019) Die Energie von morgen. Anergienetz Campus Hönggerberg - ein dynamisches Erdspeichersystem. Abteilung Immobilien, 6 pp.

[106] Energie Schweiz (2018) Fallbeispiele "Thermische Netze". Zusammenfassung, 143 pp.

[107] Hardenbrook T (2019) Accelerating Cooling System Performance at University of Oregon. WM Group, 31 pp.

[108] Abdullah MO, Yii LP, Junaidi E, Tambi G and Mustapha MA (2013) Electricity cost saving comparison due to tariff change and ice thermal storage (ITS) usage based on a hybrid centrifugal-ITS system for buildings: A university district cooling perspective. Energy and Buildings 67, 70–78. doi: 10.1016/j.enbuild.2013.08.008.

[109] Cornell University (2015) Cornell University Chilled Water Management Practices Program - 2014 Annual Report. Facilities Service - Energy and Sustainability - Utilities, 14 pp.

[110] Peer T and Joyce WS (2002) Lake-Source Cooling. ASHRAE Journal, 37–39.

[111] Mitchell SM and Spitler DJ (2013) Open-loop direct surface water cooling and surface water heat pump systems—A review. HVAC &R Research, 125–140. doi: 10.1080/10789669.2012.747374.

[112] Myers A (2013) Operational Performance Comparison of Variable and Fixed Speed. Chillers at Duke University's Chilled Water Plant No. 2, 24 pp.

[113] Werner S (2021) District cooling of universities. Personal communication.

[114] Paige D District Energy Systems. Tableau Public. https://public.tableau.com/profile/paige.davis#!/vizhome/NorthAmericaDistrictEnergySystemMap_Web/DistrictEnergySystems (last accessed: 09 Apr 2021).

[115] Frederiksen S and Werner S (2013) District Heating and Cooling. Studentlitteratur, 586 pp.

[116] Mathiesen BV, Bertelsen N, Schneiderm N. C. A., Garcia LS, Paardekooper S, Thellufsen JZ and Djorup SR (2019) Towards a decarbonised heating and cooling sector in Europe. Unlocking the potential of energy efficiency and district heating. Aaalborg Universitet, 98 pp.

[117] Sayegh MA, Danielewicz J, Nannou T, Miniewicz M, Jadwiszczak P, Piekarska K and Jouhara H (2017) Trends of European research and development in district heating technologies. Renewable and Sustainable Energy Reviews 68, 1183–1192. doi: 10.1016/j.rser.2016.02.023.

[118] Lund H, Werner S, Wiltshire R, Svendsen S, Thorsen JE, Hvelplund F and Mathiesen BV (2014) 4th Generation District Heating (4GDH). Energy 68, 1–11. doi: 10.1016/j.energy.2014.02.089.

[119] Sandrock M, Maaß C, Weisleder S, Westholm H, Schulz W, Löschan G, Baisch C, Kreuter H, Reyer D, Mangold D, Riegger M and Köhler C (2020) Kommunaler Klimaschutz durch Verbesserung der Effizienz in der Fernwärmeversorgung mittels Nutzung von Niedertemperaturwärmequellen am Beispiel tiefengeothermischer Ressourcen. Abschlussbericht. Umweltbundeamt Climate Change 31, 357 pp.

[120] BMWi (2020) Verwendung von Fernwärme in Deutschland. Energiedaten- und Szenarien. https://www.bmwi.de/Redaktion/DE/Infografiken/Energie/Energiedaten/Energietraeger/energiedaten-energietraeger-32.html (last accessed: 13 Apr 2021).

[121] Tomerius S (2016) Der Anschluss- und Benutzungszwang für kommunale Nah- und Fernwärmesysteme. Aktuelle rechtliche Vorgaben und Ausgestaltungsmöglichkeiten. Der ABZ für kommunale Nah- und Fernwärmesysteme, 61–66.

[122] Metzger S, Jahnke K, Walikewitz N, Otto M, Grondey A and Fritz S (2019) Wohnen und Sanieren. Empirische Wohngebäudedaten seit 2002 - Hintergrundbericht. Climate Change Umweltbundesamt 22, 131 pp.

[123] Werner S (2021) District cooling at universities. Personal communication.

[124] Bayer P, Attard G, Blum P and Menberg K (2019) The geothermal potential of cities. Renewable and Sustainable Energy Reviews 106, 17–30. doi: 10.1016/j.rser.2019.02.019.

[125] Brosi D and Siems L (2018) Anbindung eines Erdsondenfelds zur Wärmeabfuhr der Prozeswärme eines technischen Laboratoriums. Projetkarbeit, Hochschule Karlsruhe, Karlsruhe, 59 pp.

[126] IEA (2018) The Future of Cooling. Opportunities for energy-efficient air conditioning. doi: 10.1787/9789264301993-en.

[127] IPCC (2014) Climate Change 2014. Impacts, Adaptation, and Vulnerability. New York NY: Cambridge University Press, 1101 pp. pp.

[128] Santamouris M (2016) Cooling the buildings – past, present and future. Energy and Buildings 128, 617–638. doi: 10.1016/j.enbuild.2016.07.034.

[129] Jakubcionis M and Carlsson J (2017) Estimation of European Union residential sector space cooling potential. Energy Policy 101, 225–235. doi: 10.1016/j.enpol.2016.11.047.

[130] Mohammadi S, Vries B de and Schaefer W (2013) A Comprehensive Review of Existing Urban Energy Models in the Built Environment. In: Geertman S, Toppen F and Stillwell J (eds). Planning Support Systems for Sustainable Urban Development. Berlin, Heidelberg: Springer Berlin Heidelberg, 249–265. doi: 10.1007/978-3-642-37533-0_14.

[131] Swan LG and Ugursal VI (2009) Modeling of end-use energy consumption in the residential sector: A review of modeling techniques. Renewable and Sustainable Energy Reviews 13, 1819–1835. doi: 10.1016/j.rser.2008.09.033.

[132] Frayssinet L, Merlier L, Kuznik F, Hubert J-L, Milliez M and Roux J-J (2018) Modeling the heating and cooling energy demand of urban buildings at city scale. Renewable and Sustainable Energy Reviews 81, 2318–2327. doi: 10.1016/j.rser.2017.06.040.

[133] Chingcuanco F and Miller EJ (2012) A microsimulation model of urban energy use: Modelling residential space heating demand in ILUTE. Computers, Environment and Urban Systems 36, 186–194. doi: 10.1016/j.compenvurbsys.2011.11.005.

[134] Andreou A, Barrett BJ, Taylor CPG, Brockway DPE and Wadud EZ (2020) Decomposing the drivers of residential space cooling energy consumption in EU-28 countries using a panel data approach. Energy and Built Environment. doi: 10.1016/j.enbenv.2020.03.005.

[135] Werner S (2016) European space cooling demands. Energy 110, 148–156. doi: 10.1016/j.energy.2015.11.028.

[136] Gertec GmbH (2010) Kältemarktanalyse der Stadt Hamburg, 50 pp.

[137] Schramek E-R (2009) Taschenbuch für Heizung + Klimatechnik. München: Oldenbourg Industrieverlag 74th edn., 2311 pp.

[138] Ding G-l (2007) Recent developments in simulation techniques for vapour-compression refrigeration systems. International Journal of Refrigeration 30, 1119–1133. doi: 10.1016/j.ijrefrig.2007.02.001.

[139] Hesselbach J (2012) Energie- und klimaeffiziente Produktion. Grundlagen, Leitlinien und Praxisbeispiele. Wiesbaden: Springer Vieweg, 366 pp.

[140] Petchers N (2012) Combined Heating, Cooling & Power Handbook: Technologies & Applications. An integrated approach to energy resource optimization. Lilburn GA: The Fairmont Press 2nd edn., 818 pp.

[141] Sinopoli J (2010) Smart building systems for architects, owners, and builders. Amsterdam, Boston: Elsevier/Butterworth-Heinemann, 231 pp.

[142] Bohne D (2014) Technischer Ausbau von Gebäuden. Und nachhaltige Gebäudetechnik. Wiesbaden: Springer Vieweg 10th edn., 599 pp.

[143] Al-Ghandoor A, Al-Hinti I, Jaber JO and Sawalha SA (2008) Electricity consumption and associated GHG emissions of the Jordanian industrial sector: Empirical analysis and future projection. Energy Policy 36, 258–267. doi: 10.1016/j.enpol.2007.09.020.

[144] Gotzler W, Guernsey M, Young J, Fuhrman J and Abdelaziz O (2016) The Future of Air Conditioning for Buildings, 94 pp.

[145] Emicon (2014) ARW Trockenkühler - Dry Coolers.

[146] Trane (2008) Allgemeine Daten.

[147] Trane (2020) Luftgekühlte Verflüssiger mit bürstenlosen, ölfreien magnetgelagerten Turboverdichtern und Axialventilatoren. Baureihe CTAF, 8 pp.

[148] Hitchin R, Pout C and Riviere P (2013) Assessing the market for air conditioning systems in European buildings. Energy and Buildings 58, 355–362. doi: 10.1016/j.enbuild.2012.10.007.

[149] Bradbury K, Saboo R, L Johnson T, Malof JM, Devarajan A, Zhang W, M Collins L and G Newell R (2016) Distributed solar photovoltaic array location and extent dataset for remote sensing object identification. SciData 3, 160106. doi: 10.1038/sdata.2016.106.

[150] Malof JM, Bradbury K, Collins LM and Newell RG (2016) Automatic detection of solar photovoltaic arrys in high resolution aerial imagery. Applied Energy 183, 229–240. doi: 10.1016/j.apenergy.2016.08.191.

[151] Pezzutto S, Felice M de, Fazeli R, Kranzl L and Zambotti S (2017) Status Quo of the Air-Conditioning Market in Europe: Assessment of the Building Stock. Energies 10, 1253. doi: 10.3390/en10091253.

[152] EEA (2021) Heating and cooling degree days. https://www.eea.europa.eu/data-and-maps/indicators/heating-degree-days-2/assessment (last accessed: 07 Apr 2021).

[153] Levesque A, Pietzcker RC, Baumstark L, Stercke S de, Grübler A and Luderer G (2018) How much energy will buildings consume in 2100? A global perspective within a scenario framework. Energy 148, 514–527. doi: 10.1016/j.energy.2018.01.139.

[154] Ruijven van BJ, Cian E de and Sue Wing I (2019) Amplification of future energy demand growth due to climate change. NatCommun 10, 2762. doi: 10.1038/s41467-019-10399-3.

[155] Eveloy V and Ayou D (2019) Sustainable District Cooling Systems: Status, Challenges, and Future Opportunities, with Emphasis on Cooling-Dominated Regions. Energies 12, 235. doi: 10.3390/en12020235.

[156] Shakouri G. H (2019) The share of cooling electricity in global warming: Estimation of the loop gain for the positive feedback. Energy 179, 747–761. doi: 10.1016/j.energy.2019.04.170.

[157] Werner S (2015) European space cooling demands. Energy 110, 148–156. doi: 10.1016/j.energy.2015.11.028.

[158] Heat Roadmap Europe 2050 (2017) Heating and Cooling. Facts and figures. The transformation towards a low-carbon Heating & Cooling sector, 8 pp.

[159] Dittmann F, Riviere P and Stabat P (2017) Space Cooling Technology in Europe. Technology Data and Demand Modelling. Heat Roadmap Europe 2050. A low-carbon heating and cooling strategy, 54 pp.

[160] Persson U and Werner S (2015) Quantifying the Heating and Cooling Demand in Europe. Stratego Enhanced Heating & Cooling Plans, 25 pp.

[161] Alshuwaikhat HM and Abubakar I (2008) An integrated approach to achieving campus sustainability: assessment of the current campus environmental management practices. Journal of Cleaner Production 16, 1777–1785. doi: 10.1016/j.jclepro.2007.12.002.

[162] Saadatian O, Sopian KB and Salleh E (2013) Adaptation of sustainability community indicators for Malaysian campuses as small cities. Sustainable Cities and Society 6, 40–50. doi: 10.1016/j.scs.2012.08.002.

[163] Guerrieri M, La Gennusa M, Peri G, Rizzo G and Scaccianoce G (2019) University campuses as small-scale models of cities: Quantitative assessment of a low carbon transition path. Renewable and Sustainable Energy Reviews 113, 109263. doi: 10.1016/j.rser.2019.109263.

[164] Kolokotsa D, Gobakis K, Papantoniou S, Georgatou C, Kampelis N, Kalaitzakis K, Vasilakopoulou K and Santamouris M (2016) Development of a web based energy management system for University Campuses: The CAMP-IT platform. Energy and Buildings 123, 119–135. doi: 10.1016/j.enbuild.2016.04.038.

[165] Murshed M (2020) Electricity conservation opportunities within private university campuses in Bangladesh. Energy & Environment 31, 256–274. doi: 10.1177/0958305X19857209.

[166] Opel O, Strodel N, Werner KF, Geffken J, Tribel A and Ruck WKL (2017) Climate-neutral and sustainable campus Leuphana University of Lueneburg. Energy 141, 2628–2639. doi: 10.1016/j.energy.2017.08.039.

[167] Chung MH and Rhee EK (2014) Potential opportunities for energy conservation in existing buildings on university campus: A field survey in Korea. Energy and Buildings 78, 176–182. doi: 10.1016/j.enbuild.2014.04.018.

[168] Yildiz Y and Koçyiğit M (2020) A study on the energy-saving potential of university campuses in Turkey. Proceedings of the Institution of Civil Engineers - Engineering Sustainability 173, 379–396. doi: 10.1680/jensu.20.00006.

[169] Rezaie B and Rosen MA (2012) District heating and cooling: Review of technology and potential enhancements. Applied Energy 93, 2–10. doi: 10.1016/j.apenergy.2011.04.020.

[170] DHC+ (2012) District Heating & Cooling. A vision towards 2020-2030-2050, 36 pp.

[171] Zhu X (2015) A Feasibility Study of Using River Water in University Cooling System. Master Thesis, University of Gävle, Gävle, Sweden, 94 pp.

[172] Montagud C, Corberán JM and Ruiz-Calvo F (2013) Experimental and modeling analysis of a ground source heat pump system. Applied Energy 109, 328–336. doi: 10.1016/j.apenergy.2012.11.025.

[173] Schüppler S, Fleuchaus P, Zorn R, Salomon R and Blum P (2021) Quantifiying Installed Cooling Capacities by Aerial Images. Journal of Photogrammetry, Remote Sensing and Geoinformation Science. News item. doi: 10.1007/s41064-021-00137-0.

[174] Calderoni M, Dourlens-Qarante S, Sreekumar BB, Lennard Z, Rämä M, Klobut K, Wang Z, Duan X, Zhang Y, Nilsson J and Hargö L (2019) Suistanable District Cooling Guidelines. IAE DHC/CHP Report, 162 pp.

[175] UK Green Building Council (2011) Carbon Reductions in Existing Non-Domestic Buildings. A UK-GBC Task Group on Display Energy Certificates and the Carbon Reduction Commitment Energy Efficiency Scheme, 40 pp.

[176] Papash A, Blomley E, Boltz T, Brosi M, Bründermann E, Casalbuoni S, *et al. (eds)* New Operation Regimes at the Storage Ring KARA at KIT (2019), 4 pp.

[177] Karlsruhe Institute of Technology (2020) Facility management (FM). Versorgungsmanagement (VM). http://www.fm.kit.edu/112.php (last accessed: 07 Dec 2020).

[178] Energie Baden-Württemberg EnbW (2020) EnbW. https://www.enbw.com/ (last accessed: 07 Dec 2020).

[179] Dinçer İ and Rosen M (2015) Exergy analysis of heating, refrigerating, and air conditioning. Methods and applications. Amsterdam, Boston: Elsevier, 387 pp.

[180] Fairey P, Wilcox B, Parker SD and Lombardi M (2004) 4710.fm. ASHRAE Transactions: Reseach, 178–188.

[181] Hao X, Zhu C, Lin Y, Wang H, Zhang G and Chen Y (2013) Optimizing the pad thickness of evaporative air-cooled chiller for maximum energy saving. Energy and Buildings 61, 146–152. doi: 10.1016/j.enbuild.2013.02.028.

[182] Hansen K (2019) Decision-making based on energy costs: Comparing levelized cost of energy and energy system costs. Energy Strategy Reviews 24, 68–82. doi: 10.1016/j.esr.2019.02.003.

[183] Yang IT (2008) Distribution-Free Monte Carlo Simulation: Premise and Refinement. Journal of Construction Engineering and Management 134, 352–360. doi: 10.1061/ASCE.

[184] Vořechovský M (2012) Correlation control in small sample Monte Carlo type simulations II: Analysis of estimation formulas, random correlation and perfect uncorrelatedness. Probabilistic Engineering Mechanics 29, 105–120. doi: 10.1016/j.probengmech.2011.09.004.

[185] LUBW (2019) Probenahmestelle Karlsruhe-Nordwest. https://www.lubw.baden-wuerttemberg.de/documents/10184/705223/DEBW081_KA-NW.pdf (last accessed: 17 Aug 2020).

[186] Ayou DS and Coronas A (2020) New Developments and Progress in Absorption Chillers for Solar Cooling Applications. Applied Sciences 10, 4073. doi: 10.3390/app10124073.

[187] Pieper H, Ommen T, Buhler F, Paaske BL, Elmegaard B and Markussen WB (2018) Allocation of investment costs for large-scale heat pumps supplying district heating. Energy Procedia 147, 358–367. doi: 10.1016/j.egypro.2018.07.104.

[188] European Commission (2016) Mapping and analyses of the current and future (2020 - 2030) heating/cooling fuel deployment (fossil/renewables). Work package 2: Assessment of the technologies for the year 2012. Final report. Prepared for: European Commission under contract N°ENER/C2/2014-641, 215 pp.

[189] Schöpfer MD (2015) Absorption chillers: their feasibility in district heating networks and comparison to alternative technologies. Master thesis, Tecnico Lisboa, Lisbon, 98 pp.

[190] Verbič M, Filipović S and Radovanović M (2017) Electricity prices and energy intensity in Europe. Utilities Policy 47, 58–68. doi: 10.1016/j.jup.2017.07.001.

[191] IEA (2020) World Energy Prices - Overview. Statistics report, 19 pp.

[192] ASHRAE (2013) District Cooling Guide, 238 pp.

[193] IDEA (2008) District Cooling Best Practice Guide. Published to inform, connect and advance the global district cooling industry. Westborough, Massachusetts, USA 1st edn., 175 pp.

[194] Vetterli N, Sulzer M and Menti U-P (2017) Energy monitoring of a low temperature heating and cooling district network. Energy Procedia 122, 62–67. doi: 10.1016/j.egypro.2017.07.289.

[195] Engie Refrigeration (2016) Effiziente Fernkälte mit Power, 2 pp.

[196] Drenkelfort G, Kieseler S, Pasemann A and Behrendt F (2015) Aquifer thermal energy storages as a cooling option for German data centers. Energy Efficiency 8, 385–402. doi: 10.1007/s12053-014-9295-1.

[197] Schüppler S, Fleuchaus P and Blum P (2019) Techno-economic and environmental analysis of an Aquifer Thermal Energy Storage (ATES) in Germany. GeothermEnergy 7, 669. doi: 10.1186/s40517-019-0127-6.

[198] Andersson O (2005) ATES for District Cooling in Stockholm. In: Paksoy HÖ (ed). Thermal Energy Storage for Sustainable Energy Consumption. Fundamentals, Case Studies and Design. Springer, 239–243.

[199] Hellström G (2011) UTES Experiences from Sweden. Proceedings of the REHAU, 58 pp.

[200] Im P, Liu X and Henderson H (2016) Case Study for the ARRA-Funded Ground-Source Heat Pump Demonstration at Ball State University. Energy and Transportation Science Division, 42 pp.

[201] Kizilkan O and Dincer I (2012) Exergy analysis of borehole thermal energy storage system for building cooling applications. Energy and Buildings 49, 568–574. doi: 10.1016/j.enbuild.2012.03.013.

[202] Larsen HH and Sønderberg PL (2015) DTU International Energy Report 2015. Energy systems integration for the transition to non-fossil energy systems. Technical University of Denmark (DTU), 103 pp.

[203] Looney CM and Oney SK (2007) Seawater District Cooling and Lake Source District Cooling. Energy Engineering 104, 34–45. doi: 10.1080/01998590709509510.

[204] McClintock C (2009) District cooling case study – James Cook University, Townsville. Ecolibrium, 10 pp.

[205] Meulen T (2017) Smartgrid Warmte - Koude Opslag TU/e. WKO bedrijventerreinen, 22 pp.

[206] Moià-Pol A, Martínez-Moll V, Nadal RP and Serra JMR (2014) Solar Thermal Potential for Collective Systems in Palma Beach (Balearic Island's). Energy Procedia 48, 1118–1123. doi: 10.1016/j.egypro.2014.02.126.

[207] Pretzman R (2021) District cooling system at Arizona State University. Personal communication. Arizona State University.

[208] Seymour S (2021) District cooling system University of Florida. Personal communication.

[209] Terouanne D, Francouse Y and Veerapen PJ (2011) Climespace - City of Paris: A District Cooling System to control impact of air-conditioning in Paris. Climespace Application File for the Global District Energy Climate Awards 2011, 16 pp.

[210] Vanhoudt D, Desmedt J, van Bael J, Robeyn N and Hoes H (2011) An aquifer thermal storage system in a Belgian hospital: Long-term experimental evaluation of energy and cost savings. Energy and Buildings 43, 3657–3665. doi: 10.1016/j.enbuild.2011.09.040.

[211] Wigstrand I (2009) The ATES project - a sustainable solution for Stockholm-Arlanda airport. 11th International Conference on Thermal Energy Storage for Energy Efficiency and Sustainability. Stockholm, Sweden., 5 p.

[212] Kazanci OB, Shukuya M and Olesen BW (2016) Theoretical analysis of the performance of different cooling strategies with the concept of cool exergy. Building and Environment 100, 102–113. doi: 10.1016/j.buildenv.2016.02.013.

[213] Arghand T (2021) Direct Ground Cooling Systems for Office Buildings. Dissertation, Chalmers University of Technology, Gothenburg, 101 pp.

[214] Eindhoven University of Technology (2021) Sustainability. Cold and heat storage. https://www.tue.nl/en/tue-campus/discover-your-campus/sustainability/atlas/the-most-sustainable-building-of-education/cold-and-heat-storage/ (last accessed: 24 Feb 2021).

[215] Institut für Technologie und Management im Baubetrieb (2021) OPIK - Optimierung und Analyse von Prozessen in Krankenhäusern. https://www.tmb.kit.edu/1144_1197.php (last accessed: 22 Feb 2021).

[216] Ricaurte E (2017) Hotel Sustainability Benchmarking Index 2017: Energy, Water, and Carbon. Cornell Hospitality Report 17, 19 pp.

[217] Bloemendal M, Olsthoorn T and Boons F (2014) How to achieve optimal and sustainable use of the subsurface for Aquifer Thermal Energy Storage. Energy Policy 66, 104–114. doi: 10.1016/j.enpol.2013.11.034.

[218] Dickinson J, Buik N, Matthews M and Snijders A (2008) Aquifer thermal energy storage: theoretical and operational analysis. Géotechnique 58, 1–12. doi: 10.1680/geot.2008.58.00.1.

[219] Hähnlein S, Bayer P and Blum P (2010) International legal status of the use of shallow geothermal energy. Renewable and Sustainable Energy Reviews 14, 2611–2625. doi: 10.1016/j.rser.2010.07.069.

[220] Kangas TA and Lund PD (1994) Modelling and simulation of aquifer storage energy systems. Solar Energy 53, 237–247. doi: 10.1016/0038-092X(94)90630-0.

[221] Dincer I and Rosen MA (2011) Thermal energy storage. Systems and applications. Wiley 2nd ed., 599 pp.

[222] Kalaiselvam S and Parameshwaran R (2014) Thermal Energy Storage Technologies for Sustainability. Systems Design, Assessment, and Applications. Amsterdam, Boston: Elsevier 1st ed., 430 pp.

[223] Rosen MA and Koohi-Fayegh S (2017) Geothermal Energy. Sustainable Heating and Cooling Using the Ground. Chichester West Sussex United Kingdom: Wiley, 277 pp.

[224] Andersson O, Ekkestubbe J and Ekdahl A (2013) UTES (Underground Thermal Energy Storage) - Applications and Market Development in Sweden. Journal of Energy and Power Engineering 7, 669–678.

[225] Bloemendal M and Olsthoorn T (2018) ATES systems in aquifers with high ambient groundwater flow velocity. Geothermics 75, 81–92. doi: 10.1016/j.geothermics.2018.04.005.

[226] Bridger DW and Allen DM (2010) Heat transport simulations in a heterogeneous aquifer used for aquifer thermal energy storage (ATES). CanGeotechJ 47, 96–115. doi: 10.1139/T09-078.

[227] Bridger DW and Allen DM (2005) Designing Aquifer Thermal Energy Storage Systems. ASHRAE 47, 32–37.

[228] van Beek D and Godschalk B (2013) Regulative framework in The Netherlands, 32 pp.

[229] Bonte M, van Breukelen BM and Stuyfzand PJ (2013) Environmental impacts of aquifer thermal energy storage investigated by field and laboratory experiments. Journal of Water and Climate Change 4, 77–89. doi: 10.2166/wcc.2013.061.

[230] Eggen G and Vangsnes G (2005) Heat pump for district cooling and heating at Oslo Airport Gardermoen. Proceedings of the 8th IEA Heat Pump Conference: Global Advances in Heat Pump Technoloy, Applications and Market. Las Vegas, NV., 7 pp.

[231] Sommer W, Valstar J, van Gaans P, Grotenhuis T and Rijnaarts H (2013) The impact of aquifer heterogeneity on the performance of aquifer thermal energy storage. Water Resources Research 49, 8128–8138. doi: 10.1002/2013WR013677.

[232] Snijders AL (2005) Aquifer Thermal Energy Storage in the Netherlands. Status beginning of 2005. IFTech International B.V., 3 pp.

[233] Reilly RW, Brown DR and Huber HD (1981) Aquifer Thermal Energy Storage Costs with a Seasonal Heat Source. doi: 10.2172/5233922.

[234] Zimmerman PW and Drost MK (1989) Cost Analysis of Power Plant Cooling Using Aquifer Thermal Energy Storage. doi: 10.2172/5962306.

[235] Andersson O and Sellberg B (1992) Swedish ATES Applications: Experiences after Ten Years of Development. In: Jenne EA (ed). Aquifer Thermal Energy (Heat and Chill) Storage: Proceedings of the 27th 521 Intersociety Energy Conversion Engineering Conference. San Diego, CA, 1–9.

[236] Chant V and Morofsky E (1992) Overview of Projects with Seasonal Storage for Cooling from Four Countries. In: Jenne EA (ed). Aquifer Thermal Energy (Heat and

Chill) Storage: Proceedings of the 27th 521 Intersociety Energy Conversion Engineering Conference. San Diego, CA, 17–21.

[237] van Hove J (1993) Productivity of Aquifer Thermal Energy Storage (ATES) in The Netherlands. Tunnelling and Underground Space Technology 8, 47–52. doi: 10.1016/0886-7798(93)90136-J.

[238] Paksoy H, Snijder A and Stiles L (2009) State-of-the-Art Review of Aquifer Thermal Energy Storage Systems for Heating and Cooling Buildings. In: Proceedings Effstock. 11th International Conference on Thermal Energy Storage for Energy Efficiency and Sustainability. Stockholm, Sweden, 9 pp.

[239] Hendriks M and Velvis H (2012) Operational management of large scale UTES systems in Hospitals. Proceedings Innostock. The 12th International Conference on Energy Storage. Lleida, Spain, 10 pp.

[240] viamedica (2009) Erneuerbare Energien und Energieeffizienz in deutschen Kliniken, 40 pp.

[241] Natural Resources Canada (2019) RETScreen. https://www.nrcan.gc.ca/energy/software-tools/7465 (last accessed: 29 Jan 2019.).

[242] Behi M, Mirmohammadi SA, Suma AB and Palm BE (2014) Optimized Energy Recovery in Line With Balancing of an ATES. Proceedings of the ASME 2014 Power Conference, Balitmore, Maryland. doi: 10.1115/POWER2014-32017.

[243] GHJ (2017) Ingenieurgesellschaft für Geo- und Umwelttechnik. Kostenschätzung Geothermieanlage.

[244] Bloomquist RG (2000) Geothermal Heat Pumps Five plus decades of Experience in the United States. Proceedings World Geothermal Congress, Kyushu - Tohoku, Japan, 6 pp.

[245] Liang X and Fleming E (2012) Power Consumption Evaluation for Electrical Submersible Pump Systems. IEEE/IAS 48th Industrial & Commercial Power Systems Technical Conference (I&CPS), Louisville, KY, 1–6. doi: 10.1109/ICPS.2012.6229611.

[246] Bakema G, Snijders AL and Nordell B (1995) Underground Thermal Energy Storage. State of the art 1994. In: International Energy Agency (ed). International Energy Agency. Implementing Agreement for a Programme Implementing Agreement for a

Programm of Research and Development on Energy Conservation through Energy Storage, 89 pp.

[247] Hartog N, Drijver B, Dinkla I and Bonte M (2013) Field assessment of the impacts of Aquifer Thermal Energy Storage (ATES) systems on chemical and microbial groundwater composition. Proceedings of the European Geothermal Conference, Pisa, Italy, 8 pp.

[248] Seider WD (2006) Equipment Sizing and Capital Cost Estimation. University of Pennsylvania, Philadelphia, Pennsylvania, 10 pp.

[249] GWE (2017) Preisliste. German Water and Energy Group, 146 pp.

[250] LANUV (2015) Leistungsbuchs Altlasten und Flächenentwicklung. Landesamt für Natur, Umwelt und Verbraucherschutz Nordrhein-Westfalen. http://www.leistungsbuch.de/Frontend/lbuKatalog/KatalogForm.aspx (last accessed: 29 Jan 2019.).

[251] Palisade (2019) @Risk ein neuer Standard für die Risikoanalyse. https://www.palisade.com/risk/de/ (last accessed: 11 Apr 2021).

[252] Blohm H, Lüder K and Schaefer C (1995) Investition: Schwachstellenanalyse des Investitionsbereichs und Investitionsrechnung. München. 345 pp.: Vahlen 9th edn., 345 pp.

[253] MacKenzie W and Cusworth N (2007) The Use and Abuse of Feasibility Studies. Project Evaluation Conference, Melbourne, Vic., 12 pp.

[254] Chiasson A and Culver G (2006) Final report feasibility study for HVAC retrofit with a geothermal system Mount Grant General Hospital, Hawthorne, NV. Geo-Heat Center, Oregon Institute of Technology, 48 pp.

[255] Sanderson J (2018) Costs reverse rotary drilling. Personal Communication.

[256] Boissavy C (2015) Cost and Return on Investment for Geothermal Heat Pump Systems in France. Proceedings World Geothermal Congress, Melbourne, Australia, 19-25 April 2015, 9 pp.

[257] IEA (2007) Renewables for Heating and Cooling. Untapped Potential. International Energy Agency, Paris., 210 pp.

[258] Stindl R (2017) Electricity costs. Personal communication. Städtisches Klinikum Karlsruhe.

[259] Stadtwerke Karlsruhe (2017) Umwelterklärung 2017 mit Klimareport und Energiebericht. Aktualisierte Kennzahlen, 40 pp.

[260] Engie (2018) Der Weg zum gesunden Klima. Energieeffiziente Kältemaschinen und Serbives für Kliniken und Krankenhäuser, 5 pp.

[261] Stadtwerke Sindelfingen (2007) Planbare Kosten - die Hausanschlusspauschalen., 3 pp.

[262] Stadtwerke Sindelfingen (2018) Hausanschlusskosten Fernwärme., 1 pp.

[263] Stadtwerke Waldkraiburg (2018) Preisblatt geothermale Fernwärmeversorgung der Stadtwerke Waldkraiburg GmbH., 6 pp.

[264] HallamICS (2012) Montpelier District Heating Cost Estimate. HallamICS. South Burlington, VT., 19 pp.

[265] Stadtwerke Karlsruhe (2018) Fernwärme. Ohne Heizung heizen und dabei das Klima schützen?, 4 pp.

[266] Stadtwerke Ulm (2018) SWU Energie GmbH Preisblatt für Fernwärme., 4 pp.

[267] Stadtwerke Pforzheim (2019) Fernwärmeversorgung der SWP. Available at: https://www.stadtwerke-pforzheim.de/fernwaerme/preise (last accessed: 29 Jan 2019.).

[268] Stadtwerke Emmendingen (2019) Preisblatt Wärmelieferung – Preisstand 01.01.2019, 4 pp.

[269] Gudmundsson O, Thorsen JE and Zhang L (2013) Cost analysis of district heating compared to its competing technologies. WIT Transactions on Ecology and The Environment 176, 3–13. doi: 10.2495/ESUS130091.

[270] Konstantin P (2017) Praxisbuch Energiewirtschaft. Energieumwandlung, -transport und -beschaffung, Übertragungsnetzausbau und Kernenergieaussstieg. Springer Vieweg 4th edn., 590 pp.

[271] IUTA (2002) Preisatlas - Ableitung von Kostenfunktionen für Komponenten der rationellen Energienutzung. Institut für Energie- und Umwelttechnik e.V., Duisburg-Rheinhausen., 356 pp.

[272] Schäfer V and Negele B (2009) Absorptionskältemaschinen - Anwendungsbeispiele. Kl Kälte Luft Klimatechnik, 26–31.

[273] Schlott S (2001) Kälteerzeugung für die Klimatechnik mit einer Kompressions- oder Absorptionsmaschine mit Fernwärme. Schlott & Partner GmbH, Zwickau, 19 pp.

[274] Department of Transport and Main Roads (2015) Project Cost Estimating Manual - 6th Edition. Queensland Government, 116 pp.

[275] Engie (2016) ENGIE Refrigeration kühlt den WDR rund um die Uhr, 2 pp.

[276] Heinrich C, Wittig S, Albring P, Richter L, Safarik M, Böhm U and Hantsch A (2014) Nachhaltige Kälteversorgung in Deutschland an den Beispielen Gebäudeklimatisierung und Industrie. Im Auftrag des Umweltbundesamtes. Umweltbundesamt, Dresden, 226 pp.

[277] BMWi (2017) Zahlen und Fakten Energiedaten: Nationale und internationale Entwicklung. Entwicklung von Energiepreisen und Preisindizes zu nominalen Preisen Deutschland. Bundesministerium für Wirtschaft und Energie.

[278] EnbW (2017) CO_2-Fußabdruck und Energieeffizienz: Spezifische CO_2-Emissionen. Spezifische CO_2-Emissionen der Eigenerzeugung Strom. Energie Baden-Württemberg AG. Available at: https://www.enbw.com/unternehmen/konzern/ueber-uns/umweltschutz/co2/ (last accessed: 29 Jan 2019.).

[279] Fair Energy (2018) TÜV Zertifikat CO2 Emissionsfaktor. Available at: https://www.fairenergie.de/inhalt/privatkunden/fernwaerme.html (last accessed: 29 Jan 2019.).

[280] Stadtwerke Emmendingen (2019) Fernwärme. Available at: https://swe-emmendingen.de/fernwarme/ (last accessed: 29 Jan 2019.).

[281] Kabus F, Wolfgramm M, Seibt A, Richlak U and Beuster H (2009) Aquifer Thermal Energy Storage in Neubrandenburg - Monitoring throughout three years of regular operation. Proceedings of the 11th international conference on energy storage, 9 pp.

[282] Sanner B (2000) High Temperatur Underground Thermal Energy Storage. Fifth report to the Executive Committee. ECES Annex 12, 10 pp.

[283] Snijders AL and van Aarssen MM (2003) Big is beautiful? Application of large-scale energy storage in the Netherlands. Futurestock' 9th International Conference on the Thermal Energy Storage, Warsaw, Poland, 6 pp.

[284] Baxter G, Srisaeng P and Wild G (2018) An Assessment of Airport Sustainability, Part 2—Energy Management at Copenhagen Airport. Resources 7, 32. doi: 10.3390/resources7020032.

[285] Worthington MA (2011) Aquifer Thermal Energy Storage: An Enabling Green Technology for Campus District Energy Systems. IDEA's 24th Annual Campus Energy Conference - Campus Energy/CHP/Clean Energy. Miami, Florida, 30 pp.

[286] Hoes H, Desmedt J, Robeyn N and van Bael J (2006) Experience with ATES applications in Belgium. Operational results and energy savings. Ecostock - Conference Proceedings. Stockton University, NJ, USA, 8 pp.

[287] Desmedt J and Hoes H (2007) Monitoring results of aquifer thermal energy storage system in a Belgian hospital. 2nd PALENC COnference and 28th AIVC COnference on Building Low Energy Cooling and Advanced Ventilation Technologies in the 21st Century, 4 pp.

[288] Stadtwerke Karlsruhe (2016) Allgemeine Preise im Rahmen der Grundversorgung, 1 pp.

[289] Kranz S and Frick S (2013) Efficient cooling energy supply with aquifer thermal energy storages. Applied Energy, 321–327. doi: 10.1016/j.apenergy.2012.12.002.

[290] Bozkaya B and Zeiler W (2019) The effectiveness of night ventilation for the thermal balance of an aquifer thermal energy storage. Applied Thermal Engineering 146, 190–202. doi: 10.1016/j.applthermaleng.2018.09.106.

[291] Holstenkamp L, Meisel M, Neidig P, Opel O, Steffahn J, Strodel N, Lauer JJ, Vogel M, Degenhart H, Michalzik D, Schomerus T, Schönebeck J and Növig T (2017) Interdisciplinary Review of Medium-deep Aquifer Thermal Energy Storage in North Germany. Energy Procedia 135, 327–336. doi: 10.1016/j.egypro.2017.09.524.

[292] Kabus F and Seibt P (2000) Aquifer Thermal Energy Storage for the Berlin Reichtstag building - New seat of the German parliament. Proceedings World Geothermal Congress. Kyushu - Tohoku, Japan, 5 pp.

[293] Umweltbundesamt (2018) Hohe Kosten durch unterlassenen Umweltschutz. Available at: https://www.umweltbundesamt.de/presse/pressemitteilungen/hohe-kosten-durch-unterlassenen-umweltschutz (last accessed: 29 Jan 2019.).

[294] Yang H, Cui P and Fang Z (2010) Vertical-borehole ground-coupled heat pumps: A review of models and systems. Applied Energy 87, 16–27. doi: 10.1016/j.apenergy.2009.04.038.

[295] Lund JW, Freeston DH and Boyd TL (2005) Direct application of geothermal energy: 2005 Worldwide review. Geothermics 34, 691–727. doi: 10.1016/j.geothermics.2005.09.003.

[296] Rivera JA, Blum P and Bayer P (2017) Increased ground temperatures in urban areas: Estimation of the technical geothermal potential. Renewable Energy 103, 388–400. doi: 10.1016/j.renene.2016.11.005.

[297] Gaia Geothermal (2009) Ground Loop Design. Geothermal Design Studio, 178 pp.

[298] Hellström G and Sanner B (2000) EED Earth Energy Designer. User Manual, 43 p.

[299] Spitler JD (2000) GLHEPRO - A Design Tool For Commercial Building Ground Loop Heat Exchangers. Proceedings of the Fourth International Heat Pumps in Cold Climates Conference, Aylmner, Quebec, 17-18 August, 2000, 16 pp.

[300] Chiasson AD (2016) Geothermal Heat Pump and Heat Engine Systems: Theory and Practice. West Sussex, United Kingdom: Wiley, 494 pp.

[301] Kavanaugh S (2010) Ground Source Heat Pump System Designer. GshpCalc Version 5.0, 56 pp.

[302] sia (2010) Erdwärmesonden SIA 384/6-C1:2010. Schweizerischer Ingenieur- und Architektenverein, 76 pp.

[303] Nordell B (1993) Borehole Heat Store Design Optimization. Doctoral Thesis, Lulea University of Technology, Lulea, Sweden, 275 pp.

[304] Spitler JD and Bernier M (2016) Vertical borehole ground heat exchanger design methods. In: Rees S (ed). Advances in Ground-Source Heat Pump Systems. Elsevier, 1st edn., 29–61. doi: 10.1016/B978-0-08-100311-4.00002-9.

[305] Beier RA (2011) Vertical temperature profile in ground heat exchanger during in-situ test. Renewable Energy 36, 1578–1587. doi: 10.1016/j.renene.2010.10.025.

[306] Gwadera M, Larwa B and Kupiec K (2017) Undisturbed Ground Temperature—Different Methods of Determination. Sustainability 9, 1–14. doi: 10.3390/su9112055.

[307] Ouzzane M, Eslami-Nejad P, Badache M and Aidoun Z (2015) New correlations for the prediction of the undisturbed ground temperature. Geothermics 53, 379–384. doi: 10.1016/j.geothermics.2014.08.001.

[308] Radioti G, Sartor K, Charlier R, Dewallef P and Nguyen F (2017) Effect of undisturbed ground temperature on the design of closed-loop geothermal systems: A case study in a semi-urban environment. Applied Energy 200, 89–105. doi: 10.1016/j.apenergy.2017.05.070.

[309] Fluker BJ (1958) Soil temperatures. Soil Science, 35–46.

[310] Givoni B and Katz L (1985) Earth Temperature and Underground Buildings. Energy and Buildings 8, 15–25. doi: 10.1016/0378-7788(85)90011-8.

[311] Hillel D (2013) Introduction to Soil Physics. Academic Press 1st edn., 392 pp. pp.

[312] Kusuda T and Archenbach P (1965) Earth temperature and thermal diffusivity at selected stations in the United States. ASHRAE Transactions 71, 233 pp.

[313] Wu J and Nofziger DL (1999) Incorporating Temperature Effects on Pesticide Degradation into a Management Model. Journal of Environmental Quality 28, 92–100. doi: 10.2134/jeq1999.00472425002800010010x.

[314] Badache M, Eslami-Nejad P, Ouzzane M, Aidoun Z and Lamarche L (2016) A new modeling approach for improved ground temperature profile determination. Renewable Energy 85, 436–444. doi: 10.1016/j.renene.2015.06.020.

[315] Acuña J and Palm B (2013) Distributed thermal response tests on pipe-in-pipe borehole heat exchangers. Applied Energy 109, 312–320. doi: 10.1016/j.apenergy.2013.01.024.

[316] Sanner B, Hellström G, Gehlin S and Spitler J (2005) Thermal Response Test - Current Status and World-Wide Application. Proceedings World Geothermal Congress 2005, Antalya, Turkey, 24-29 April 2005, 9 pp.

[317] Gehlin S (2002) Thermal response test: method development and evaluation. Doctoral thesis, Lulea University of Technology, Lulea, 191 pp.

[318] Gehlin S and Nordell B (2003) Determining Undisturbed Ground Temperature for Thermal Response Test. ASHRAE Transactions 109, 151-156.

[319] Claesson J and Eskilson P (1988) Conductive Heat Extraction to a Deep Borehole: Thermal Analyses and Dimensioning Rules. Energy 13, 509–527

[320] Bayer P, Rivera JA, Schweizer D, Schärli U, Blum P and Rybach L (2016) Extracting past atmospheric warming and urban heating effects from borehole temperature profiles. Geothermics 64, 289–299. doi: 10.1016/j.geothermics.2016.06.011.

[321] Acuña J, Mogensen P and Palm B (2009) Distributed Thermal Response Test on a U-Pipe Borehole Heat Exchanger. Proceedings of 11th International Conference on Energy Storage EFFSTOCK, Stockholm, Sweden, 14-17 June, 8 pp.

[322] Cao D, Shi B, Zhu H-H, Wei G, Bektursen H and Sun M (2018) A field study on the application of distributed temperature sensing technology in thermal response tests for borehole heat exchangers. BullEngGeolEnviron 109, 312. doi: 10.1007/s10064-018-1407-2.

[323] Fujii H, Okubo H, Nishi K, Itoi R, Ohyama K and Shibata K (2009) An improved thermal response test for U-tube ground heat exchanger based on optical fiber thermometers. Geothermics 38, 399–406. doi: 10.1016/j.geothermics.2009.06.002.

[324] Luo J, Rohn J, Xiang W, Bayer M, Priess A, Wilkmann L, Steger H and Zorn R (2015) Experimental investigation of a borehole field by enhanced geothermal response test and numerical analysis of performance of the borehole heat exchangers. Energy 84, 473–484. doi: 10.1016/j.energy.2015.03.013.

[325] Shim BO and Song Y (2011) Interpretation of Thermal Response Tests using the Fiber Optic Distributed Temperature Sensing Method. The 11th international conference on energy storage EFFSTOCK, Stockholm, Sweden, 5 pp

[326] Soldo V, Boban L and Borović S (2016) Vertical distribution of shallow ground thermal properties in different geological settings in Croatia. Renewable Energy 99, 1202–1212. doi: 10.1016/j.renene.2016.08.022.

[327] Aranzabal N, Martos J, Steger H, Blum P and Soret J (2019) Novel Instrument for Temperature Measurements in Borehole Heat Exchangers. IEEETransInstrumMeas 68, 1062–1070. doi: 10.1109/TIM.2018.2860818.

[328] Aranzabal N, Martos J, Stokuca M, Mazzotti Pallard W, Acuña J, Soret J and Blum P (2020) Novel instruments and methods to estimate depth-specific thermal properties in

borehole heat exchangers. Geothermics 86, 101813. doi: 10.1016/j.geothermics.2020.101813.

[329] Raymond J, Lamarche L and Malo M (2016) Extending thermal response test assessments with inverse numerical modeling of temperature profiles measured in ground heat exchangers. Renewable Energy 99, 614–621. doi: 10.1016/j.renene.2016.07.005.

[330] Ministerium für Umwelt, Klima und Energiewirtschaft Baden-Württemberg (2018) Leitlinien Qualitätssicherung Erdwärmesonden (LQS EWS). Stuttgart, 35 pp.

[331] Rohner E, Rybach L and Schaerli U (2005) A New, Small, Wireless Instrument to Determine Ground Thermal Conductivity In-Situ for Borehole Heat Exchanger Design. Proceedings World Geothermal Congress 2005. Antalya, Turkey, 24-29 April 2005, 4 pp.

[332] Wagner R and Rohner E (2008) Improvements of Thermal Response Tests for Geothermal Heat Pumps. 9th International IEA Heat Pump Conference, 20-22 May, Zürich, Switzerland, 9 pp.

[333] Martos J, Torres J and Montero Á (2008) Wireless sensor network for measuring thermal properties of borehole heat exchangers. IEEE International Conference Sustain. Energy Technol., 944–948. doi: 10.1109/ICSET.2008.4747125.

[334] Martos J, Montero Á, Torres J, Soret J, Martínez G and García-Olcina R (2011) Novel wireless sensor system for dynamic characterization of borehole heat exchangers. Sensors(Basel) 11, 7082–7094. doi: 10.3390/s110707082.

[335] Aranzabal N, Martos J, Steger H, Blum P and Soret J (2019) Temperature measurements along a vertical borehole heat exchanger: A method comparison. Renewable Energy. doi: 10.1016/j.renene.2019.05.092.

[336] Gottlieb J, Tilg M-A, Fischer D, Zorn R and Meier S (2018) Messmethoden für Monitoring, Qualitätskontrolle und Beweissicherung bei Erdwärmesonden. In: Bauer M, Freeden W, Jacobi H and Neu T (eds). Handbuch Oberflächennahe Geothermie. Springer Spektrum, 637–652. doi: 10.1007/978-3-662-50307-2_20.

[337] Heraeus Sensor Technology (2017) Heraus Sensorbroschüre. Präzise und zuverlässig messen, optimieren, steuern., 2 pp.

[338] Taylor HR (1997) Data Acquisition for Sensor Systems. Springer-Science Business Media, 332 pp.

[339] Bernhard F (2014) Handbuch der Technischen Temperaturmessung. Berlin Heidelberg: Springer Vieweg 2. Auflage, 1631 pp.

[340] Grote K-H and Antonsson EK (2008) Springer Handbook of Mechanical Engineering. Springer, 1589 pp.

[341] JCGM (2008) Evaluation of measurement data - Guide to the expression of uncertainty in measurement, 134 pp.

[342] Eurachem (2012) Quantifying Uncertainty in Analytical Measurement Third Edition, 141 pp.

[343] Scheller G (2003) Error Analysis of a Temperature Measurement System. with worked examples 1st edition, 34 pp.

[344] Taylor BN and Kuyatt CE (1993) Guidelines for evaluating and expressing the uncertainty of NIST measurement results. NIST Technical Note 1297, 24 pp.

[345] Deutsche Akkreditierungsstelle GmbH (2010) Kalibrierung von Widerstandsthermometern. DKD-R 5-1, 24 pp.

[346] Kurzweil P, Frenzel B and Gebhard Florian (2008) Physik Formelsammlung. Ingenieure und Naturwissenschaftler. Vieweg 1st edn., 388 pp.

[347] Michalski L, Eckersdorf K, Kucharski J and McGhee J (2001) Temperature measurement. John Wiley & Sons, Ltd 2nd edn., 514 pp.

[348] Nau M (2002) Electrical Temperature Measurement with thermocouples and resistance thermometers, 163 pp.

[349] Li Y, Zhang Z, Hao X and Yin W (2018) A Measurement System for Time Constant of Thermocouple Sensor Based on High Temperature Furnace. Applied Sciences 8, 2585. doi: 10.3390/app8122585.

[350] Wang S, Tang J and Younce F (2003) Temperature Measurement. Encyclopedia of Agricultural, Food, and Biological Engineering, 987–993. doi: 10.1081/E-EAFE.

[351] Focaccia S and Tinti F (2013) An innovative Borehole Heat Exchanger configuration with improved heat transfer. Geothermics 48, 93–100. doi: 10.1016/j.geothermics.2013.06.003.

[352] Li Y, An Q, Liu L and Zhao J (2014) Thermal Performance Investigation of Borehole Heat Exchanger with Different U-tube Diameter and Borehole Parameters. Energy Procedia 61, 2690–2694. doi: 10.1016/j.egypro.2014.12.278.

[353] Eggeling L and Schneider J (2018) Auswirkungen der Grundwasserbeschaffenheit auf Bau und Betrieb Oberflächennaher Geothermieanlagen. In: Bauer M, Freeden W, Jacobi H and Neu T (eds). Handbuch Oberflächennahe Geothermie. Springer Spektrum, 281–294.

[354] Klotzbücher T, Kappler A, Straub KL and Haderlein SB (2007) Biodegradability and groundwater pollutant potential of organic anti-freeze liquids used in borehole heat exchangers. Geothermics 36, 348–361. doi: 10.1016/j.geothermics.2007.03.005.

[355] Umweltministerium Baden-Württemberg (2005) Leitfaden zur Nutzung von Erdwärme mit Erdwärmesonden, 28 pp.

[356] Benz SA, Bayer P, Menberg K, Jung S and Blum P (2015) Spatial resolution of anthropogenic heat fluxes into urban aquifers. SciTotalEnviron 524-525, 427–439. doi: 10.1016/j.scitotenv.2015.04.003.

[357] Menberg K, Blum P, Schaffitel A and Bayer P (2013) Long-term evolution of anthropogenic heat fluxes into a subsurface urban heat island. EnvironSciTechnol 47, 9747–9755. doi: 10.1021/es401546u.

[358] Agilent Technologies (2007) Agilent N4385A/N4386A Distributed Temperature System User's Guide, 72 pp.

[359] Hausner MB, Suárez F, Glander KE, van de Giesen N, Selker JS and Tyler SW (2011) Calibrating single-ended fiber-optic Raman spectra distributed temperature sensing data. Sensors(Basel) 11, 10859–10879. doi: 10.3390/s111110859.

[360] van de Giesen N, Steele-Dunne SC, Jansen J, Hoes O, Hausner MB, Tyler S and Selker J (2012) Double-ended calibration of fiber-optic Raman spectra distributed temperature sensing data. Sensors(Basel) 12, 5471–5485. doi: 10.3390/s120505471.

[361] Des Tombe B, Schilperoort B and Bakker M (2020) Estimation of Temperature and Associated Uncertainty from Fiber-Optic Raman-Spectrum Distributed Temperature Sensing. Sensors(Basel) 20. doi: 10.3390/s20082235.

[362] Kurevija T, Vulin D and Krapec V (2011) Influence of Undisturbed Ground Temperature and Geothermal Gradient on the Sizing of Borehole Heat Exchangers.

World Renewable Energy Congress 2011 – Sweden, 8-11 May 2011, Linköping, Sweden, 1360–1367. doi: 10.3384/ecp110571360.

[363] Urban K (2010) External and intrinsic influences on Thermal Response Test evaluation using the line source model. Diplomarbeit, Eberhard-Karls-Universität, Tübingen, 84 pp.

[364] Sommer WT, Doornenbal PJ, Drijver BC, van Gaans PFM, Leusbrock I, Grotenhuis JTC and Rijnaarts HHM (2014) Thermal performance and heat transport in aquifer thermal energy storage. HydrogeolJ 22, 263–279. doi: 10.1007/s10040-013-1066-0.

[365] Vogt T, Schneider P, Hahn-Woernle L and Cirpka OA (2010) Estimation of seepage rates in a losing stream by means of fiber-optic high-resolution vertical temperature profiling. Journal of Hydrology 380, 154–164. doi: 10.1016/j.jhydrol.2009.10.033.

[366] Smolen JJ and van der Spek A (2003) Distributed Temperature Sensing. A DTS Primer for Oil & Gas Production. Techn. Report, Shell, 97 pp.

[367] Ukil A, Braendle H and Krippner P (2011) Distributed Temperature Sensing: Review of Technology and Applications. IEEE Sensors Journal, 885–892. doi: 10.1109/JSEN.2011.2162060.

[368] Shatarah SMI and Olbrycht R (2017) Distributed temperature sensing in optical fibers based on Raman scattering: theory and applications. Measurement Automation Monitoring 63, 41–44

[369] Lee D, Ooka R, Ikeda S and Choi W (2019) Artificial neural network prediction models of stratified thermal energy storage system and borehole heat exchanger for model predictive control. Science and Technology for the Built Environment 25, 534–548. doi: 10.1080/23744731.2018.1557464.

[370] Woernle MI (2008) Anwendbarkeit künstlicher neuronaler Netze zur Untergrundbewertung in der oberflächennahen Geothermie. Dissertation, Karlsruhe, 126 pp.

[371] Menberg K, Bayer P, Zosseder K, Rumohr S and Blum P (2013) Subsurface urban heat islands in German cities. SciTotalEnviron 442, 123–133. doi: 10.1016/j.scitotenv.2012.10.043.

[372] Schüppler S, Roman Z, Schindler L, Neuner F, Steger H and Blum P (2020) Monitoring of Borehole Heat Exchanger Using Wireless Temperature Measurements. Proceedings World Geothermal Congress 2020 Reykjavik, Iceland, April 26 – May 2, 2020

[373] Kolb M (2021) Besprechung Projekte mit Saisonspeicher. Personal communication. Anex.

[374] Blum P, Fleuchaus P, Koenigsdorff R, Ryba M, Zorn R, Schüppler S, Braun J, Giannelli G, Moormann C, Buhmann P, Liaghi M, Isenbeck-Schröter M, Ritter S, Breyer-Mayländer T. and Doherr D (2020) Forschungsbericht BWPLUS. Abschlussbericht Geospeicher.bw, 103 pp.

[375] Gautschi T and Amiet R (2006) ETH Zürich Masterplan Energie- und Medienversorgung Hönggerberg. Gesamtbericht. Amstein + Walthert AG, 147 pp.

[376] Lowe WJ (2016) Ball State University. Ground Source Geothermal District Heating and Cooling System, 233 pp.

[377] Andersson O (2021) Best practice ATES systems. Personal communication

[378] Godschalk B (2021) Feasibilities of ATES. Personal communication. IF Technology.

[379] Haussler-Pause R (2021) Machbarkeitsanalysen ETH Hönggerberg. Personal communication. ETH Zürich.

[380] Barth F (2020) Luftbildanalyse zur Bestimmung der Kälteleistung im Raum Freiburg im Breisgau. Projektstudie, Karlsruher Institut für Technologie (KIT), Karlsruhe, 59 pp.

[381] Tissen C, Menberg K, Benz SA, Bayer P, Steiner C, Götzl G and Blum P (2021) Identifying key locations for shallow geothermal use in Vienna. Renewable Energy 167, 1–19. doi: 10.1016/j.renene.2020.11.024.

[382] Zhang Y, Soga K and Choudhary R (2014) Shallow geothermal energy application with GSHPs at city scale: study on the City of Westminster. Géotechnique Letters 4, 125–131. doi: 10.1680/geolett.13.00061.

[383] Bozkaya B, Li R and Zeiler W (2018) A dynamic building and aquifer co-simulation method for thermal imbalance investigation. Applied Thermal Engineering 144, 681–694. doi: 10.1016/j.applthermaleng.2018.08.095.

[384] Gillingham K and Stock JH (2018) The Cost of Reducing Greenhouse Gas Emissions. Journal of Economic Perspectives 32, 53–72. doi: 10.1257/jep.32.4.53.

[385] McKinsey&Company (2007) Kosten und Potenziale der Vermeidung von Treibhausgasemissionen in Deutschland, 70 pp.

[386] van den Bergh K and Delarue E (2015) Quantifying CO2 abatement costs in the power sector. Energy Policy 80, 88–97. doi: 10.1016/j.enpol.2015.01.034.

[387] Antelmi M, Alberti L, Angelotti A, Curnis S, Zille A and Colombo L (2020) Thermal and hydrogeological aquifers characterization by coupling depth-resolved thermal response test with moving line source analysis. Energy Conversion and Management 225, 113400. doi: 10.1016/j.enconman.2020.113400.

[388] Witte HJL (2013) Error analysis of thermal response tests. Applied Energy 109, 302–311. doi: 10.1016/j.apenergy.2012.11.060.

Publications and contributions

Peer-reviewed journal publications

Schüppler S, Fleuchaus P, Duchesne A, Blum P (2021) Cooling supply costs of a university campus. *Submitted to Energy.*

Stemmle R, Blum P, **Schüppler S**, Fleuchaus P, Limoges M, Bayer P, Menberg K (2020) Environemntal impacts of aquifer thermal energy storage (ATES). *Submitted to Renewable and Sustainable Energy Reviews.*

Schüppler S, Fleuchaus P, Zorn R, Salomon R, Blum P (2021) Quantifying installed cooling capacities using aerial images. Journal of Photogrammetry, Remote Sensing and Geoinformation Science. doi: 10.1007/s41064-021-00137-0.

Schüppler S, Zorn R, Hagen S, Blum P (2021). Uncertainty analysis of wireless temperature measurement (WTM) in borehole heat exchanger. Geothermics. doi: 10.1016/j.geothermics.2020.102019.

Fleuchaus P, **Schüppler S**, Kathrin M, Stemmle R, Blum P (2020) Aquiferspeicher in Deutschland. Grundwasser. doi: 10.1007/s00767-021-00478-y.

Fleuchaus P, **Schüppler S**, Bloemendal M, Guglielmetti L, Opel O, Blum P (2020) Risk analysis of High Temperature Aquifer Thermal Energy Storage (HT-ATES). Renewable and Sustainable Energy Reviews. doi: 10.1016/j.rser.2020.110153.

Fleuchaus P, **Schüppler S**, Bakema G, Godschalk B, Blum P (2020) Performance analysis of Aquifer Thermal Energy Storage (ATES). Renewable Energy, 146, 1536-1548. doi: 10.1016/j.renene.2019.07.030.

Schüppler S, Fleuchaus P, Blum P (2019) Techno-economic analysis of an Aquifer Thermal Energy Storage (ATES) in Germany. Geothermal Energy 7. doi: 10.1186/s40517-019-0127-6.

Conference proceedings

Schüppler S, Zorn R, Makni L, Neuner F, Steger H, Blum P (2020) Monitoring of Borehole Heat Exchangers Using Wireless Temperature Measurements. World Geothermal Congress (WGC), Reykjavic, Iceland, 7 pp.

Fleuchaus P, **Schüppler S**, Godschalk B, Bakema G, Zorn R, Blum P (2020) Techno-economic performance evaluation of Aquifer Thermal Energy Storage. World Geothermal Congress (WGC), Reykjavik, Iceland, 11 pp.

Godschalk B, Fleuchaus P, **Schüppler S**, Velvis H, Blum P (2019) Aquifer Thermal Energy Storage (ATES) systems at universities. European Geothermal Congress (EGC), Den Haag, The Netherlands, June 11-14, 7 pp.

Conference contributions (first author)

Schüppler S, Zorn R, Steger H, Blum P (2021) Wireless probes for measuring vertical temperature profiles in borehole heat exchanger (2021). European Geoscience Union General Assembly, online, April 19-30 2021, EGU21-9948. doi: 10.5194/egusphere-egu21-9948 (vPICO presentation).

Schüppler S, Fleuchaus P, Godschalk B, Bakema G, Zorn R, Blum P (2020) Aquifer Thermal Energy Storage (ATES) systems – current global practical experience. European Geoscience Union General Assembly, online, May 4-8 2020, EGU2020-21396. doi: 10.5194/egusphere-egu2020-21396 (online presentation).

Schüppler S, Zorn R, Makni L, Steger H, Blum P (2020) Kabellose Messkugeln zur Aufzeichnung tiefenorientierter Temperaturprofile. 28. Tagung der Fachsektion Hydrogeologie (FH-DGGV), Leipzig, Germany (*cancelled* - selected as presentation).

Schüppler S, Fleuchaus P, Godschalk B, Bakema G, Zorn R, Blum P (2019) Technische und ökonomische Analyse von Aquiferspeichern (ATES). Der Geothermiekongress (DGK), München, Germany, November 20-21 (presentation).

Schüppler S, Zorn R, Steger H, Blum P (2019) Errors and uncertainties of wireless temperature measurements (WTMs) in borehole heat exchangers (BHEs). IEA ECES Annex 27 – Quality Management Design, Construction and operation of Borehole Systems – 8th Experts Meeting, Subtask 4, Garching, Germany, September 9-11 (presentation).

Schüppler S, Fleuchaus P, Blum P (2019) Economic and environmental analysis of an Aquifer Thermal Energy Storage (ATES) of a hospital in Germany. European Geoscience Union General Assembly, Vienna Austria, April 7-12 2019, Geophysical Research Abstracts Vol. 21, EGU2019-15035 (poster).

Schüppler S, Fleuchaus P, Blum P (2019) Techno-economic analysis of an Aquifer Thermal Energy Storage (ATES) in Germany. 10th European Geothermal PhD Days (EGPD), Potsdam, Germany, February 25-27 (poster).

Schüppler S, Zorn R, Eyler D (2018) Geothermal Heat Storage in Baden-Württemberg. Towards Energy Transition, Scientific Workshop and Forum for Students, Paris-Saclay, France, November 6-8 (poster).

Co-supervised degree theses

- Florian Barth (2021) Estimating Cooling Capacities from Aerial Images Using Convolutional Neural Networks, *M.Sc.-Thesis*. Karlsruhe Institute of Technology (KIT).
- Lukas Cnauer (2021) Analytische Modellierung von tiefenorientierten Temperaturprofilen, *B.Sc.-Thesis.* Karlsruhe Institute of Technology (KIT).
- Johannes Klein (2020) Techno-economic feasibility study of a Cooling Network at the KIT Campus North. *M.Sc.-Thesis*. Karlsruhe Institute of Technology (KIT).
- Susanna Grahovac (2019) Wärmeeintrag durch das Aquadrom Hockenheim in den Untergrund: ein Wärmetransportmodell. *M.Sc.-Thesis.* Karlsruhe Institute of Technology (KIT).
- Antoine Duchesne (2019) Wirtschaftlichkeitsanalyse der Kälteversorgung eines Forschungszentrums. *M.Sc.-Thesis.* Karlsruhe Institute of Technology (KIT).
- Robert Salomon (2019) Analyse der installierten Kälteleistung am KIT CN mittels Luftbildern. *M.Sc.-Thesis*. Karlsruhe Institute of Technology (KIT).
- Mélissa Limoges (2019) Life Cycle Assessment of Aquifer Thermal Energy Storage Systems. *B.Sc.-Thesis*. Technische Hochschule Ingolstadt (THI).